JAMES COOK CYCLONE STRUCTURAL TESTING STATION

CYCLONE TESTING STATION

FINITE ELEMENT ANALYSIS OF PROFILED ROOFING SHEETS SUBJECT TO SIMULATED WIND UPLIFT

Technical Report No. 40

August 1993

Cyclone Structural Testing Station
James Cook University of North Queensland

Finite Element Analysis of Profiled Roofing Sheets Subject to Simulated Wind Uplift

by

Y. L. Xu

Technical Report No. 40

Xu, Y. L. (You Lin), 1952-
Finite element analysis of profiled roofing sheets
subject to simulated wind uplift

ISBN 0 86443 480 4.
ISSN 0158 - 8338.

1. Roofs - Aerodynamics. 2. Roofing, Iron and steel - Testing.
3. Sheet-metal - Testing. 4. Building, Stormproof. 5. Metals -
Fatigue. I. James Cook University of North Queensland.
Cyclone Testing Station. II. Title. (Series : Technical Report
(James Cook University of North Queesnland. Cyclone
Testing Station) ; no 40).

690.15

FINITE ELEMENT ANALYSIS OF PROFILED ROOFING SHEETS SUBJECT TO SIMULATED WIND UPLIFT

Synopsis

Field investigations and laboratory experiments have shown that screw fastened light gauge steel profiled roofing sheets may fail locally in the vicinity of screw fasteners by plastic collapse under strong peak wind loads or by cracking due to low cycle fatigue under sustained fluctuating wind loads. The problem however remains unclear with respect to characteristics of local plastic collapse and fatigue damage. This report therefore presents a finite element study of screw fastened profiled roofing sheets, from which severe sheeting distortions and complex stress distributions in the vicinity of screw fasteners can be demonstrated.

Three commonly-used types of profiled roofing sheets were modelled in this study. Both linear elastic and elastic-plastic large deflection analyses were carried out. The upward deflections, fastener reaction forces and failure loads of the roofing sheets predicted by the finite element method were compared with those from previously conducted experiments, and a close agreement was found. The finite element analysis performed here not only provided clear pictures on global deformations, local deformations, yield zones and cross-sectional distortions of the roofing sheets, but also identified highly stressed areas around the fastener holes where local plastic collapse and fatigue cracks originate. Furthermore, the relationships between wind uplift and sheeting stresses at critical areas brought out mechanisms of local plastic collapse and characteristics of sheeting fatigue. The large difference between load-stress relations of three types of roofing sheets indicates that different profiled roofing sheets would exhibit different fatigue performances.

The successful application of the finite element method to light gauge steel profiled sheets offers a method of conducting extensive parametric studies of the structural behaviour of marketing roofing sheets under arbitrarily distributed wind pressure. It also opens the way for the initial design of new sheeting profiles and serves as a transfer function from cyclone induced wind load characterisation to sheeting fatigue life prediction.

CONTENTS

1 INTRODUCTION

Light gauge steel profiled sheeting is widely used as roof claddings in houses, low rise commercial and industrial buildings due to its high lateral (bending) stiffness and competitive cost. Most sheet roof systems in Australia are constructed by screw-fastening light gauge steel sheeting of various profiles to cold-formed steel purlins or high quality timber battens. When such roof systems are used in wind prone areas, the strength of roofing sheets under wind loads becomes the most important criterion for structural design.

A large number of wind tunnel studies and field measurements (e.g. Eaton *et al*, 1975; Holmes and Best, 1978; Stathopoulos, 1984; Metha *et al*, 1992) show that roofing sheets in strong wind are predominantly subjected to wind suction, i.e., wind uplift, and very high suction is developed at roof eaves close to the corner or at the roof ridge near the gable end. Field damage investigations after tropical cyclones (e.g., Walker, 1975, 1980) and laboratory structural experiments (e.g., Beck and Stevens, 1976; Morgan and Beck, 1977; Beck and Stevens, 1979; and Mahendran, 1990) further show that screw fastened roofing sheets mainly fail in the vicinity of screw fasteners by plastic collapse under strong peak wind uplift or by cracking due to low cycle fatigue under sustained fluctuating wind uplift. The problem however remains unclear with respect to mechanisms of local sheeting failure and characteristics of wind loads causing sheeting fatigue damage. This has led to a serious debate in Australia on the current criteria of roof sheeting design and tests (Holmes, Walker and Melbourne, 1991).

With the rapid development in recent years of computer science and numerical structural analysis technology, it becomes possible to use computer-based finite element method to determine complex stress distributions and severe shape distortions in the vicinity of screw fasteners, to identify highly stressed areas where local plastic collapse and fatigue cracks originate, to find relationships between loads and stresses at critical areas, and to explain local failure mechanisms. The finite element analysis can also serve as a transfer function from external load characterisation to sheeting fatigue life prediction as suggested in ASCE (1982) and SAE (1988), and as an effective tool for sheeting design, especially for the initial design of new sheeting products.

To the extent of the author's knowledge, very limited numerical analysis work currently exists on roofing sheets under laterally applied concentrated or distributed loads, though the numerical analysis of light gauge metal shear diaphragms (Nilson, 1973) can be occasionally found. Salaheldin, Schmidt and Upfold (1987) used the finite element method to simulate responses of corrugated sheets under a laterally applied, static, concentrated load. Mahendran (1990) conducted a numerical study on structural behaviour of wind-loaded roofing sheets of arc-tangent profile, but his results were somewhat restricted to a low load level, so sheeting local failure mechanisms were not studied.

In this report, a detailed study is presented on finite element analysis of full range structural behaviour of wind-loaded screw fastened roofing sheets. Three commonly-used types of profiled roofing sheets are concerned here, the profiles of which are trapezoidal profile (Spandek profile), ribbed profile (Trimdek profile) and arc-tangent profile (Custom Orb profile), as shown in Fig. 1.1. The proposed finite element modelling procedure is validated through the comparison between the finite element results and the experimental results with regard to the upward deflections, fastener reaction forces and failure loads of the roofing sheets. Characteristics of fluctuating wind loads causing sheeting fatigue damage and the application of the finite element results to sheeting fatigue life prediction are not included in this report.

2 FINITE ELEMENT MODELLING OF ROOFING SHEETS

2.1 Sheeting Test Arrangement

This section is a brief description of the test arrangement associated with the midspan load method and used in the previous roofing sheet experiments by Xu and Reardon, 1992. The finite element modelling of the roofing sheets in this report is based on this kind of test arrangement so that the previous test results can be used to validate finite element results. Nevertheless, the proposed finite element modelling procedure can also be applied to the roofing sheets tested by other methods, such as a vacuum chamber method (Redfearn,1984; Gerhardt and Kramer, 1986; and Hancock, 1991).

In most roof sheeting tests, a multi-span prototype assembly of roof cladding is conservatively represented by a two-span prototype roofing assembly since wind induced high suction is usually developed at roof eaves close to the corner, or at the roof ridge near the gable end. The critical second support from the eaves or

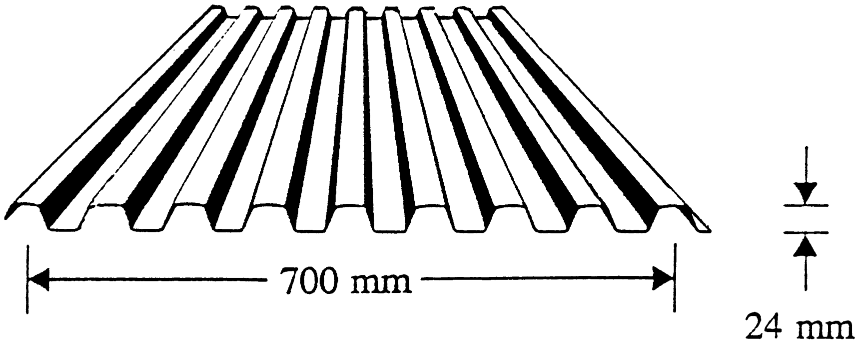

Trapezoidal Profile Sheet
(Spandek Profile)

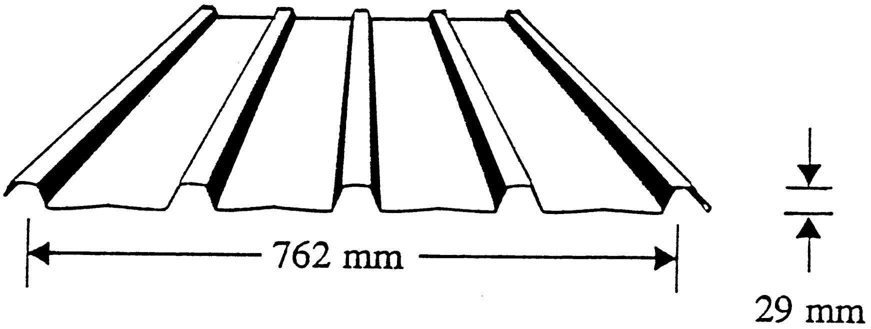

Ribbed Profile Sheet
(Trimdek Profile)

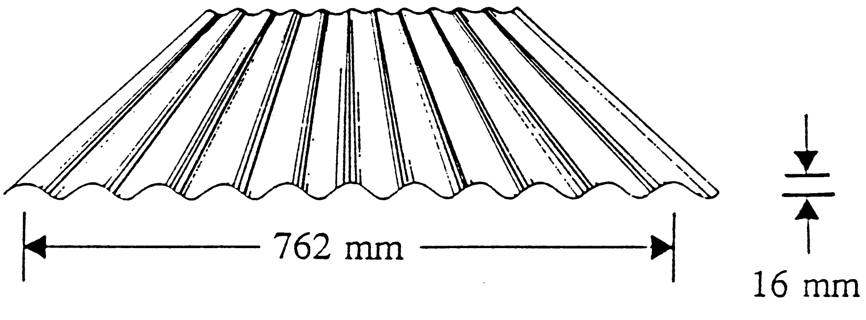

Arc-Tangent Profile Sheet
(Custom Orb Profile)

FIG.1.1 SHEETING PROFILES USED IN ANALYSIS the ridge of the roof prototype is represented by the central support of the two-span prototype roofing assembly. When the midspan load method is used to test roofing sheets in laboratory, distributed pressure, which is assumed to uniformly act on the entire sheeting surface, is further replaced by limited band pressure exerted by rubber loading pads at the midspan of the sheeting. Correspondingly, an equivalent sheeting span should be used to replace the sheeting span in the two-span prototype roofing assembly such that the fastener reaction force and bending moment of the test sheet at the central support are the same as those of the two-span prototype roofing assembly (as a two-span continuous beam). A force relationship between the midspan line load on the test sheet and the average wind pressure on the two-span prototype roofing assembly is also established from the above modelling requirements.

The experimental set-up corresponding to the midspan load method used in the previous experiments is shown schematically in Fig. 2.1, with a serve-controlled hydraulic testing machine (Instron) being the major apparatus. Roofing sheets were symmetrically screw fastened to three high quality timber battens to construct a two-span roofing assembly. Two different roofing spans were adopted: a 648 mm short span which is equivalent to 900 mm span in prototype, and a 868 mm long span which is equivalent to 1200 mm span in prototype. An alternate crest fastening system was adopted for the trapezoidal and arc-tangent profile sheets. For ribbed profile roofing sheets, all ribs were screw fastened, which is considered as an equivalent alternate crest fastening system due to the wide pan between two ribs. Each self-drilling screw was used together with a neoprene washer of 2.5 mm thickness. Flexible rubber loading pads were used to apply a narrow band of pressure to the bottom surface of test sheet to simulate wind uplift. The band width was 28 mm and the upper face of the loading pads was formed to coincide with the shape of the sheeting profiles. The loading pads for the trapezoidal and ribbed profile sheets later were found to exert some additional restraint to sheeting deformations. Subsequently, loading pads with a flat surface which applied normal pressures to the valleys only were also used for the trapezoidal profile roofing sheet to ascertain the effect of the additional restraint. For the arc-tangent profile roofing sheet, a thin rubber tube filled with water was fixed on the top of the loading pads to achieve a uniform normal pressure. The total reaction at the central support was measured by an Instron load cell. This total reaction force was then divided by the number of fasteners to obtain average reaction force on each fastener. A Kyowa load cell of a capacity of 20 kN was employed to measure total uplift load on the roofing sheet, which was then divided by 2b (b = the sheeting width) to calculate

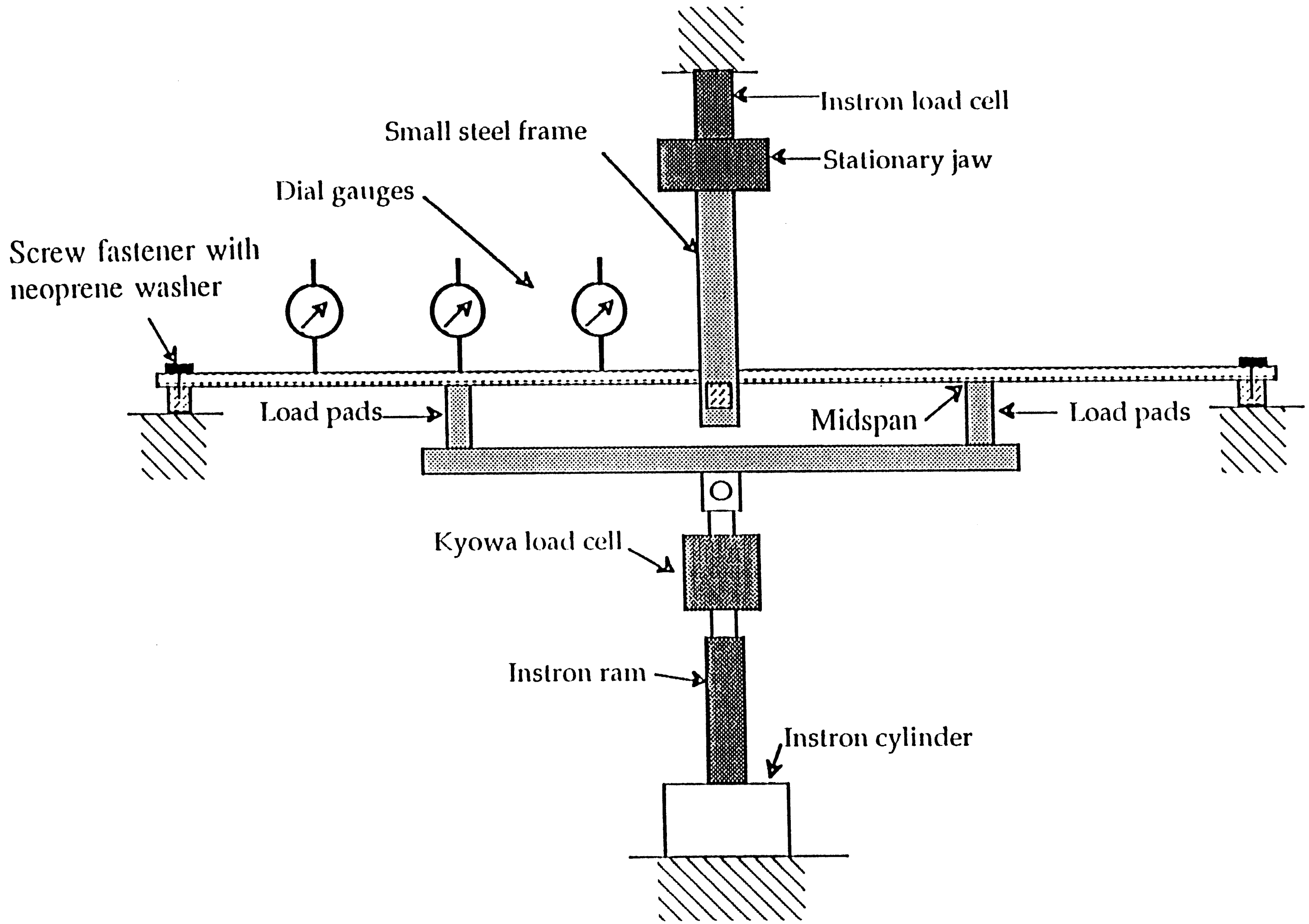

FIG.2.1 EXPERIMENTAL SET-UP

average line load applied to the test sheet by the loading pads.

All tests were conducted by controlling the displacement of the movable ram of the Instron machine in order to follow the entire load-deflection path through any unstable failure stages. However, since dial gauges were used to measure sheeting upward deflections, sheeting local buckling or plastic collapse behaviour could not be satisfactorily recorded on load-deflection curves. A few measurements of upward deflection during sheeting snap-through or plastic collapse were taken in dynamic equilibrium with an effort of simultaneously reading both load and deflection values, but they may still not be good enough.

2.2 Finite Element Modelling

For the two-span roofing sheet assembly described above, symmetry conditions are satisfied along the line of central support with regard to both geometry and loading. Symmetry conditions were also assumed along the longitudinal centre line of each crest (or each rib and pan in the ribbed profile sheets). The latter symmetry assumption was not satisfied exactly by the test sheets due to the limited sheeting width and the two unrestrained sheeting edges, but it is justified when prototype roof sheeting with a large number of crests or ribs is considered. The use of symmetry led to much reduced computational work.

From above symmetry considerations, only a one-span model of one nominal corrugation is needed to consider in the finite element modelling. The one nominal corrugation in the trapezoidal or arc-tangent profile sheet means the part of the sheet from one screwed crest to adjacent unscrewed crest, as shown in Fig. 2.2 or Fig. 2.4. In the ribbed profile sheet, it means the part from one screwed rib to the middle of adjacent pan (see Fig. 2.3). The finite element models shown in Figs. 2.2 and 2.3 represent long span roofing sheets whilst the finite element model shown in Fig. 2.4 represents short span roofing sheet. For all three types of finite element models, both longitudinal edges of the model were restrained against rotations about the edges and transverse translations (translations in the x-direction) from symmetry considerations. For the same reason, the central support edge was prevented from rotating about the edge and from longitudinal translation (translation in the y-direction). The edge near the end support was assumed to be free to move since a two-span roofing assembly was considered.

As the fastener holes in the sheeting were produced by self-drilling screws, and

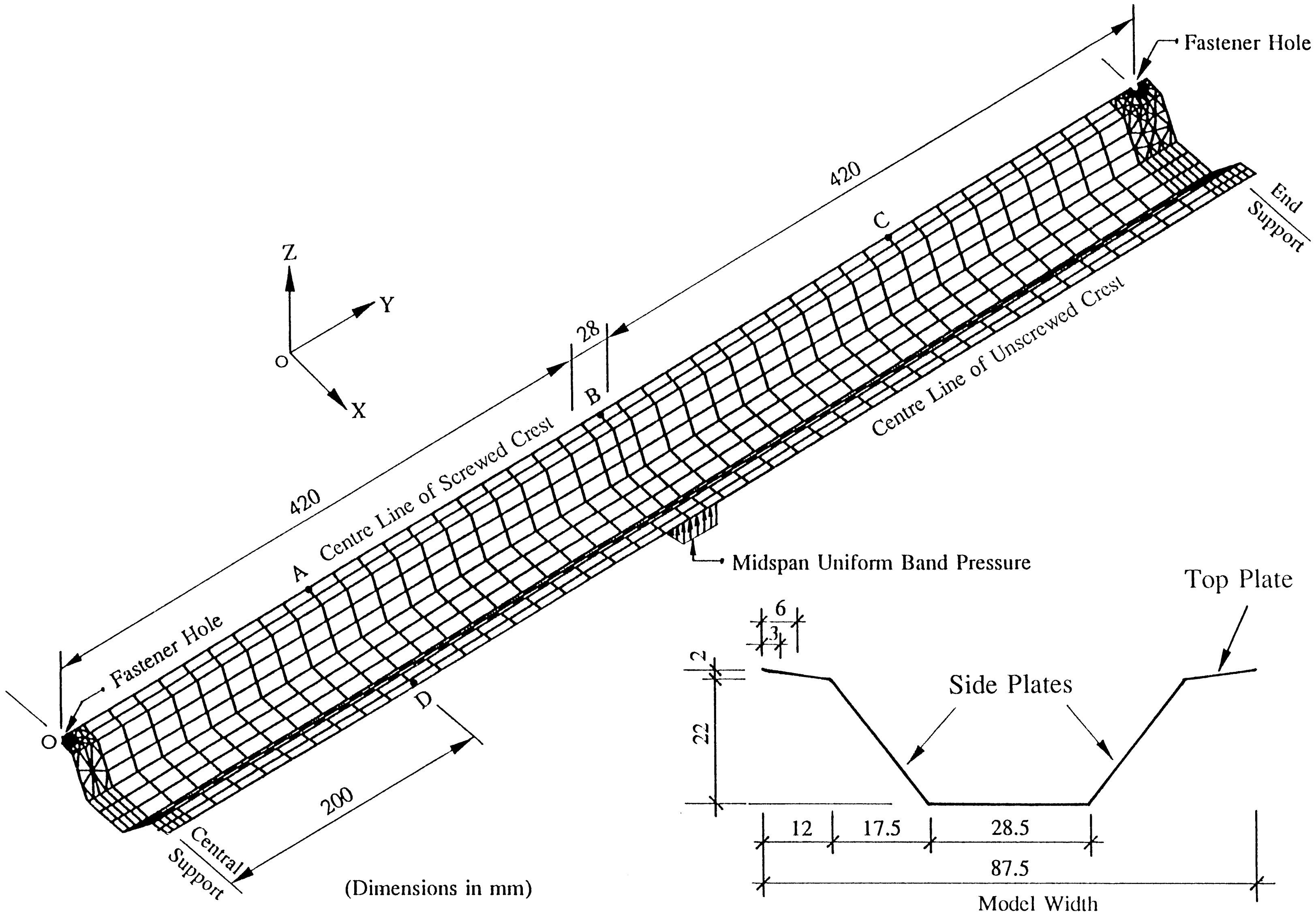

FIG.2.2 FINITE ELEMENT MODEL OF TRAPEZOIDAL PROFILE ROOFING SHEET

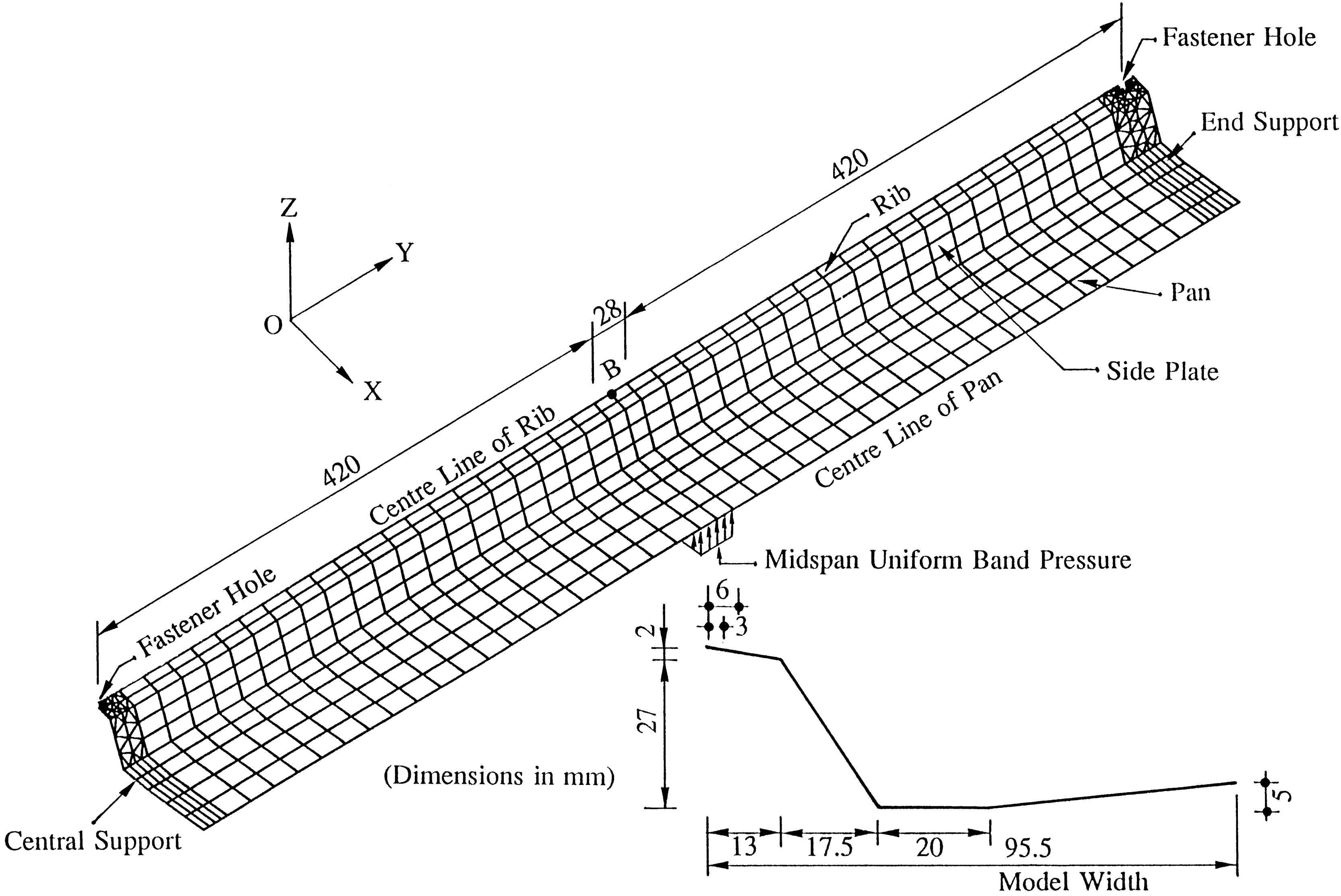

FIG.2.3 FINITE ELEMENT MODEL OF RIBBED PROFILE ROOFING SHEET

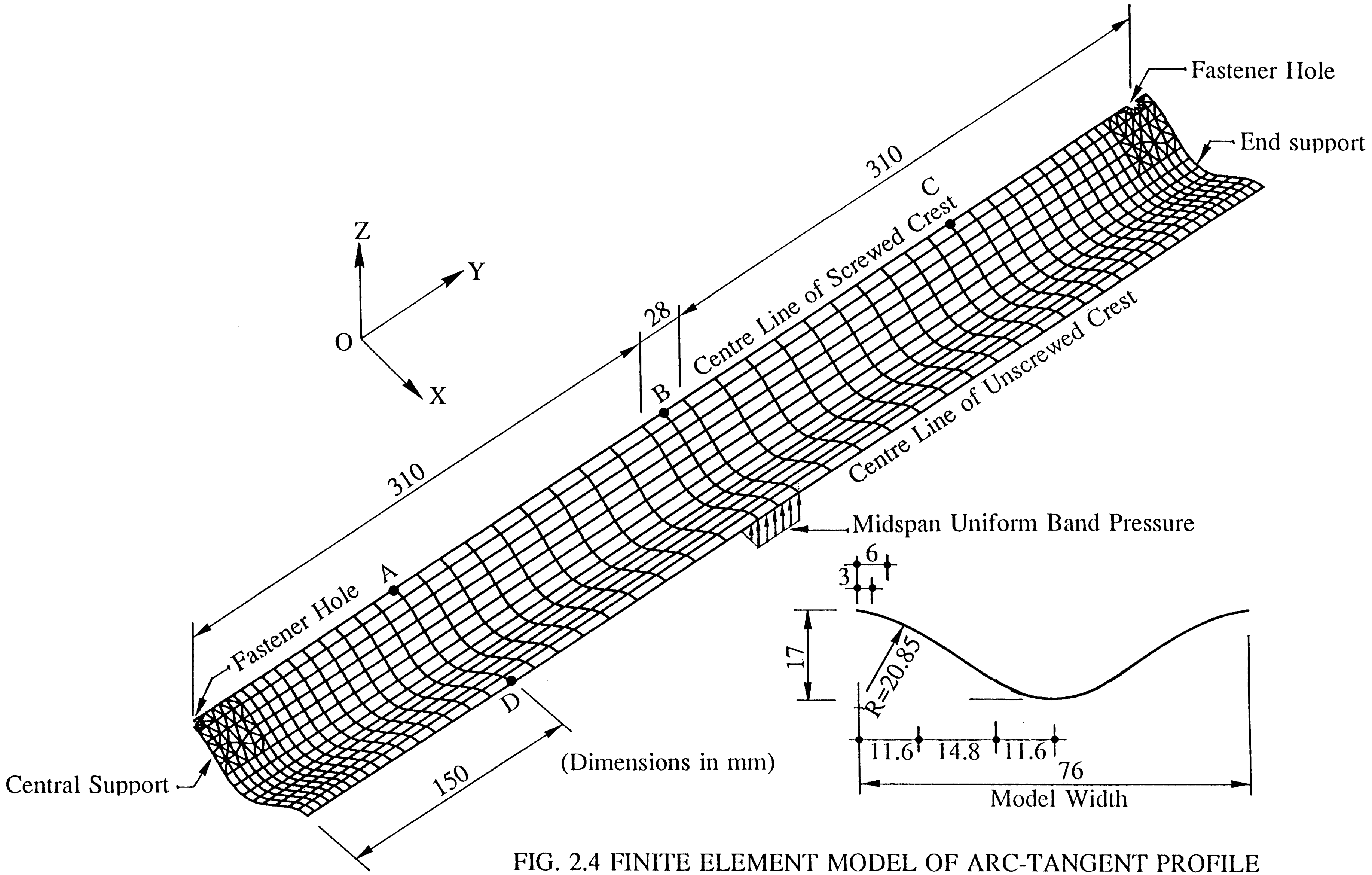

FIG. 2.4 FINITE ELEMENT MODEL OF ARC-TANGENT PROFILE ROOFING SHEET

the screw fasteners at the central support were in symmetrical conditions, the hole edges, which were in direct contact with the screw shafts, were assumed to be restrained against translations in both x- and y- directions. This assumption is valid for the static analysis of the roofing sheets, but may not be well suitable for the fatigue analysis as a relative movement of the hole edges to the fastener shaft was observed during sheet fatigue tests. In addition, it was mentioned in Section 2.1 that the roofing sheets under uplift load were supported by screw heads via neoprene washers. When the uplift load is small, the neoprene washer deforms elastically, so ideally the washer should be modelled as an elastic restraint to the sheeting. However, plastic deformations of the washer appear quickly as external load becomes larger, and the degree of pre-tightening of the screws with neoprene washers is variable to some extent in practice. As an approximation, the area in contact with the washer was assumed to be prevented from vertical displacements (the z-direction translations) in the static analysis of the roofing sheets. The rigid body displacement caused by washer deformations can then be deducted from the measured upward sheeting deflections by assuming the washer deformations to be linear and elastic. In fact, this rigid body displacement was small comparing with roof sheeting deflections at the midspan, especially for the unscrewed crest. As to the pressure generated between the loading pads and the sheeting surface, it was assumed to be normal to the sheeting surface and uniformly distributed over a band width of 28 mm. The line load can be easily obtained from the product of the band pressure and the band width in accordance to the test results.

The Semi-Loof curved thin shell element available in the LUSAS finite element system (FEA, 1990) was used in the analysis because of its capability of modelling shell intersections. Details of the Semi-Loof shell element may be found in the LUSAS Theory Manual or elsewhere (e.g., Irons, 1976; Javaherian *et al*, 1979; Martins and Owen, 1981). As shown in Figs. 2.2 to 2.4, a fine mesh with eight-noded quadrilateral elements was generated throughout the span, except in the vicinity of the fastener hole where a much finer mesh with 6-noded triangular elements was used to model rapidly varying high local stresses and deformations. For the arc-tangent profile roofing sheet, planar triangular elements were used to replace curved triangular elements in the vicinity of the fastener holes (see Fig. 2.4) because triangular elements could not be generated on curved surfaces in the current LUSAS system (Version 10.0). This element discretisation created more than 700 Semi-Loof curved thin shell elements and about 2000 nodes. The adequacy of the mesh was established via a convergence study in which several linear analyses using different meshes were carried out.

The finite element analysis to be described in this paper considered both geometrical nonlinearity due to large sheeting deflections and material nonlinearity due to local plastic deformations. The results from linear elastic analysis were also provided to estimate effects of geometric and material nonlinearities. The total Lagrangian approach was adopted in the finite element analysis, and the plastic behaviour of steel was modelled using the J_2 flow theory of plasticity assuming no strain hardening (i.e. von Mises yield criterion with Prandtl-Reuss flow rule). Solution of the nonlinear equations was achieved by the modified Newton-Raphson method in conjunction with a variable arc-length constraint to trace possible nonlinear snap-through behaviour of the sheeting.

2.3 Effective Sheeting Thickness

The profiled roofing sheets used in the test were roll-formed from Zincalume-coated high strength steel plate sheets and were supplied by Lysaght Building Industries, Australia. Several small pieces of steel carefully cut from the sample flat plates were scanned using an electron microscope to determine accurately both the base metal and coating thicknesses. Fig. 2.5 shows a typical micrograph of the sheeting total thickness, in which the base steel and Zincalume coating were clearly identified.

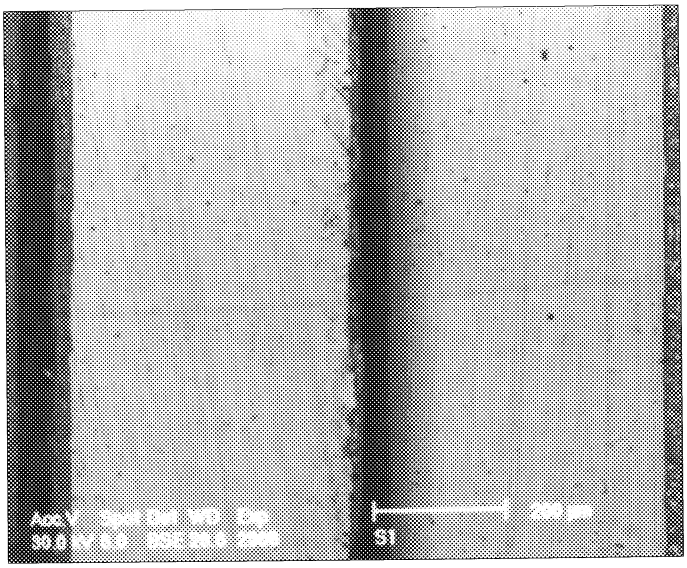

FIG.2.5 ELECTRON MICROGRAPH OF SHEETING THICKNESS

The mean value of the base steel thickness from electron microscope measurements is 0.43 mm whilst the nominal base steel thickness specified by the manufacturer is 0.42 mm (Lysaght Building Industries, 1991). The mean measured total sheeting thickness is 0.49 mm whilst the nominal total sheeting thickness is 0.47 mm. Although it has been suggested (AS 1397, 1984) that the base steel thickness be used as an effective sheeting thickness (t_{ef}) in the structural analysis, the author is not aware of any rigorous justification of ignoring the coating thickness. The reasoning behind the suggestion is perhaps that the contribution of the coating is small and it is conservative to ignore the coating. In this study, two different effective sheeting thicknesses, 0.43 mm and 0.45 mm, were employed in some cases to investigate the effect of a small change in effective thickness.

2.4 Material Properties

Standard tensile tests were carried out to determine material properties of the steel (Xu and Reardon, 1992). Tensile test specimens were cut according to the Australian Standard AS1391 (1991) from sample flat plates supplied by the roofing manufacturer taken during intervals between rolling periods of the roofing sheets used in the test. Both specimens with their long edges cut along (longitudinal specimens) and across (transverse specimens) the final rolling direction were made.

Stress-strain relations of the longitudinal specimens showed an approximate elastic-perfectly plastic behaviour (see Fig. 2.6). Different values may be deduced for the material properties depending on the use of different effective thicknesses. If the sheeting effective thickness is assumed to be 0.45 mm, the mean yield stress defined by the 0.2% proof stress is 690 MPa, which is only slightly smaller than the ultimate tensile strength in this case, but larger than the minimum yield stress of 550 MPa specified in AS1397 (1984) for G550 steel. The corresponding mean Young's modulus is 2.0×10^5 MPa. No strain hardening was found and the fracture strain is about 2%. When the base metal thickness of 0.43 mm is used as the effective thickness as done in most existing works, the 0.2% proof stress becomes 722 MPa and the Young's modulus becomes 2.1×10^5 MPa.

Material properties of the transverse specimens were found to differ from those of the longitudinal specimens. These specimens show a brittle behaviour and their ultimate tensile strengths are reached before attaining a strain of 0.2%. Assuming an effective thickness of 0.45 mm, the average ultimate tensile strength of the transverse specimens is 760 MPa.

Ideally, a nonlinear orthotropic material model in conjunction with some cracking criteria should be developed to analyse the roofing sheets investigated here. However, it is believed that the difference in the material properties between the two directions is secondary factors in the static analysis of the roofing sheets, and to avoid the problem being further complicated the material was modelled as isotropic, elastic-perfectly plastic only, with its properties given by the mean value obtained from the longitudinal specimens. Initial geometric imperfections and residual stresses were not considered either.

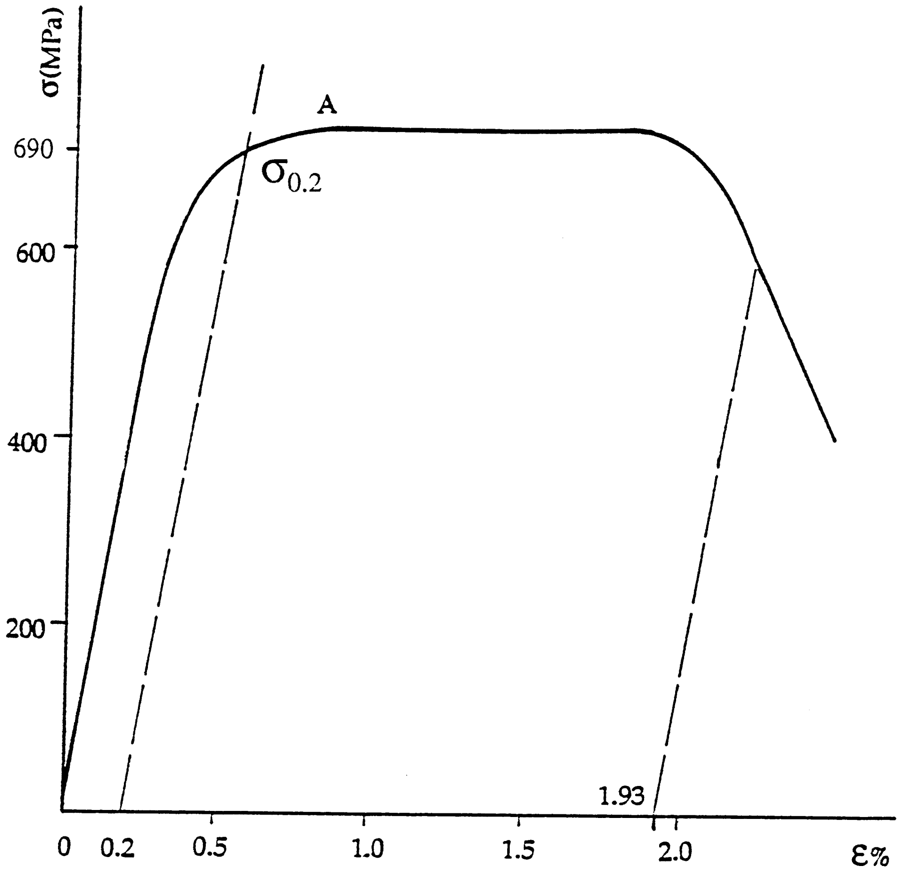

FIG.2.6 STRESS-STRAIN RELATION OF SHEETING MATERIAL IN LONGITUDINAL DIRECTION

3 ANALYSIS OF ROOFING SHEETS OF TRAPEZOIDAL PROFILE

3.1 Sheeting Deflections and Local Plastic Collapse

The upward deflections of point D located on the longitudinal centre line of the unscrewed crest at the midspan (see Fig. 2.2) are plotted in Fig. 3.1 against uplift line load for the trapezoidal profile roofing sheet of a 868 mm span. Results from nonlinear analyses using both 0.43 mm and 0.45 mm effective sheeting thicknesses are compared with experimental results. The midspan band pressure adopted in the numerical analysis has been converted into the uplift line load to make it consistent with the experimental results. Linear elastic analysis results using 0.45 mm sheeting thickness are also plotted in Fig. 3.1.

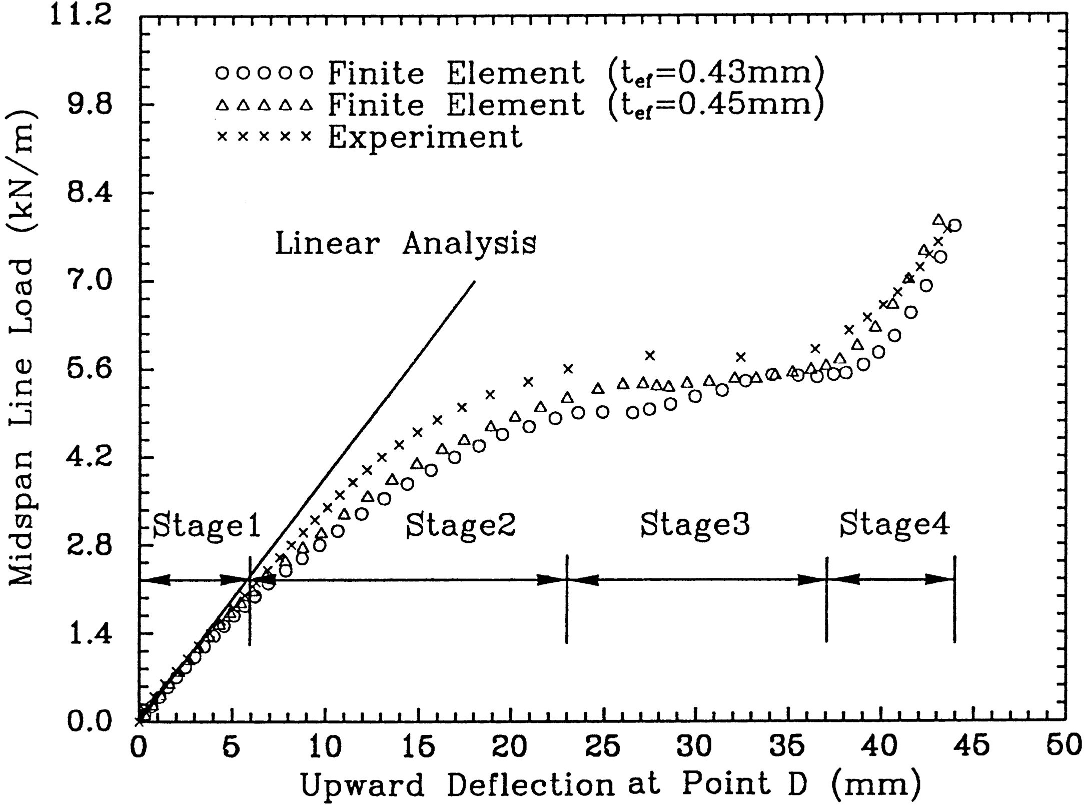

FIG.3.1 LOAD-DEFLECTION CURVES FOR POINT D: TRAPEZOIDAL PROFILE ROOFING SHEET

It is seen that the numerical results from the nonlinear analyses are in close agreement with the experimental results in the full range load-deflection curves of the trapezoidal profile roofing sheet. The load-deflection behaviour may be seen as consisting of four stages (Fig. 3.1). These include the elastic deformation stage when the uplift line load is small, the elastic-plastic transition stage where the sheeting starts to soften quickly due to the spreading of yielding, the local plastic collapse stage where large cross-sectional distortion occurs with little change in its load carrying capacity and the geometrically stiffening stage due to a gross change in the profile of sheeting cross-section. The boundaries between the different stages are, of course, not clearly cut, but such distinctions are useful in describing the behaviour of the trapezoidal profile roofing sheet.

The elastic deformation stage is restricted to an uplift line load of less than 1.68 kN/m. Under such a line load, the overall structural behaviour of the roofing sheet seems to be predominantly linear and elastic, as the load-deflection curve deviates only slightly from that predicted by the linear elastic analysis. It should be noted, however, that the deflections are already many times the sheeting thickness. In a smooth-surfaced plate or shell, such large deflections are bound to cause large geometrical nonlinear effects. However, for the profiled sheeting, the load-deflection curves shown in Fig. 3.1 represent the global rather than local behaviour of the sheeting, so the ratio between deflection and corrugation depth seems more indicative of geometrical nonlinearity. In the elastic deformation stage, finite element results match those from experiments very well.

As the load increased further, a small dimple was observed to appear under each screw fastener head at the central support in both the experiment and the finite element analysis, and the sheeting entered its second stage of deformations. These dimples developed progressively with increasing load, and the sheeting distortions became apparent. The deformations of part of the longitudinal centre line of the screwed crest near the central support predicted by finite element analysis are shown in Fig. 3.2 for different load levels. It is seen that as the load became larger, the deformations near the central support became more and more localised till the local plastic collapse stage was reached at a midspan line load of 5.32 kN/m.

When the line load was increased beyond 5.32 kN/m, the local plastic collapse stage began, in which large cross-sectional distortions occurred without any load increase, and the load-deflection curves exhibited a plateau. The change of the sheeting cross-section at the central support predicted from finite element analysis is shown in Fig. 3.3. It can be seen that the local plastic collapse is associated with large bending deformations of the two inclined side plates. The curves shown in Fig. 3.2 also indicate an abrupt change of the local deformation near the central support in the longitudinal direction. The results in both Figs. 3.2 and 3.3 were obtained using an effective sheeting thickness of 0.45 mm. The initial failure load from the test was 5.6 KN/m whilst the numerical results were 5.32 KN/m and 5.04 KN/m for an effective sheeting thickness of 0.45 mm and 0.43 mm, respectively. It is noted that the different effective sheeting thicknesses only led to a small difference in the predicted initial failure load. The experimental results of the local plastic failure load was slightly larger than the finite element results, probably due to the additional restraint provided by the curved surface loading pads.

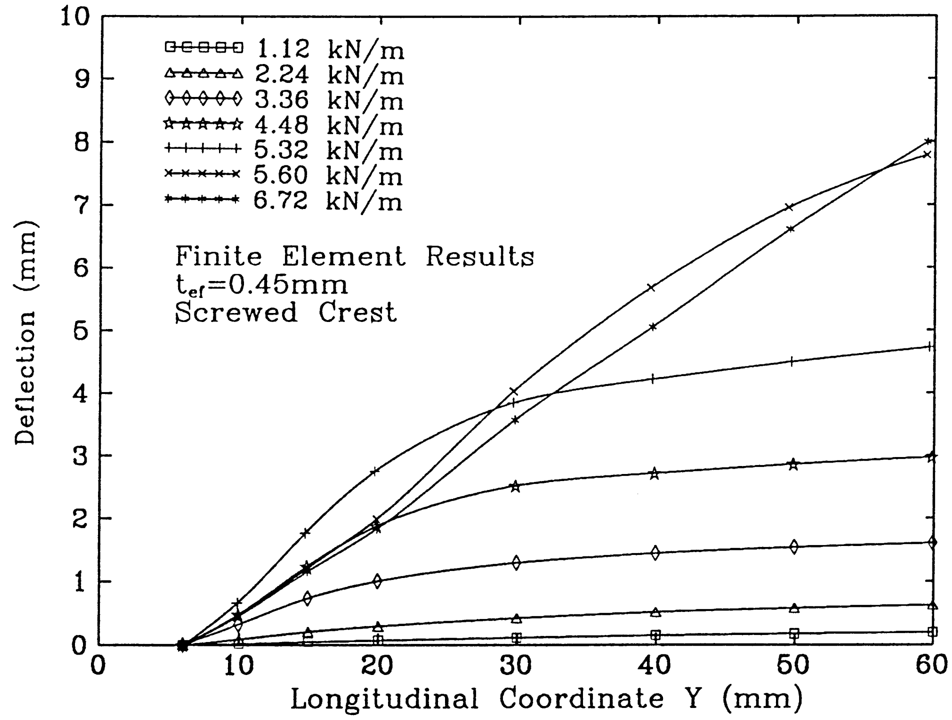

FIG.3.2 DEFLECTED SHAPES OF SCREWED CREST NEAR CENTRAL SUPPORT UNDER INCREASING LOADS: TRAPEZOIDAL PROFILE ROOFING SHEET

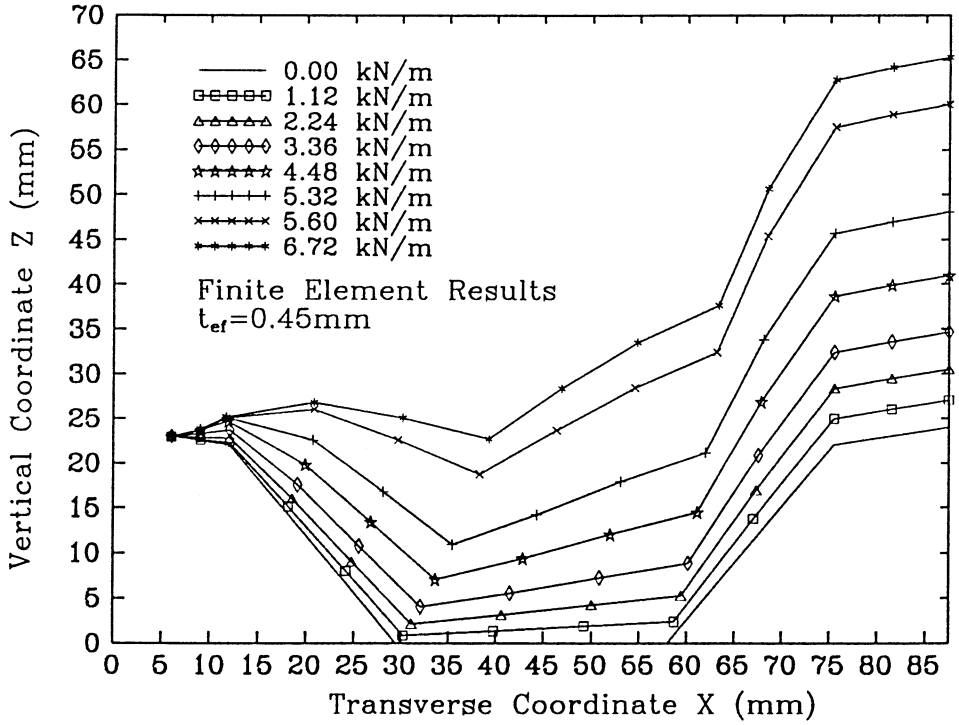

FIG.3.3 DISTORTION IN SHEETING PROFILE AT CENTRAL SUPPORT UNDER INCREASING LOADS: TRAPEZOIDAL PROFILE ROOFING SHEET

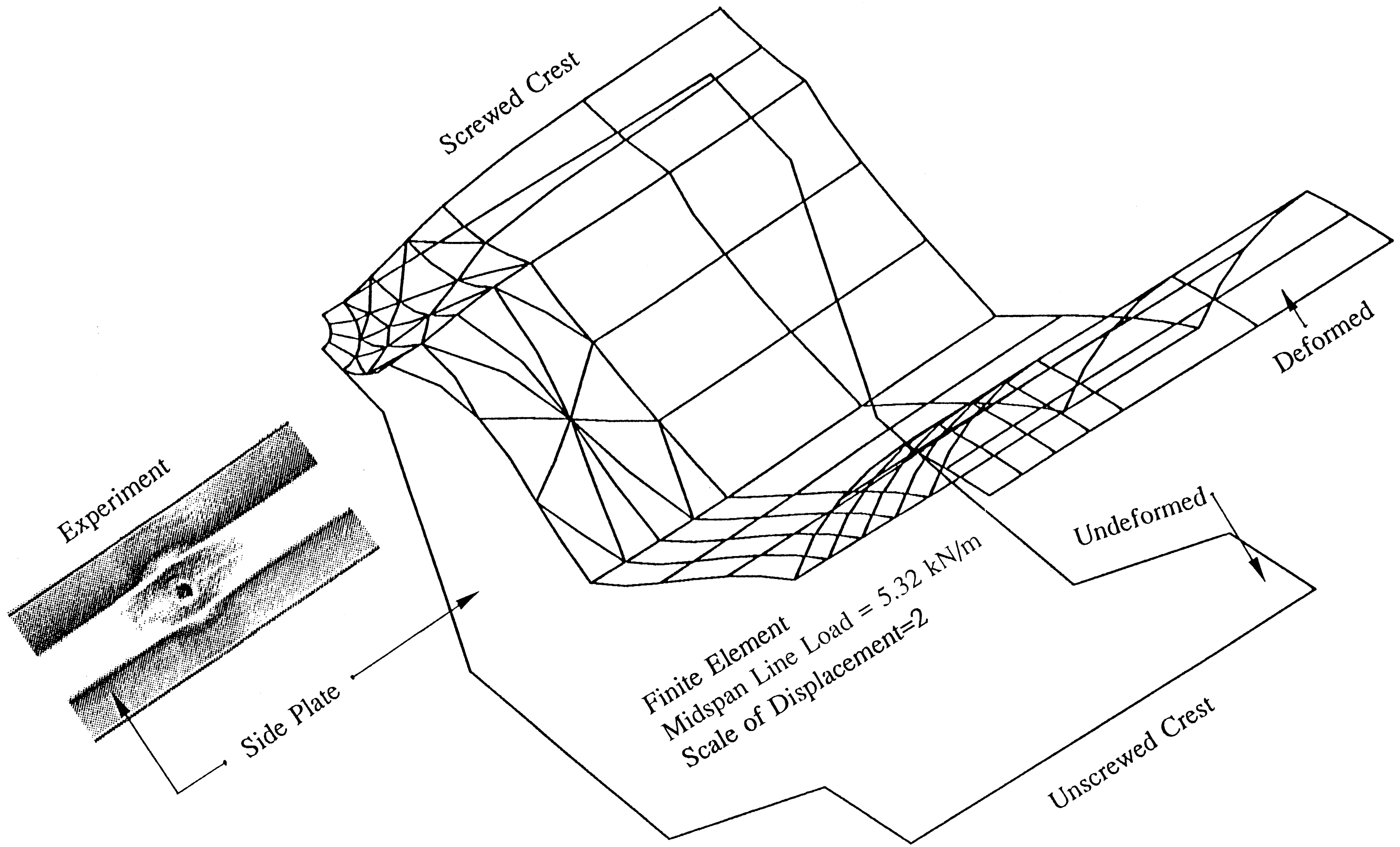

FIG.3.4 LOCAL DEFORMED SHAPE AROUND CENTRAL SUPPORT FASTENER HOLE: TRAPEZOIDAL PROFILE ROOFING SHEET

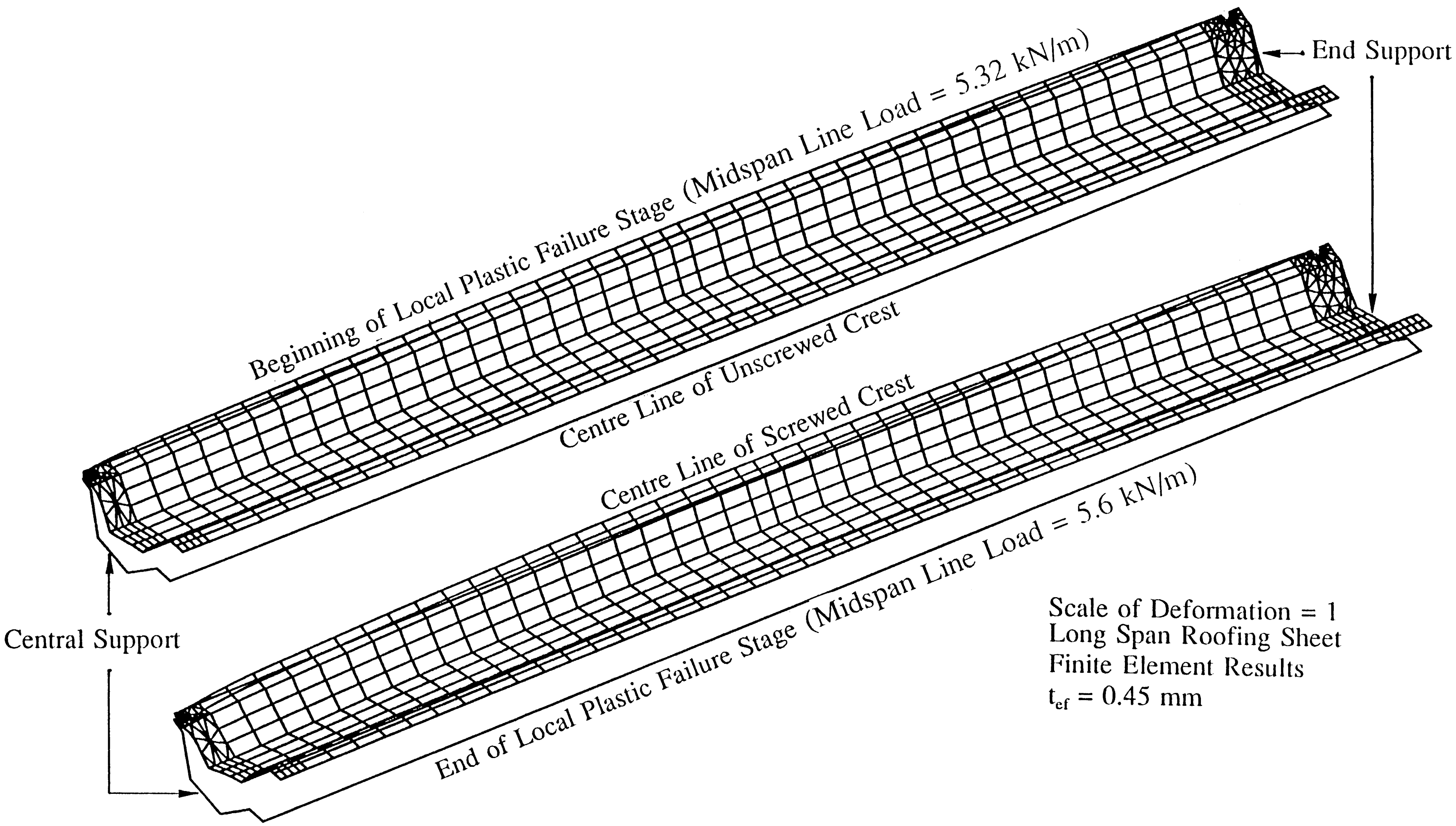

Scale of Deformation = 1
Long Span Roofing Sheet
Finite Element Results
$t_{ef} = 0.45$ mm

FIG. 3.5 GLOBAL DEFORMATIONS AT THE BEGINNING AND END OF LOCAL PLASTIC FAILURE STAGE: TRAPEZOIDAL PROFILE ROOFING SHEET

The local deformed shape around the central support fastener hole at the beginning of the local plastic failure stage is shown in Fig. 3.4 together with a photograph from the experiment showing the permanent deformations after test: they match each other's pattern very closely. It is evident that there is local plastic buckling at the upper part of the two inclined side plates. Once the side plates became locally unstable, large bending deformations of the side plates resulted and the entire sheeting exhibited large cross-sectional distortions, as shown in Fig. 3.5. Correspondingly, a plateau appeared on the load-deflection curves in both the experiment and the finite element analysis (see Fig. 3.1). By the end of the local plastic failure stage, the sheeting shape around the central support became totally different due to deformations (see Figs. 3.2 and 3.3) and a new load carrying mechanism arose.

A close examination of the distorted cross-section at the central support at a line load of 5.6 kN/m shows that the side plates were nearly flattened (Fig. 3.3). With further load increase, the top plate and the side plates around the central fastener tended towards membrane behaviour with the surrounding sheeting sustaining large bending deformations and acting as their restraint. The sheeting therefore displayed geometrically stiffening behaviour characterised by a nearly linear load-deflection response similar to that found in the post-failure behaviour of structures suffering snap-through. In the test, this stiffening behaviour continued until the valleys across the entire width at the midspan crimpled at a line load a little above 7.56 kN/m. The cross-section at the midspan is under a large hogging moment if the test sheet is viewed as a 2 span beam. This hogging moment loaded the valleys at the midspan in large longitudinal compression which led to the final crimpling at the midspan. The crimpling mode was similar to that described by Bushnell (1985) for corrugated semi-sandwich bonded panels under axial compression. This crimpling is partly due to the use of a midspan line load which leads to a much higher hogging moment on the sheeting cross-section at the midspan and may not be expected in the prototype roofing sheets under distributed pressures. The finite element analysis did not predict this crimpling. The reason appears to be that the mesh used at the midspan was too coarse to model the short wave crimpling deformations with a typical wavelength of about 10 mm.

Comparisons between the experimental and numerical load-deflection responses of points A, B and C (see Fig. 2.2) are shown in Fig. 3.6. All three points were located at the longitudinal centre line of the screwed crest. The upward deflections of all points were much smaller than that of point D at the unscrewed crest (see

Fig. 3.1). The experimental load-deflection curves showed a slightly softer structure than those from the finite element analysis. This discrepancy is believed to have been caused mainly by the deformability of rubber washers under screw fastener heads located at the screwed crest, which was not modelled in the finite element analysis. However, the local plastic failure load was not expected to be affected as washer deformations only led to predominantly rigid body displacements of the whole test sheet. If the rigid body displacements of the test sheet were deducted from the measured upward deflections by assuming the washer deformations to be linear and elastic, a closer agreement was found between the experimental and numerical load-deflection curves.

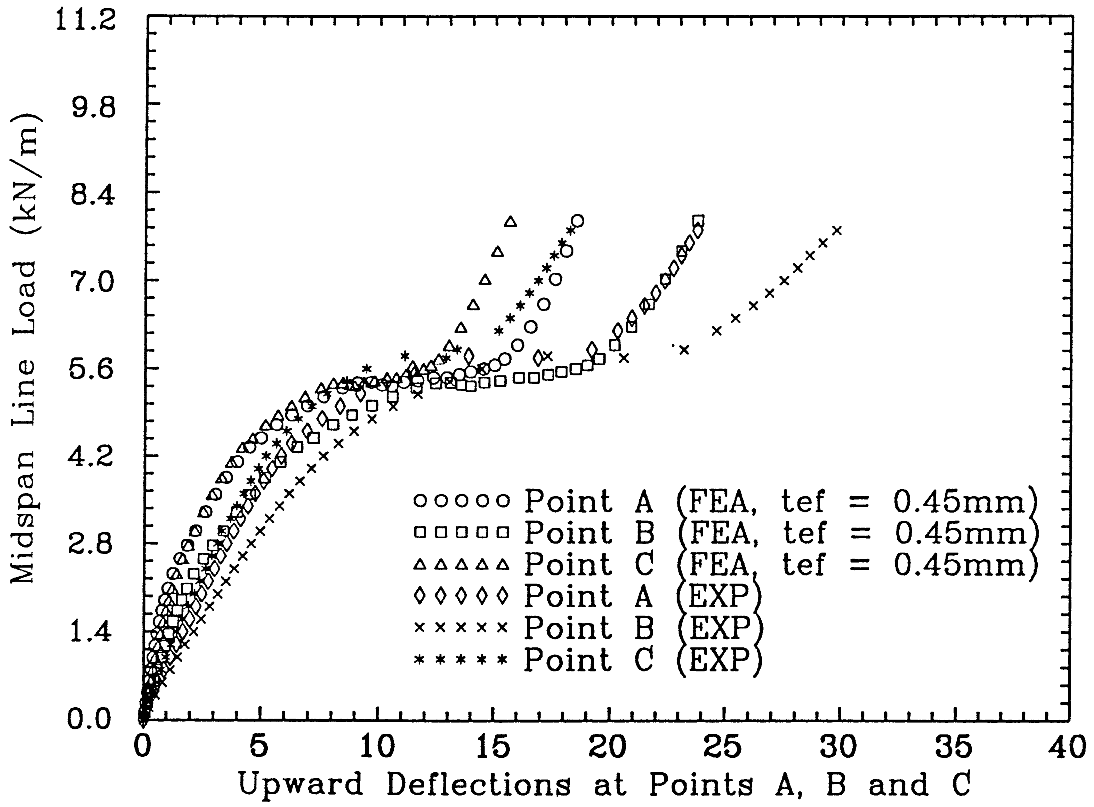

FIG.3.6 LOAD-DEFLECTION CURVES FOR POINTS A, B AND C: TRAPEZOIDAL PROFILE ROOFING SHEET

In order to investigate the effect of the additional restraint provided by the curved surface loading pads on the local plastic failure load, flat loading pads were used in some tests to apply a uniform band pressure to the flat valley plates only. A typical experimental load-deflection relationship at point D is given in Fig. 3.7

and compared with the corresponding finite element results using an effective sheeting thickness of 0.45 mm. It is seen that the numerical and experimental results, including the local plastic failure load, are in closer agreement than those shown in Fig. 3.1. Therefore, the slightly higher value of the experimental local plastic failure load shown in Fig. 3.1 was mainly caused by the additional restraint provided by the curved surface loading pads. In Fig. 3.7, the midspan line load was calculated using the widths of the flat valley plates only.

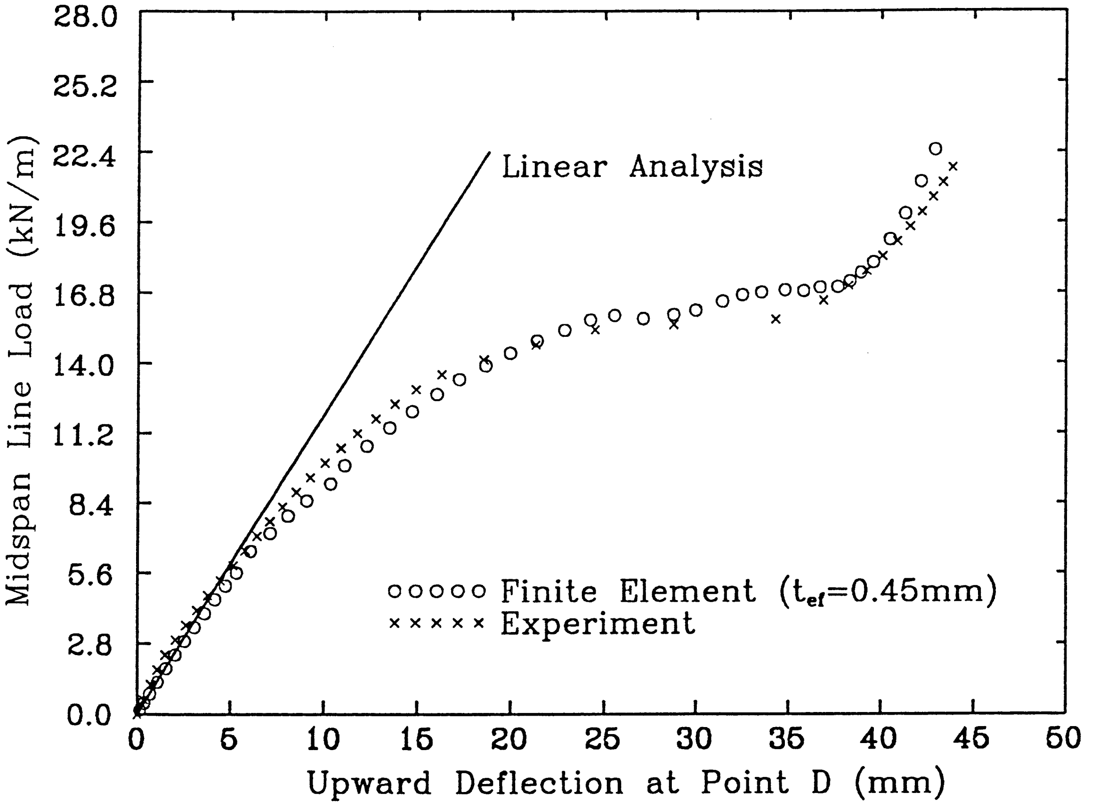

FIG.3.7 LOAD-DEFLECTION CURVES FOR POINT D: TRAPEZOIDAL PROFILE ROOFING SHEET AND FLAT LOADING PADS

3.2 Fastener Reaction Force

Both test and finite element results showed that deep dimples only occurred around screw fasteners at the central support, though some plastic deformations were also seen around the fasteners at the end supports. This is because the fastener reactions were larger at the central support, and these fastener reactions loaded the sheeting into local plastic failure. The local nature of the failure can also be demonstrated by plotting the yield zones (see Fig. 3.8) in the sheeting at the beginning and end of the local plastic failure stage. At the beginning of the local plastic failure stage, the yield zones were concentrated around the fastener holes at the central support and at the end support. The larger reaction at the central support led to more extensive yielding and then local plastic collapse there. At the end of the local plastic failure stage, the yield zones around the central support fastener penetrated much further into the span, indicating large plastic deformations there. On the other hand, the yield zones around the end support fastener stayed almost unchanged, as this region experienced no collapse and the total load was not changed significantly from the start of the local plastic failure stage.

The above discussion demonstrates that the failure of the roofing sheet is dominated by the magnitude of the fastener reaction at the central support. Therefore, most commercial tests of roofing sheets are designed to directly control the fastener reaction force or the so-called average load per fastener. This has led to the wide use of the simple panel pull-over test, especially in the United States (Ellifritt and Burnette, 1990), instead of the two-span roofing assembly test, and the midspan load method instead of applying a uniformly distributed pressure. The following discussions on the fastener reaction force provide an additional insight into both the sheeting behaviour and the midspan load method.

Figure 3.9 shows a relationship between the central fastener reaction force and the deflection of point D obtained from both the experiment and the finite element analysis. Whilst the four stages of deformations can still be identified, the fastener reaction-deflection curves display a snap-through buckling phenomenon which was not revealed in the load-deflection curves. This is because the load-deflection curves represent the overall structural behaviour, while the fastener reaction-deflection curves reflect, to some extent, local structural behaviour. This snap-through buckling behaviour is closely related to local unstable plastic collapses of the two side plates. Finite element results are again in good agreement with experimental results. The finite element peak reaction for local plastic failure for a 0.43 mm effective thickness is closer to the experimental value than that for a 0.45 mm effective thickness. The experimental lower and upper limit values of reaction force per fastener during the plastic failure stage are about 900 N and 1000 N. The corresponding numerical results are about 900 N and 1100 N for a 0.43 mm sheeting thickness and about 880 N and 1000 N for a 0.45 mm sheeting thickness.

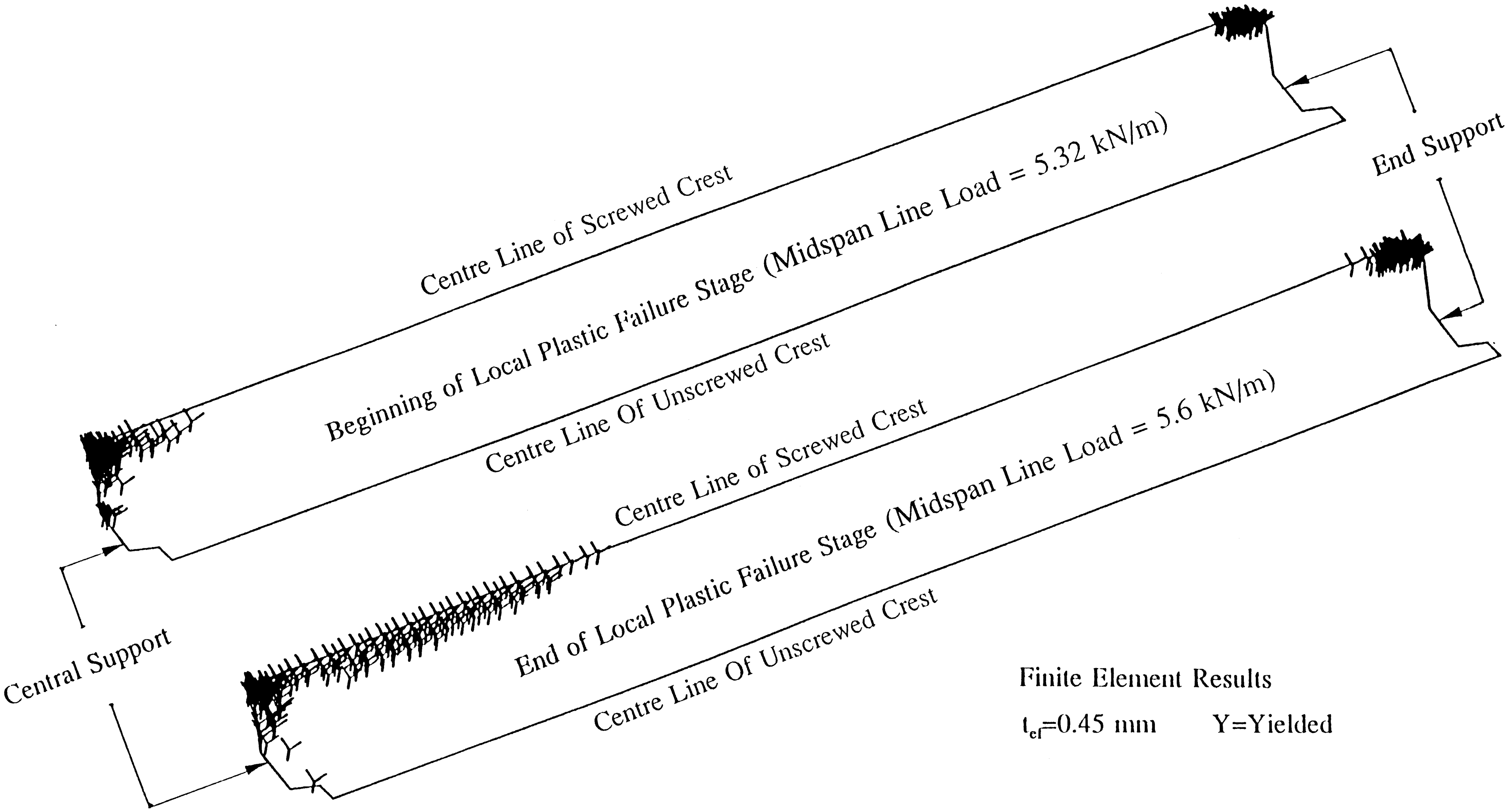

FIG.3.8 YIELD ZONES AT THE BEGINNING AND END OF LOCAL PLASTIC FAILURE STAGE:TRAPEZOIDAL PROFILE ROOFING SHEET

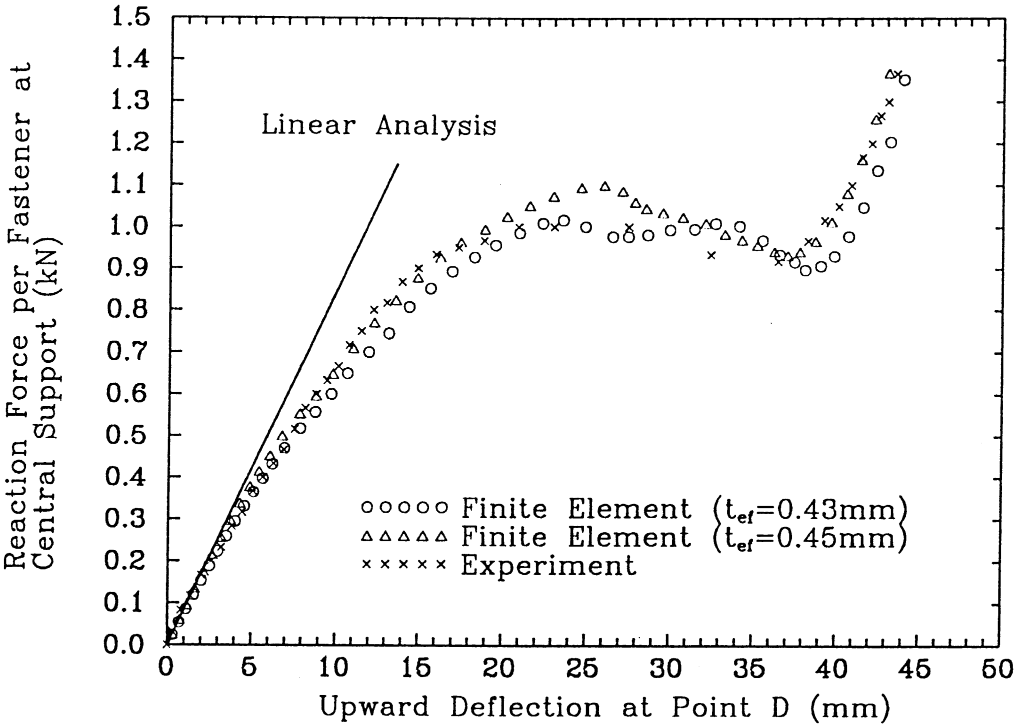

FIG.3.9 FASTENER REACTION-DEFLECTION CURVES FOR POINT D: TRAPEZOIDAL PROFILE ROOFING SHEET

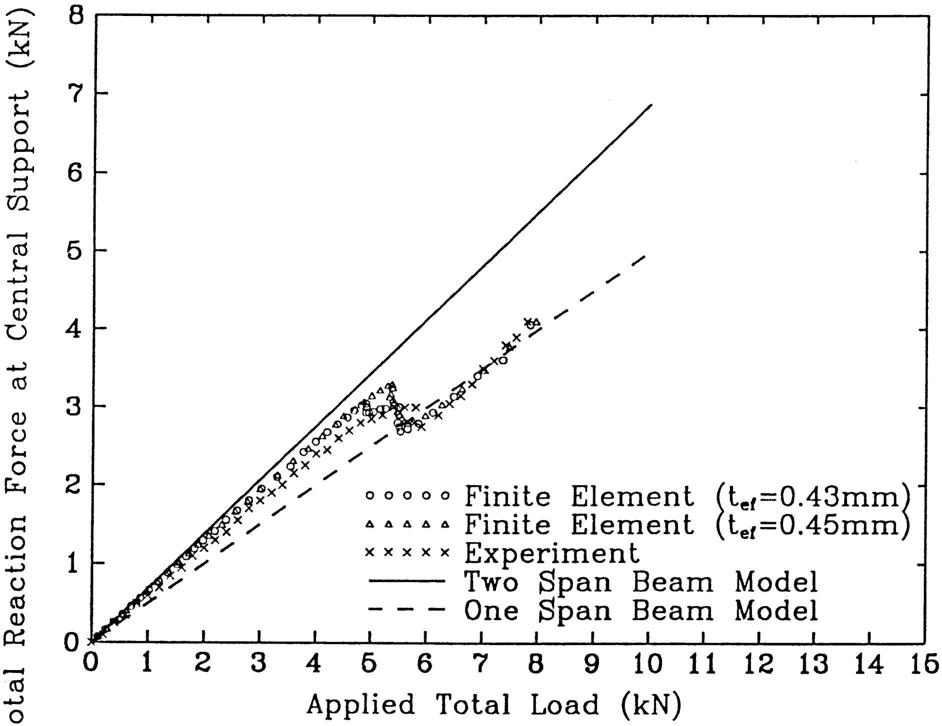

FIG.3.10 LOAD-FASTENER REACTION RELATIONSHIP: TRAPEZOIDAL PROFILE ROOFING SHEET

The relationship between the total uplift load and the total fastener reaction at the central support is shown in Fig. 3.10. The agreement between experimental and finite element results is close. The load-fastener reaction relation calculated for a two-span continuous beam with simple end supports under midspan loads was close to both finite element and experimental results well before local plastic failure, especially at loads below half of the local plastic failure load. When the roof sheeting entered the local plastic failure stage the reaction force suddenly dropped down. After local plastic failure, the load-fastener reaction relations matches closely that of a simply supported one-span beam under a midspan load, indicating that, in the post-local failure deformations, the sheeting cross-section at central support sustained only a small global bending moment. It is clear that the linear relationship between the uplift load and the fastener force approximately remains only before sheeting local plastic failure. Therefore, the midspan load method based on a linear elastic beam theory is valid only prior to local plastic failure.

3.3 Stress Distributions

The trapezoidal profile roofing sheet under wind uplift exhibits two types of deformations: those related to the sheeting global bending (global behaviour) and those due to the fastener reactions (local behaviour). The global bending behaviour dominates in the sheet away from fastener supports, but interacts strongly with local effects from the fastener reactions in the regions near the fastener holes.

From the stress contours of the long span roofing sheet of a 0.45 mm effective thickness under a midspan line load of 5.32 kN/m it was found that large transverse bending stresses existed in the sheet to match the severe cross-sectional distortions. The transverse bending stresses along the longitudinal centre line of the unscrewed crest were smaller than those along the longitudinal centre line of the screwed crest which suffered more severe transverse bending (Fig. 3.3). Transverse membrane stresses were much smaller, compared with the transverse bending stresses. Longitudinal membrane stresses in the sheet matched those expected from global bending deformations as a two-span beam. That is, at the midspan the longitudinal membrane stresses were compressive at the sheeting valley and tensile at the crest, and the situation was reversed for the central support. Both longitudinal membrane stresses and bending stresses were large. The finite element results also indicate that the shear stress component was rather small throughout the whole roofing sheet compared with the membrane and bending stresses in both longitudinal and transverse directions. The aforementioned stress distribution was only for areas away from the fastener holes.

Stresses in the vicinity of the fastener hole at the central support, however, became very high and their distribution was very complicated. Figure 3.11 shows the longitudinal membrane stress distribution in the middle layer through the sheeting thickness, obtained from finite element analysis near the central support under a midspan line load of 5.32 kN/m. Three critical areas could be identified around the fastener hole. Near the junction between the top plate and the side plate (Region 1, see Fig. 3.11), there were large longitudinal compressive membrane stresses. In Region 2 (see Fig. 3.11), large longitudinal tensile membrane stresses existed. Along the crest (Region 3), large compressive membrane stresses were also found. The transverse membrane stresses were relatively small in regions 1 and 3 and medium in region 2 (see Fig. 3.12), and were tensile in regions 1 and 2 but compressive in region 3. This local stress distribution was consistent with the local deformations obtained in the finite element analysis and observed in the tests. In particular, it was the high longitudinal compressive membrane stresses in region 1 that caused local plastic buckling of the side plates as shown in Fig. 3.4. The high tensile longitudinal membrane stresses in region 2 may be an indication that material cracks could occur most easily here. The fact that local plastic failure around the fastener hole is triggered by side plate buckling under longitudinal compressive membrane stresses casts some doubt on the suitability of using a simple panel pull-over test to determine the local failure strength of sheeting.

3.4 Load-Stress Relations at Critical Areas

Three points representative of the three regions mentioned above were chosen to investigate the variations of the four main stress resultants (membrane stress resultants and bending moments in both longitudinal and transverse directions) with midspan line load (see Figs. 3.13a-d). These stress resultants were obtained by performing a through-thickness integration. The x, y and z coordinates of the three Gauss points in millimetres are (12.97, 0.833, 20.78) for point 1, (7.936, 0.389, 22.68) for point 2 and (0.438, 8.864, 23.93) for point 3 in the global Cartesian coordinates (see Fig. 2.2). A few important observations are made as follows:

(a) When line load was small (first stage of deformations), all three points experienced compressive membrane stresses in the longitudinal direction (Fig. 3.13b), with the largest value at point 3. This is expected from the global bending of the roofing sheet as a two-span beam. Compared with other two points, point

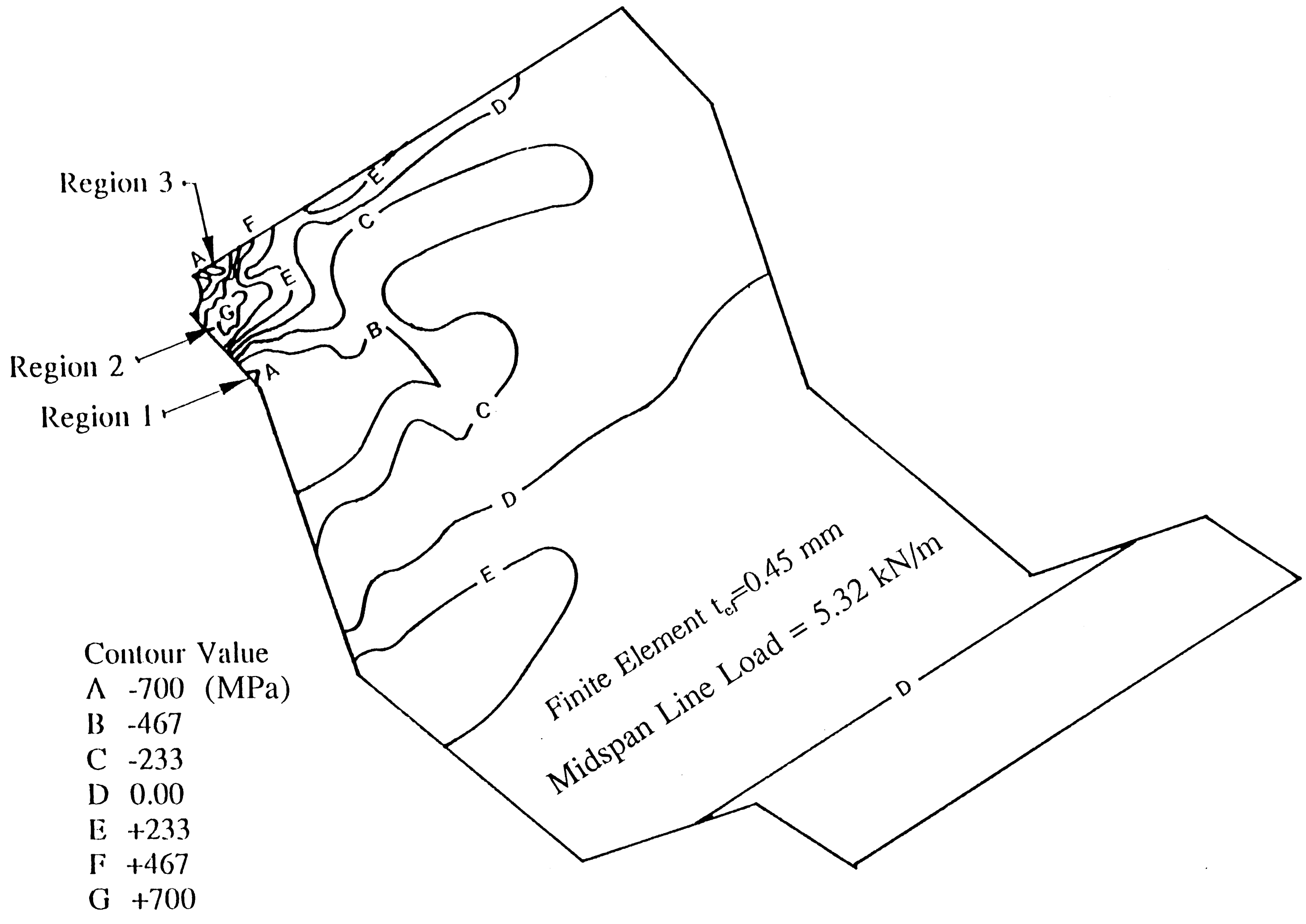

FIG.3.11 CONTOURS OF LONGITUDINAL MEMBRANE STRESSES AT THE BEGINNING OF LOCAL PLASTIC FAILURE STAGE: TRAPEZOIDAL PROFILE ROOFING SHEET

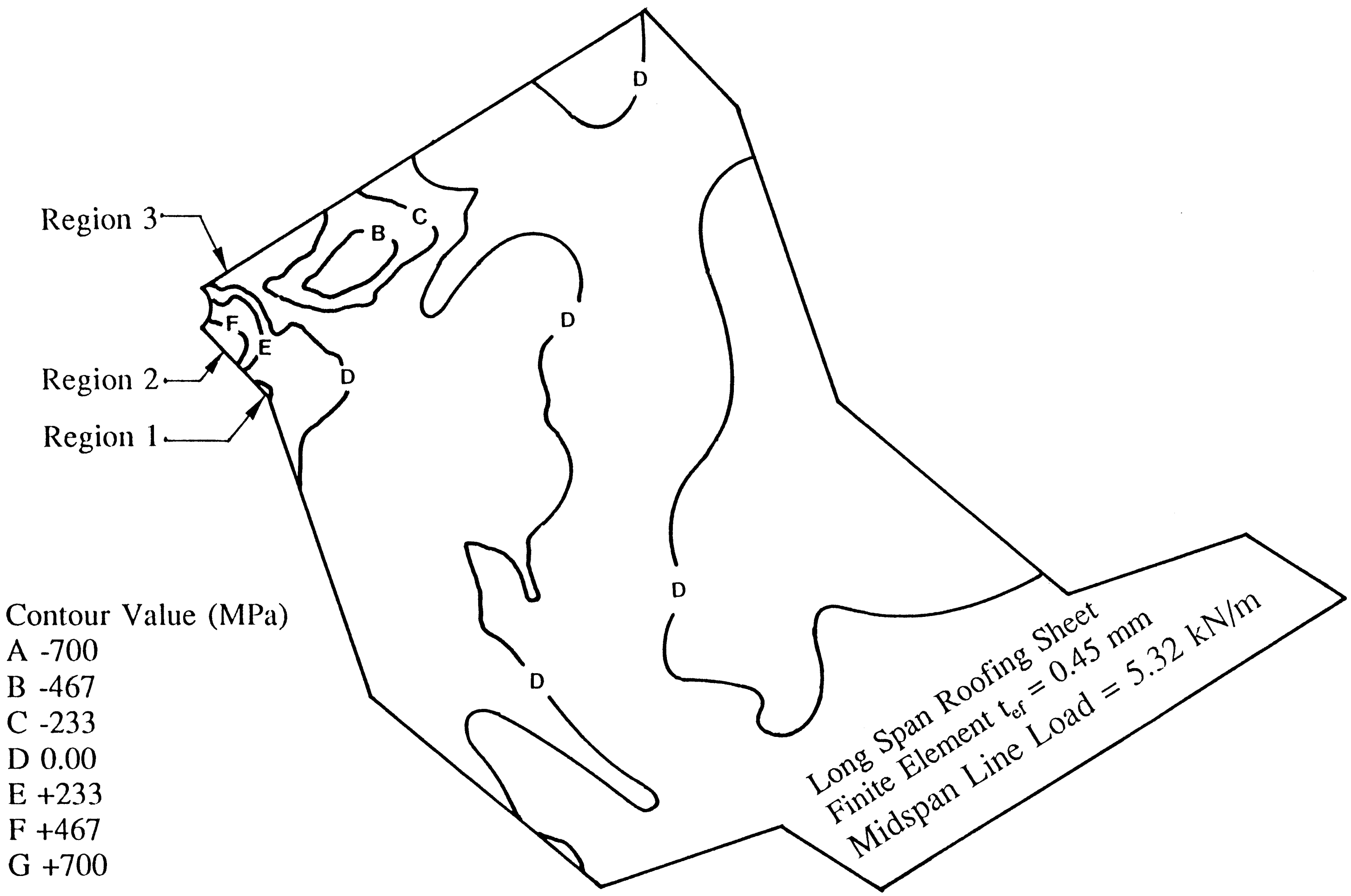

FIG. 3.12 CONTOURS OF TRANSVERSE MEMBRANE STRESSES AT THE BEGINNING OF LOCAL PLASTIC FAILURE STAGE: TRAPEZOIDAL PROFILE ROOFING SHEET

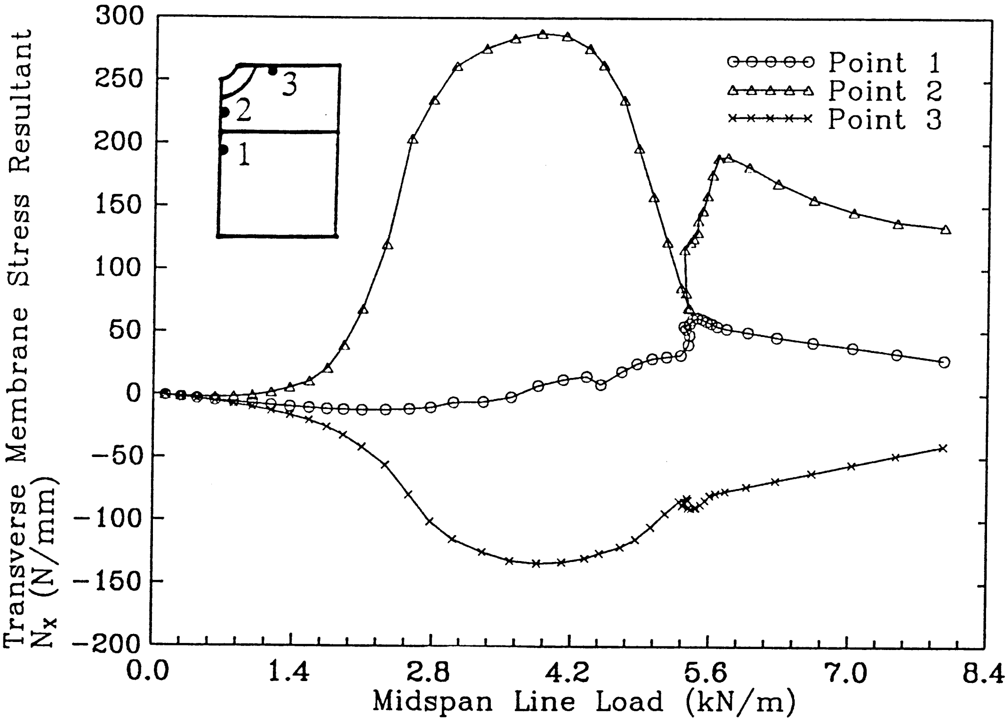

(a) Transverse Membrane Stress Resultant

FIG.3.13 VARIATION OF STRESS RESULTANTS WITH LOAD: TRAPEZOIDAL PROFILE ROOFING SHEET

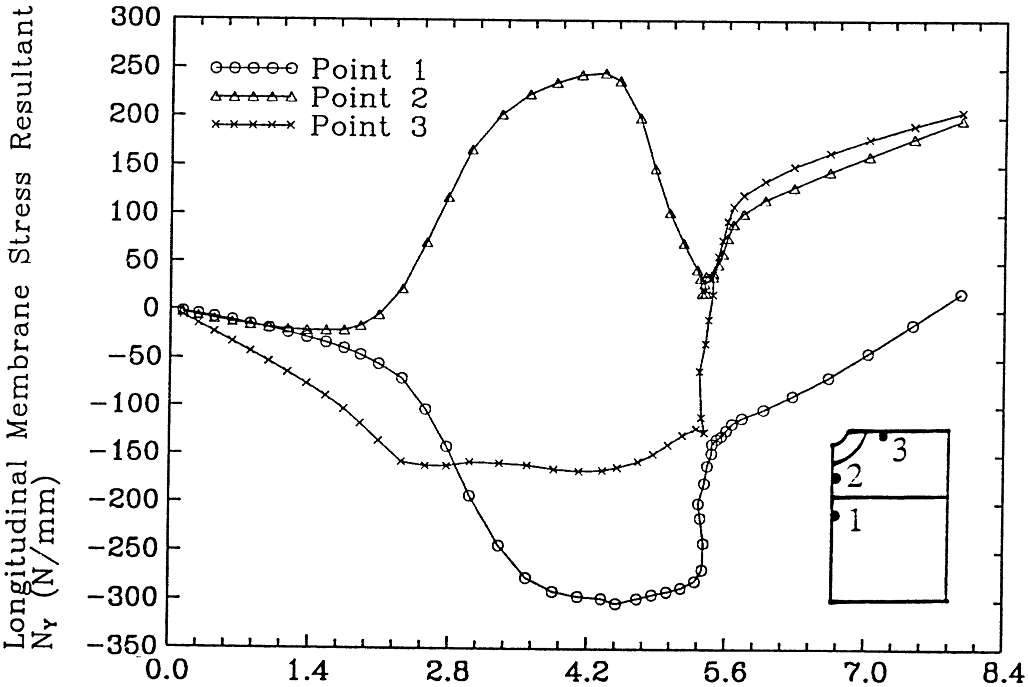

(b) Longitudinal Membrane Stress Resultant

FIG.3.13 VARIATION OF STRESS RESULTANTS WITH LOAD: TRAPEZOIDAL PROFILE ROOFING SHEET

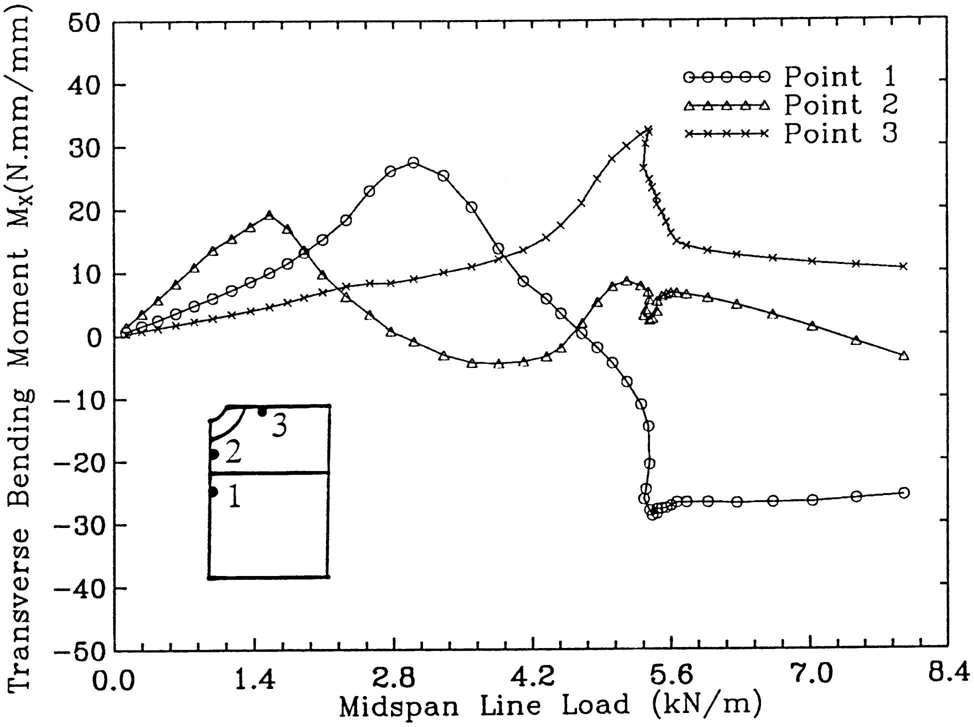

(c) Transverse Bending Moment

FIG.3.13 VARIATION OF STRESS RESULTANTS WITH LOAD: TRAPEZOIDAL PROFILE ROOFING SHEET

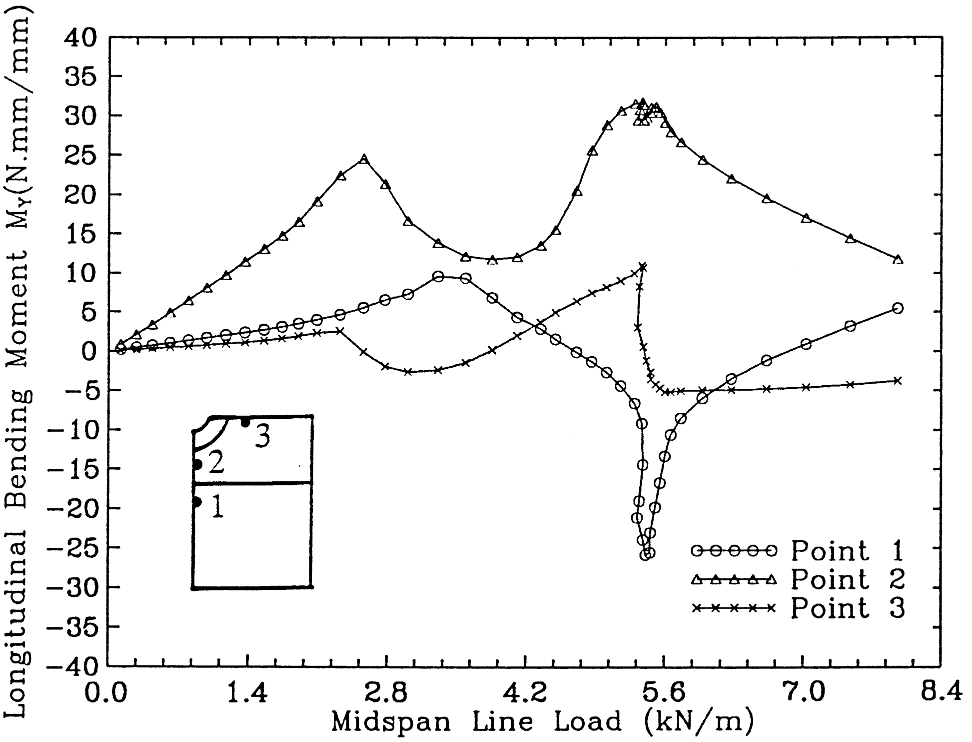

(d) Longitudinal Bending Moment

FIG.3.13 VARIATION OF STRESS RESULTNATS WITH LOAD: TRAPEZOIDAL PROFILE ROOFING SHEET

2 in region 2 had relatively large longitudinal and transverse bending moments (Figs. 3.13c-d).

(b) When the line load was increased to 1.68 kN/m, a peak appeared in the transverse bending moment curve of point 2 (see Fig. 3.13c), which corresponded to the inversion of the slope at the crest in transverse direction. After that, the transverse bending moment at point 2 decreased, but the longitudinal bending moment still increased (Fig. 3.13d) and tensile membrane stress resultants appeared in both directions. The bi-directional tensile membrane stress resultants at point 2 increased rapidly and peaked at a line load of 3.92 kN/m (Fig. 3.13a-b). From a fatigue damage point of view, the area around point 2 is a critical location where fatigue cracks easily originate due to the high bi-directional tensile membrane stress resultants and longitudinal bending moment.

(c) The increase in tensile membrane stress resultants at point 2 was accompanied by rapidly increasing compressive longitudinal membrane stress resultants at point 1 (Fig.3b), during which the transverse bending moment at point 1 reversed direction indicating that large transverse bending deformations were taking place. The compressive longitudinal membrane stress resultants at point 1 peaked at a load of about 4.2 kN/m and remained until the load reached about 5.32 kN/m when these large compressive membrane stress resultants in region 1 induced the buckling of the side plate (Fig. 3.4). The buckling of the side plate initiated the local plastic collapse stage.

(d) The failure stage saw a rapid increase in both longitudinal and transverse bending moments at point 1 which was accompanied by a large decrease in the longitudinal membrane stress resultant at point 1. The failure stage also saw a reversal in sign of the longitudinal membrane stress resultant at point 3 as the crest now played the role of valley in the distorted cross-section (Fig. 3.3). Point 3 experienced large bending moments in both directions before failure, but they were reduced substantially when failure occurred. Other stress resultants plotted also show extensive redistribution associated with the large deformations during the local plastic failure stage, despite that the applied load varied only slightly.

(e) The post-failure stage experienced a steady increase in the longitudinal tensile membrane stress resultants at points 2 and 3, and a reduction in the compressive membrane stress resultants and bending moments at all three points. That is, the sheeting around the screw fastener at the central support tended more and more to a membrane state of tension, which resulted in the geometrically stiffening post-failure behaviour.

The abovementioned observations indicate that if trapezoidal profile roofing sheets undergo cyclic loads, the sheets would exhibit different fatigue performances and cracking types at different load levels due to different stress states. However, the cyclone induced sheeting fatigue has random characteristics, making it difficulty to apply the obtained load-stress relations to the fatigue life prediction.

4 ANALYSIS OF ROOFING SHEETS OF RIBBED PROFILE

4.1 Sheeting Deflections and Local Cracking

Presented in Fig. 4.1 is the upward deflections of the ribbed profile roofing sheet at point B (see Fig. 2.3), which is located at the longitudinal centre line of rib at the midspan. Fig. 4.1a depicts the results of the short span roofing sheet whilst Fig. 4.1b shows the results of the long span roofing sheet. The finite element analyses include linear elastic analysis, material nonlinear analysis and elastic-plastic large deflection analysis. The reason for performing the analysis of material nonlinearity only is to estimate the effect of sheeting geometric nonlinearity on the structural response. Both 0.43 mm and 0.45 mm effective sheeting thicknesses were used in the finite element analyses, but for the linear elastic and material nonlinear analyses, only the results using 0.45 mm effective thickness were plotted.

It is seen that under low midspan line load, the deflection behaviour of the ribbed profile roofing sheets seems to be predominantly linear and elastic, as the load-deflection curves from both the experiment and the nonlinear analyses deviated only slightly from those predicted by the linear elastic analyses. The line load with respect to the linear elastic limiting range is about 1.4 kN/m in the long span roofing sheet case and about 1.96 kN/m in the short span roofing sheet case. The long span roofing sheet exhibited a softer stiffness than the short span roofing sheet. The use of 0.43 mm or 0.45 mm effective thickness did not cause any significant difference, and the numerical results were in good agreement with the experimental results with regard to the sheeting load-deflection behaviour.

As the line load increased, small dimples were observed to appear and grow up

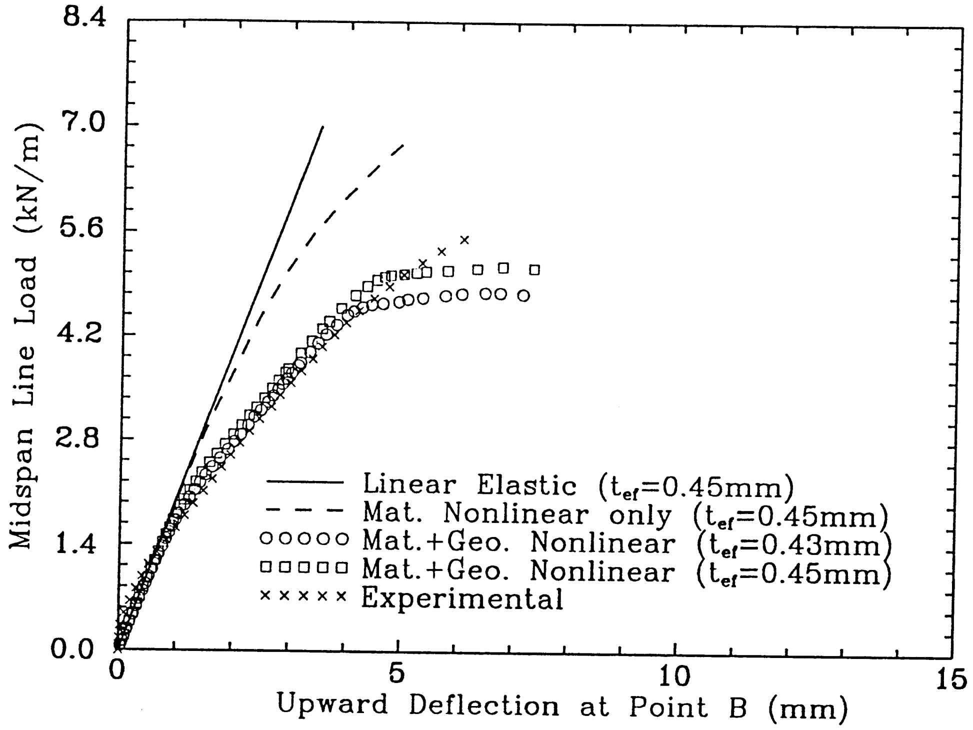

(a) Short Span Roofing Sheet

FIG.4.1 LOAD-DEFLECTION CURVES FOR POINT B: RIBBED PROFILE ROOFING SHEET

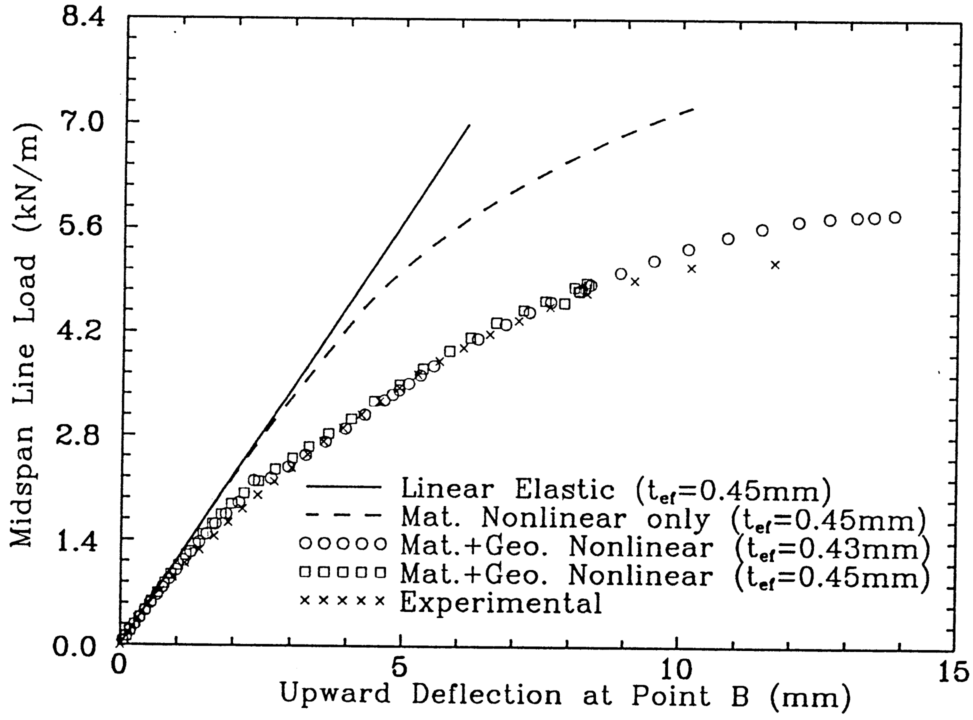

(b) Long Span Roofing Sheet

FIG.4.1 LOAD-DEFLECTION CURVES FOR POINT B: RIBBED PROFILE ROOFING SHEET under the central screw fastener heads in both experiment and elastic-plastic large deflection analysis, which is similar to the trapezoidal roof sheeting case. The geometrical nonlinearity effect on the load-deflection behaviour of the ribbed profile roofing sheets was apparent since the load-deflection curves obtained from both the experiment and the elastic-plastic large deflection analysis substantially departed from those predicted by the material nonlinear analysis. It is clear that nonlinear analysis only involving material nonlinearity could not provide a correct prediction when the line load was above 1.4 kN/m (long span case) and 1.96 kN/m (short span case). The elastic-plastic large deflection analysis is therefore required to achieve a close agreement with experimental results. It is also seen that the finite element results using a 0.43 mm effective sheeting thickness are nearly the same as those using a 0.45 mm effective sheeting thickness when the line load was below 4.2 kN/m.

The geometric nonlinearity effect mentioned above was mainly attributed to large sheeting cross-sectional distortions. Fig. 4.2a shows cross-sectional distortions along the central support of the short span roofing sheet of a 0.45 mm effective sheeting thickness whilst Fig. 4.2b shows those of the long span sheeting of a 0.43 mm effective thickness, predicted by the elastic-plastic large deflection analyses. It can be seen that when the midspan line load was above 1.68 kN/m, the sheeting pan had significant upward deflections. A dimple of reversed curvature formed gradually on the top plate of the rib, and the effective height of the rib reduced gradually due to the deformations of the inclined side plate. In the longitudinal direction, local upward deflections around the central screw fastener at the centre line of rib also exhibited a growing dimple under increasing loads (see Figs. 4.3a-b). Compared with the trapezoidal profile roofing sheet (see Fig. 3.2), the local upward deflection curvature in the longitudinal direction of the ribbed roofing sheet did not experience an inversion when the sheeting approached the local failure.

For the short span roofing sheet, it was observed from the test that when midspan line load was increased to 5.6 kN/m, local plastic collapse occurred around the central screw fastener at the junction between the top plate and the upper part of the inclined distorted side plate. Immediately after the local collapse, the sheeting split under the central screw fastener head in the x-direction, and then the load suddenly dropped. Because the finite element analysis performed here did not concern material fracture, the load-deflection curves it predicted exhibited an abrupt plateau instead (see Fig. 4.1a). However, the line load corresponding to the plateau

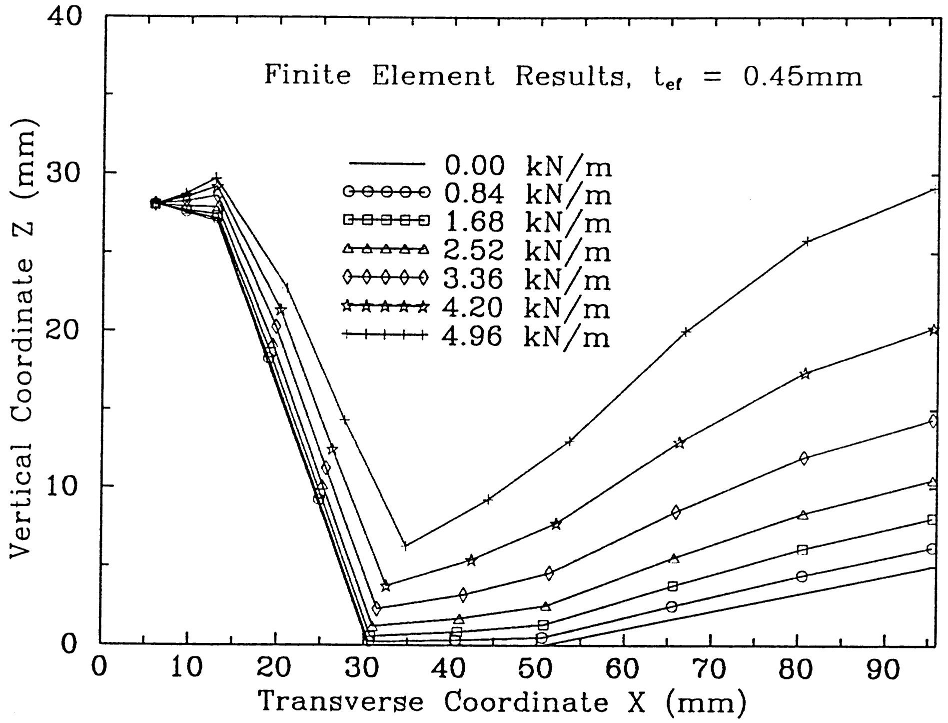

(a) Short Span Roofing Sheet

FIG.4.2 DISTORTION IN SHEETING PROFILE AT CENTRAL SUPPORT UNDER INCREASING LOADS: RIBBED PROFILE ROOFING SHEET

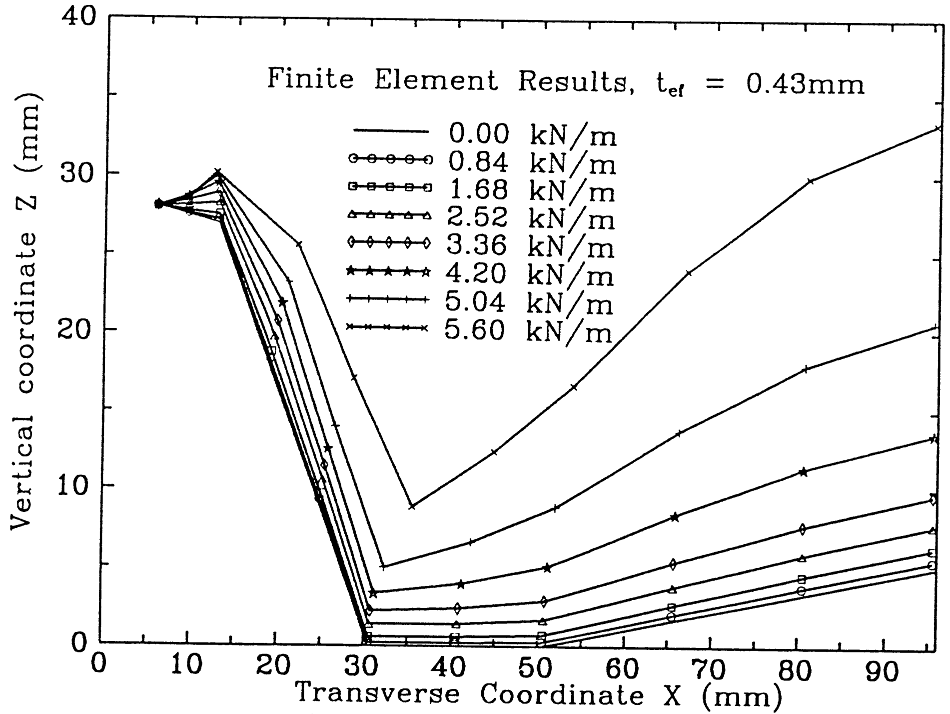

(b) Long Span Roofing Sheet

FIG.4.2 DISTORTION IN SHEETING PROFILE AT CENTRAL SUPPORT UNDER INCREASING LOADS: RIBBED PROFILE ROOFING SHEET

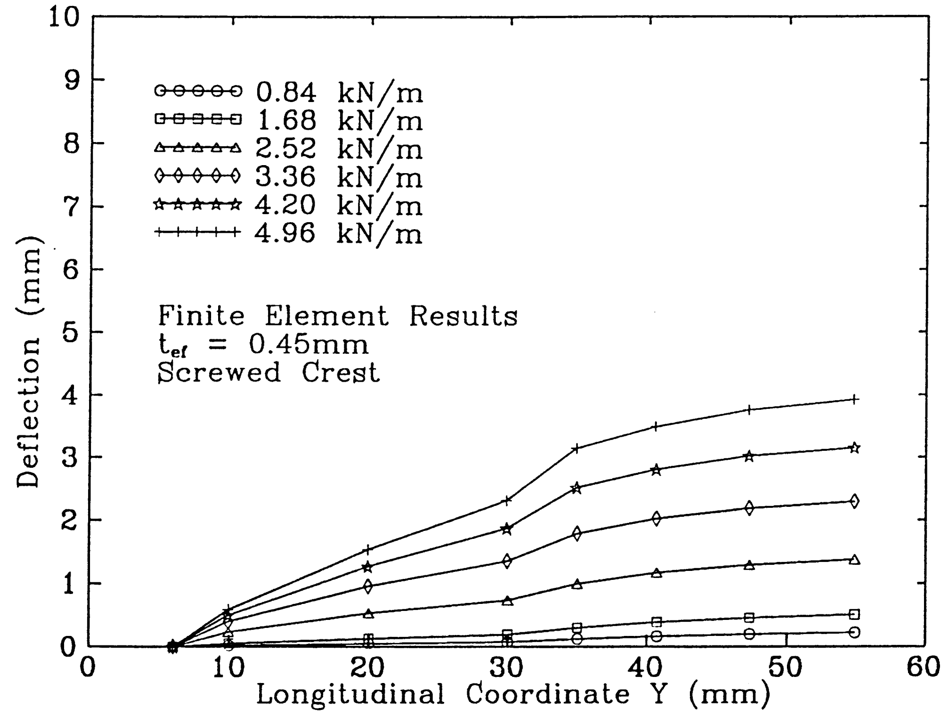

(a) Short Span Roofing Sheet

FIG.4.3 DEFLECTED SHAPES OF SCREWED CREST NEAR CENTRAL SUPPORT UNDER INCREASING LOADS: RIBBED PROFILE ROOFING SHEET

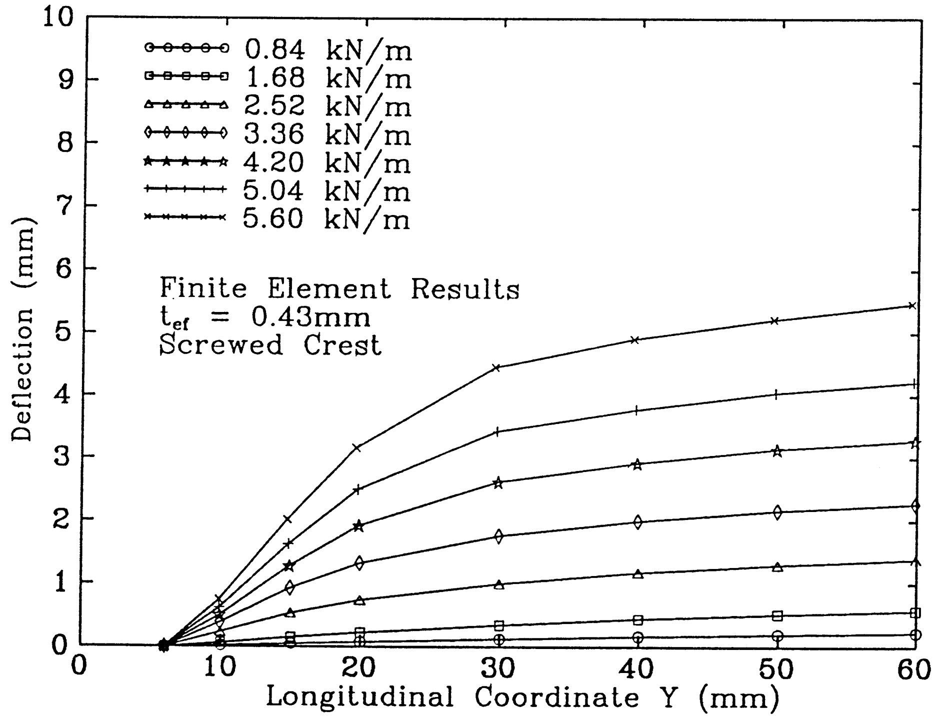

(b) Long Span Roofing Sheet

FIG.4.3 DEFLECTED SHAPES OF SCREWED CREST NEAR CENTRAL SUPPORT UNDER INCREASING LOADS: RIBBED PROFILE ROOFING SHEET indeed represents the sheeting failure load with respect to the local plastic collapse. The predicted failure load is about 5.04 kN/m in the case using a 0.45 mm effective sheeting thickness and about 4.76 kN/m in the case using a 0.43 mm effective thickness. The thinner sheeting thicknesses lead to a slightly smaller failure load than the thicker sheeting thickness as found in the trapezoidal profile roofing sheet case. The experimental failure load, however, is more than 10% larger than the finite element results. This difference is attributed to many factors, major one of which is the additional restraint provided by the curved-surface loading pads.

The local deformations of the sheeting around the central support under the failure load is shown in Fig. 4.4 together with a photograph from the experiment showing the permanent deformations around the fastener hole after test. The predicted patterns of both the local plastic dimple at the top plate and the local collapse at the upper part of the inclined side plate match the experimental results closely.

For a given midspan line load, the midspan cross-section of the long span roofing sheet was under a larger hogging moment, compared with the short span roofing sheet. This hogging moment loaded the sheeting pan at the midspan in larger longitudinal compression, especially near the junction between the pan and the side plate when line load approached the failure load. Correspondingly, it was observed in the test of the long span ribbed profile sheeting that when the line load was increased to about 5.04 kN/m, the large compressive stresses caused an overall buckling at the midspan cross the entire section, which started from the junction between the pan and the side plate. It is apparent that the sheeting under the midspan line load would be more easily exposed to this midspan buckling than the sheeting under the pressure uniformly distributed over the entire sheeting in the prototype. This is one of the disadvantages inherent in the midspan load method.

For finite element analysis of the long span roofing sheet, coarse mesh used around the midspan appears to filter the midspan buckling of a very small wavelength. As a result, finite element results show that final failure of the long span roofing sheet is also due to the local plastic collapse around the central screw fastener at the junction between the top plate and the side plate. The failure load was about 5.74 kN/m for a 0.43 mm sheeting effective thickness. This predicted failure load was higher than that of the short span sheeting of the same effective thickness, but corresponded to much larger upward deflections (see Fig. 4.1). It is

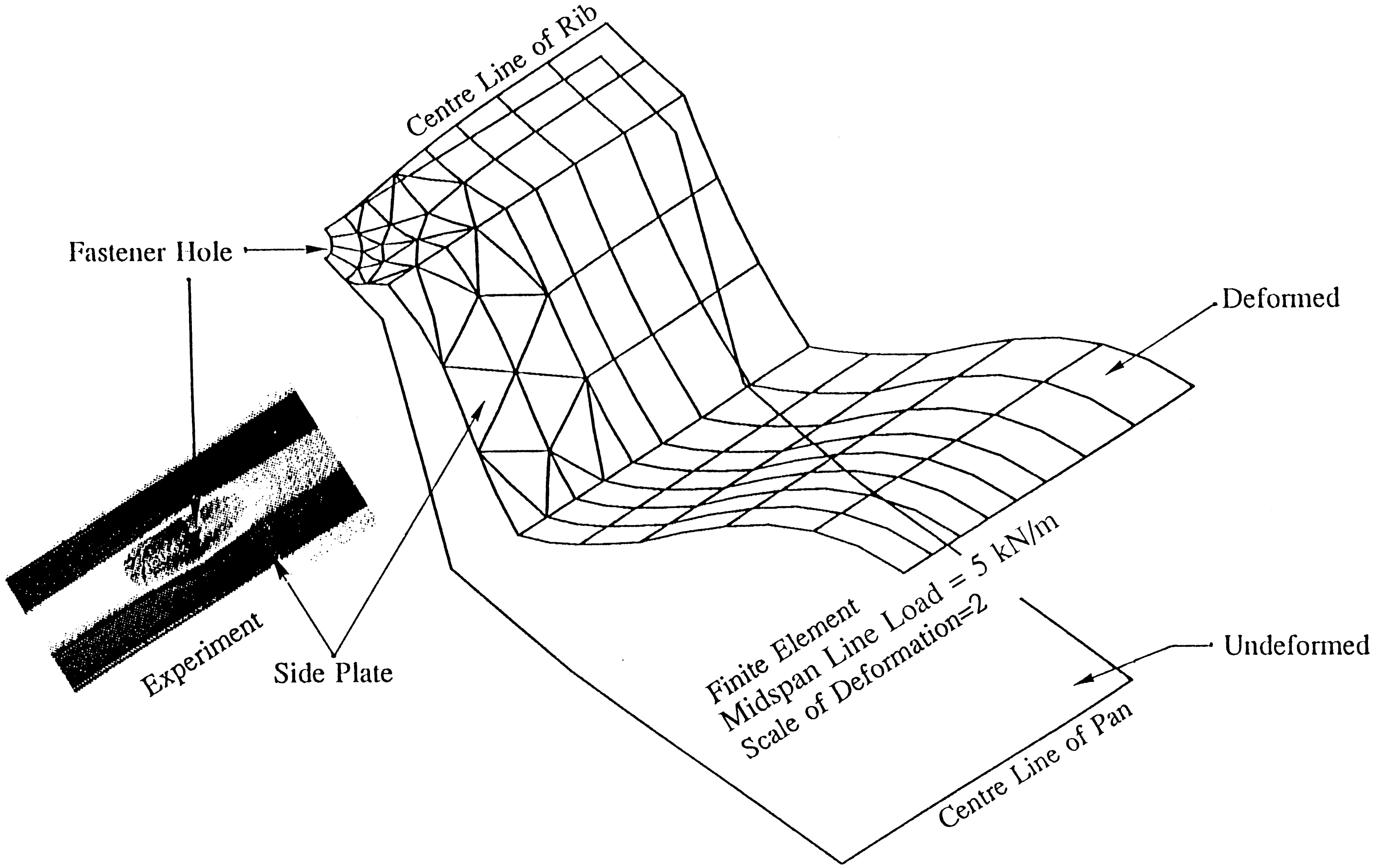

FIG.4.4 LOCAL DEFORMED SHAPE AROUND CENTRAL SUPPORT FASTENER HOLE: RIBBED PROFILE ROOFING SHEET

believed that different geometric deformations between the short and long span sheets caused this contrary to common beliefs that the long span sheeting should have a lower failure load than the short span sheeting. However, it should be kept in mind that the introduction of some cracking models in the finite element analysis may lead to a different conclusion.

For the long span sheeting of a 0.45 mm effective sheeting thickness, the finite element LUSAS system somewhat stopped running at a line load of 4.9 kN/m (see Fig. 4.1b). Different iteration and increment techniques, and different control parameters available in the LUSAS system, such as arc-length, were then tried to overcome the problem, but did not work. Nevertheless, from the theoretical viewpoint of the finite element technique used here, the line load of 4.9 kN/m can be regarded as an approximate value of the real failure load. The exact value of failure load may be expected with the improvement of the numerical technique in the coming new LUSAS version.

The global deformations and yield zones of both the short and long span roofing sheets under the failure load are shown in Figs. 4.5 and 4.6 respectively. The local plastic dimple and local collapse around the central screw fastener are clearly demonstrated. The larger reaction forces at the central screw fasteners led to more extensive yielding around the fastener. For the short span sheeting, the cross-sectional distortions were more uniform along the span than the long span sheeting. The larger upward deflections around the midspan in the long span case indicate a possibility of midspan buckling. The yield zones appearing around the junction between the pan and the inclined side plate at the midspan were caused by large longitudinal compressive stresses arising from the large hogging moment.

4.2 Fastener Reaction Force

The relationship between the fastener reaction force at the central support and the upward deflection of point A is shown in Figs. 4.7a-b for the short and long span ribbed roofing sheets respectively. The characteristics of the fastener force-deflection curves were similar to those of the load-deflection curves (Figs. 4.1a-b). When the reaction force per fastener was below 500 N (short span case) or 400 N (long span case), linear elastic analysis can provide a satisfying prediction. When reaction force per fastener exceeded the abovementioned values, elastic-plastic large deflection analysis should be used to give a close agreement with the experimental results. As to ultimate fastener force in the short span case, the experimental result

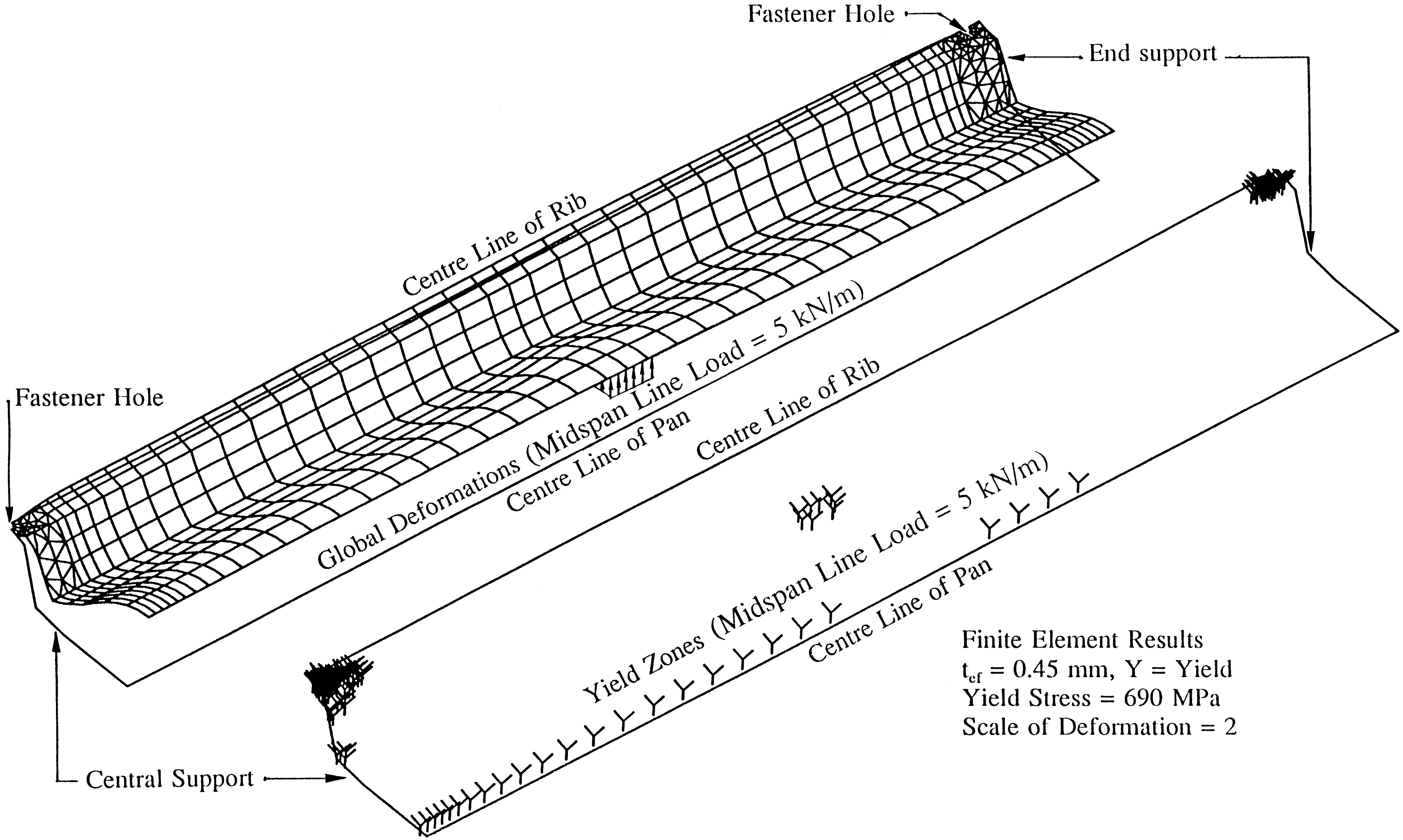

FIG. 4.5 GLOBAL DEFORMATIONS AND YIELD ZONES OF SHORT SPAN RIBBED PROFILE ROOFING SHEET UNDER FAILURE LOAD

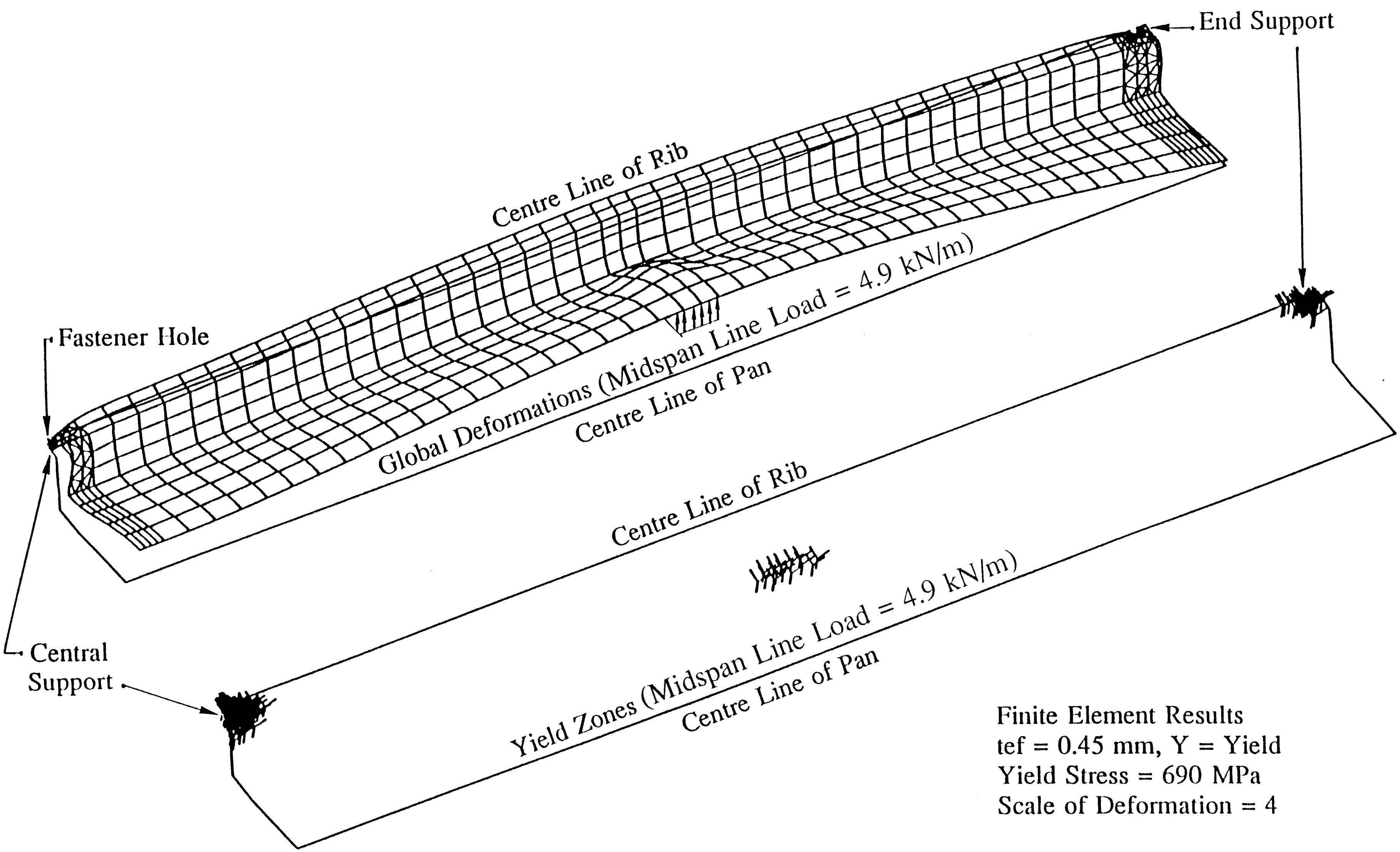

Finite Element Results
tef = 0.45 mm, Y = Yield
Yield Stress = 690 MPa
Scale of Deformation = 4

FIG.4.6 GLOBAL DEFORMATIONS AND YIELD ZONES OF LONG SPAN RIBBED PROFILE ROOFING SHEET UNDER FAILURE LOAD

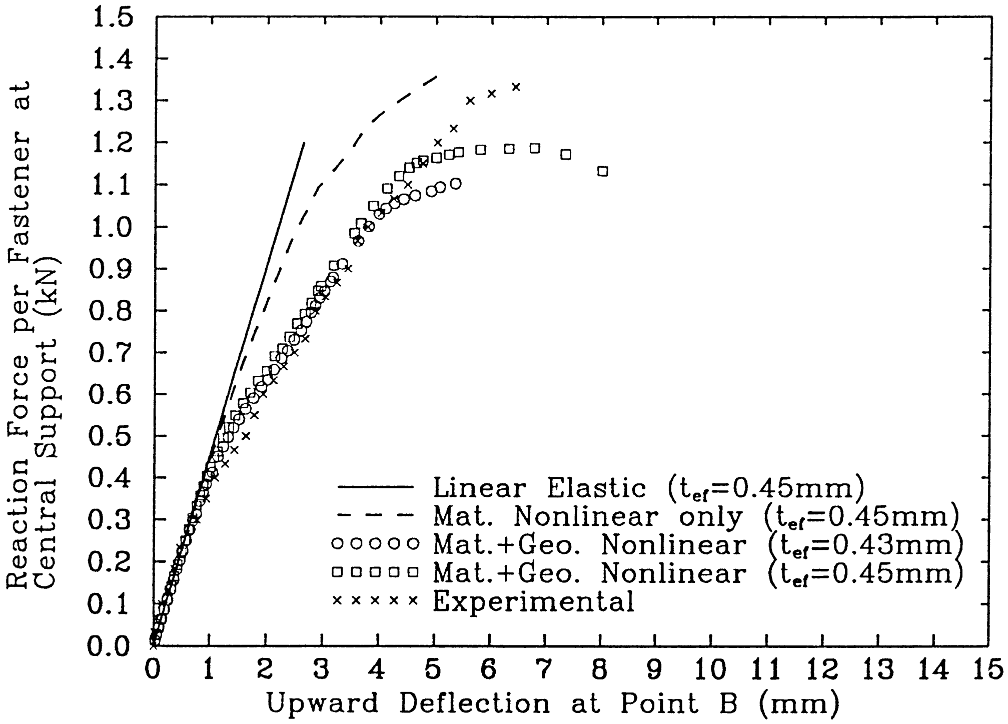

(a) Short Span Roofing Sheet

FIG.4.7 FASTENER REACTION-DEFLECTION CURVES FOR POINT B: RIBBED PROFILE ROOFING SHEET

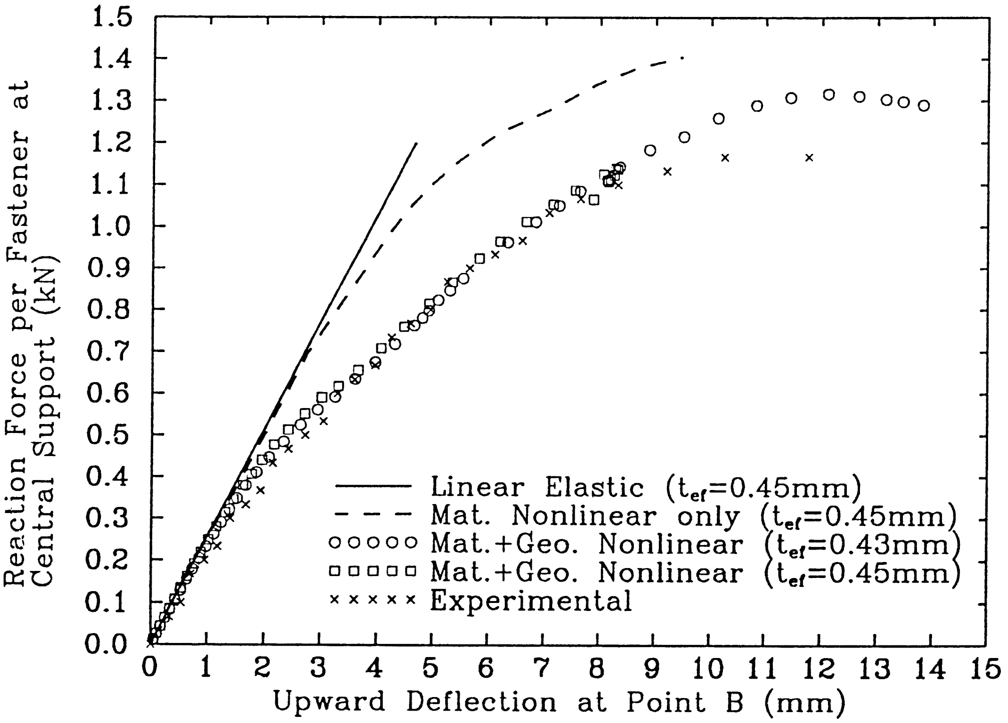

(b) Long Span Roofing Sheet

FIG.4.7 FASTENER REACTION-DEFLECTION CURVES FOR POINT B: RIBBED PROFILE ROOFING SHEET was about 1350 N per fastener whilst the numerical values were about 1200 N per fastener for the sheeting of a 45 mm effective thickness and about 1100 N per fastener for the sheeting of a 43 mm effective thickness. In the case of the long span sheeting, the numerical value of ultimate fastener force was about 1300 N per fastener for the sheeting of a 0.43 mm effective thickness while the compatible experimental result could not be given due to the overall buckling at the midspan. The numerical value of ultimate fastener force for the sheeting of a 0.45 mm effective thickness needs to be further confirmed when the new version of the LUSAS system is available.

The relationship between the total fastener reaction force at the central support and the total uplift load is shown in Fig. 4.8a and 4.8b for the short and long span ribbed profile roofing sheets respectively. It is clear that the finite element results from the elastic-plastic large deflection analysis are in good agreement with the experimental results. The load-fastener reaction force relationship calculated for a two-span continuous beam with simple end supports under a concentrated midspan load approximates both finite element and experimental results when load is less than half of the local failure load. As the load increased, the curves slightly deviated from the solid line due to the local plastic deformations around the screw fastener, but were still away from the dash line which was derived from a simply supported one span beam under a concentrated midspan load.

4.3 Stresses in Short Span Roofing Sheet

From the stress contours of the short span roofing sheet of a 0.45 mm effective thickness under a midspan line load of 5 kN/m it was found that large transverse bending stresses existed to match the severe cross-sectional distortions. The transverse bending stresses along the longitudinal centre line of the pan were much larger than those along the longitudinal centre line of the rib, a reversed situation from the trapezoidal profile roofing sheet. Compared with the transverse bending stresses, transverse membrane stresses were much smaller. In longitudinal direction, both membrane and bending stresses were also small, but became large in the midspan loading area. It is interesting to find that the shear stresses were quite large in the side plate along the entire span. The side plate therefore seems to be a major structural component to transfer the midspan load to the screw fasteners.

The aforementioned stress distribution is only for areas away from the fastener holes. Stresses in the vicinity of the fastener hole at the central support, however,

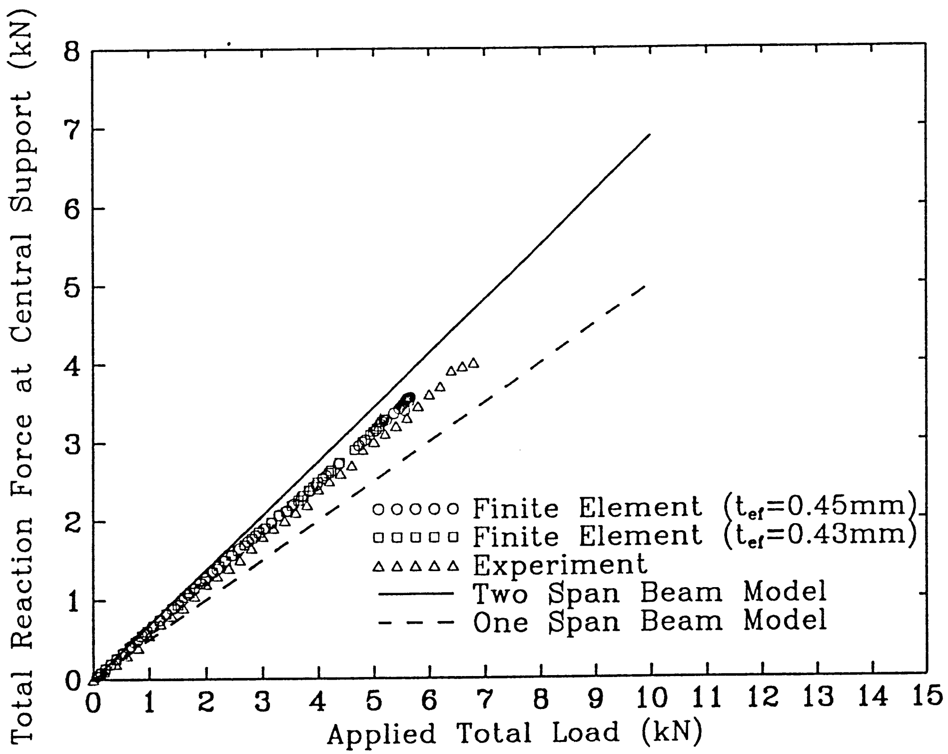

(a) Short Span Roofing Sheet

FIG.4.8 LOAD–FASTENER REACTION RELATIONSHIP: RIBBED PROFILE ROOFING SHEET

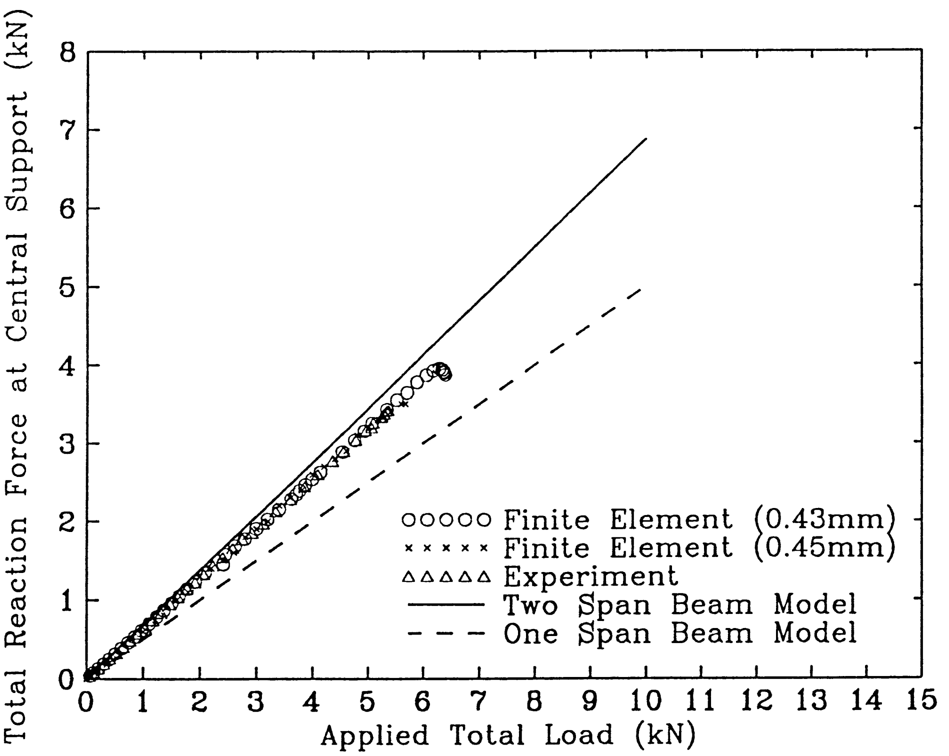

(b) Long Span Roofing Sheet

FIG.4.8 LOAD–FASTENER REACTION RELATIONSHIP: RIBBED PROFILE ROOFING SHEET became very high, and their distribution was very complicated as found in the case of the trapezoidal profile roofing sheet. Fig. 4.9 shows the longitudinal membrane stress distribution (in the middle layer through the sheeting thickness) near the central support under a midspan line load of 5 kN/m. Three critical areas could be identified around the fastener hole. Near the junction between the top plate and the side plate (Region 1), there were large longitudinal compressive membrane stresses. In Region 2 (see Fig. 4.9), large longitudinal tensile membrane stresses existed. Along the centre line of the rib (Region 3), large compressive members stresses were found in a very small area. The transverse membrane stresses, as shown in Fig. 4.10, were small in regions 1 and 3 but very large in region 2 in tension. It is interesting to see the local stress distributions of the membrane stresses of the ribbed profile roofing sheet were similar to those of the trapezoidal profile roofing sheet (Figs. 3.11 and 3.12). Both roofing sheets had three critical areas at nearly the same positions and of the same sign membrane stresses. These are believed to be attributed to the similar shapes of the screwed crest (or rib).

Three points representative of the three regions mentioned above were chosen to see the variations of the four stress resultants (membrane stress resultants and bending moments in both longitudinal and transverse directions) with midspan line load. They are shown in Figs. 4.11a-d, respectively. The x, y and z coordinates of the three points (Gauss points) in millimetres are (13.972, 0.833, 25.500) for point 1, (8.626, 0.435, 27.673) for point 2 and (0.430, 8.797, 28.934) for point 3 in the global Cartesian coordinates (see Fig. 2.3). From these figures, a few important observations are made as follows:

(a) When the line load was less than 1.96 kN/m, the load-stress relations were almost linear, which is consistent with the linear load-deflection relations described in Section 4.1. In the meanwhile, all three points were loaded in longitudinal membrane compression, with the largest value at point 3 (Fig. 4.11b). This is similar to the trapezoidal profile roofing sheet (Section 3.4) and is expected from the global bending behaviour of the sheeting as a two-span beam.

(b) As the line load increased, the longitudinal compressive membrane stress resultant at point 1 increased rapidly and monotonicly until sheeting failure (Fig. 4.11b). In the meantime, both the longitudinal and transverse membrane stress resultants at point 2 became tensile and increased significantly until the sheeting failure. It was the large longitudinal compressive membrane stresses in region 1 that induced the buckling of the side plate and initiated the local plastic collapse.

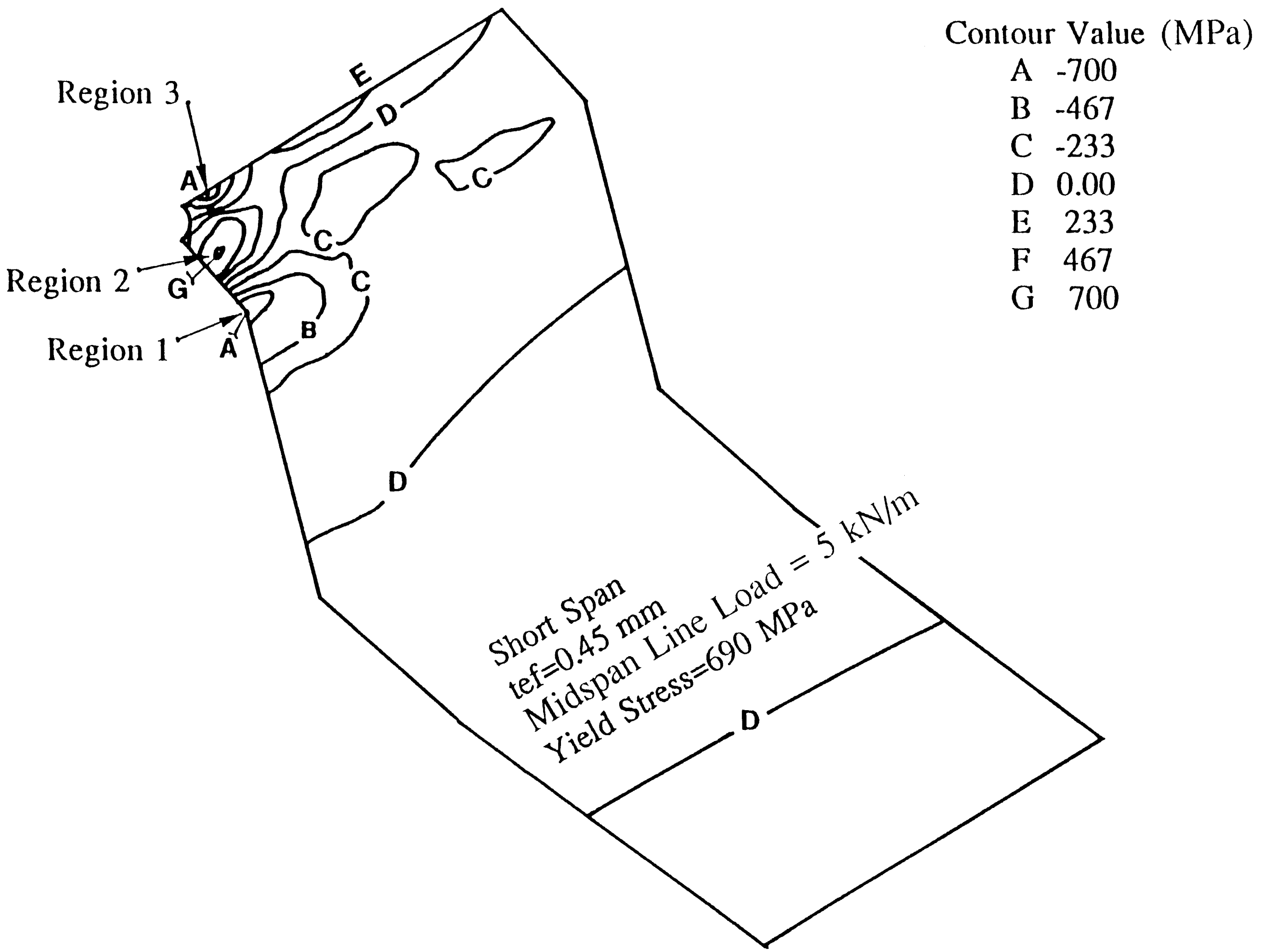

FIG.4.9 CONTOURS OF LONGITUDINAL MEMBRANE STRESSES UNDER FAILURE LOAD: RIBBED PROFILE ROOFING SHEET

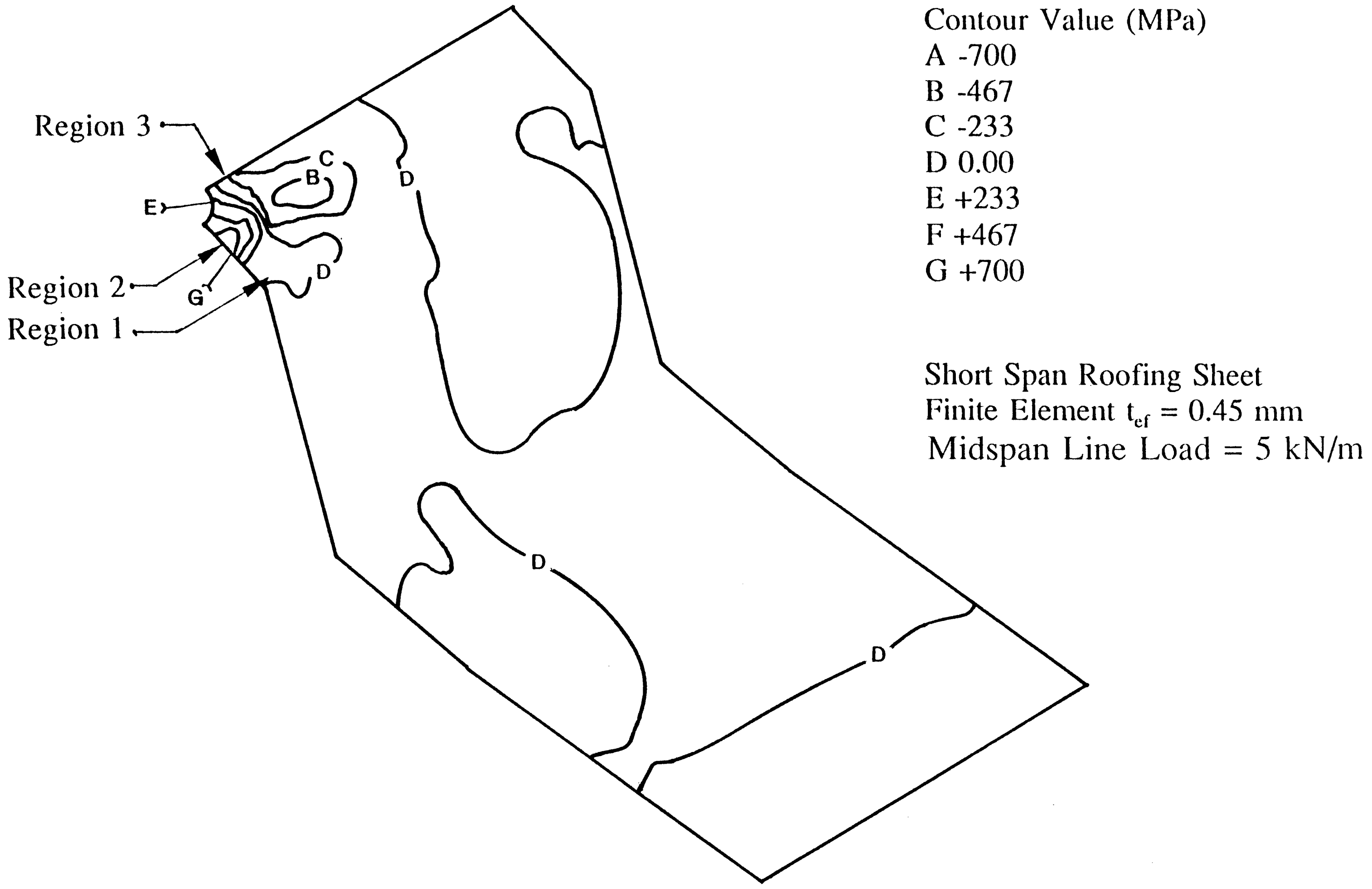

FIG. 4.10 CONTOURS OF TRANSVERSE MEMBRANE STRESSES UNDER LOCAL FAILURE LOAD: RIBBED PROFILE ROOFING SHEET

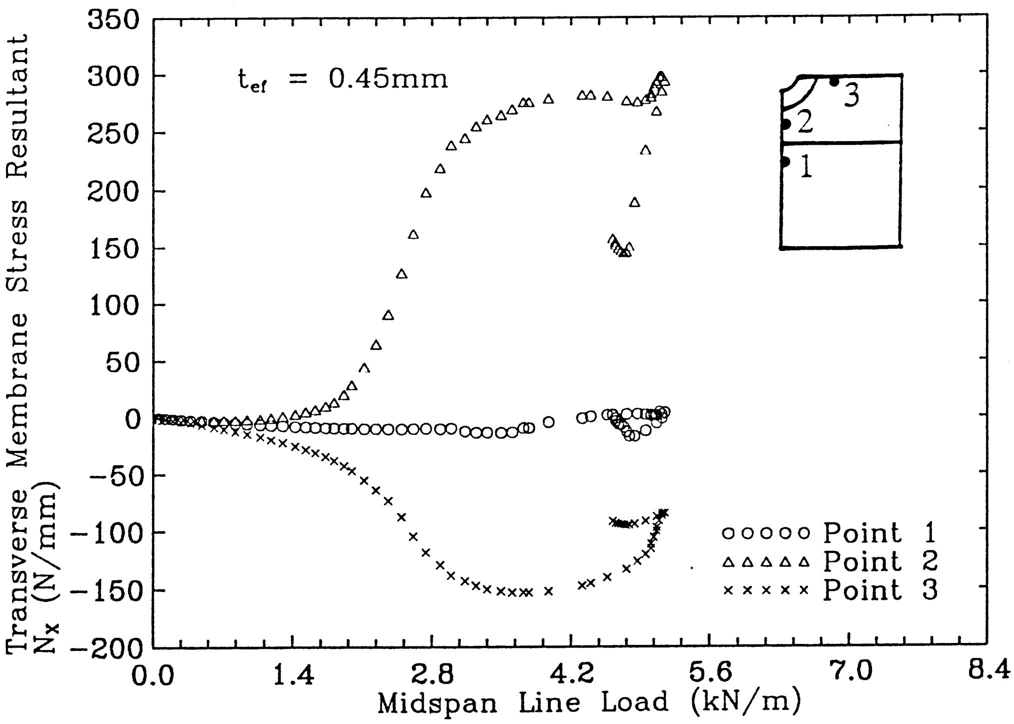

(a) Transverse Membrane Stress Resultant

FIG.4.11 VARIATION OF STRESS RESULTANTS WITH LOAD: SHORT SPAN RIBBED PROFILE ROOFING SHEET

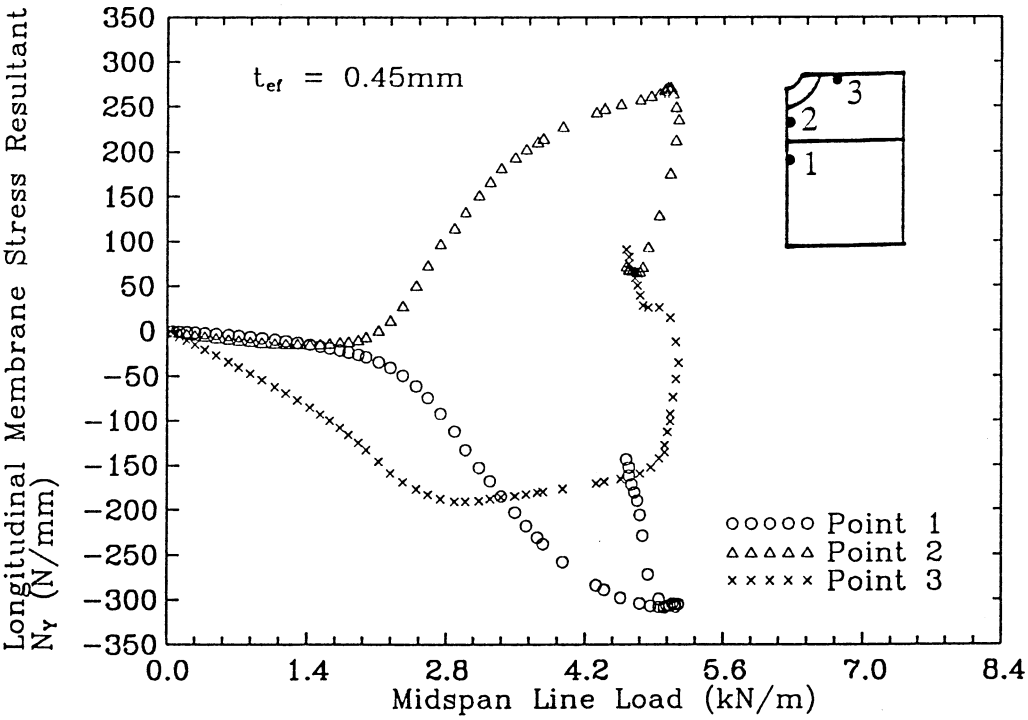

(b) Longitudinal Membrane Stress Resultant

FIG.4.11 VARIATION OF STRESS RESULTANTS WITH LOAD: SHORT SPAN RIBBED PROFILE ROOFING SHEET

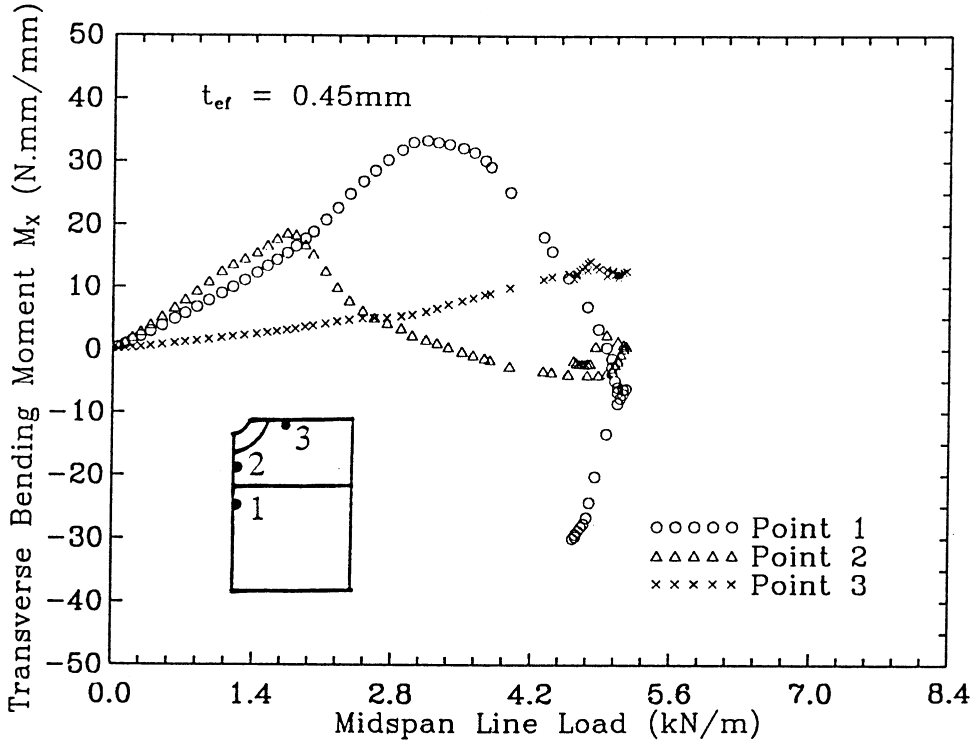

(c) Transverse Bending Moment

FIG.4.11 VARIATION OF STRESS RESULTANTS WITH LOAD: SHORT SPAN RIBBED PROFILE ROOFING SHEET

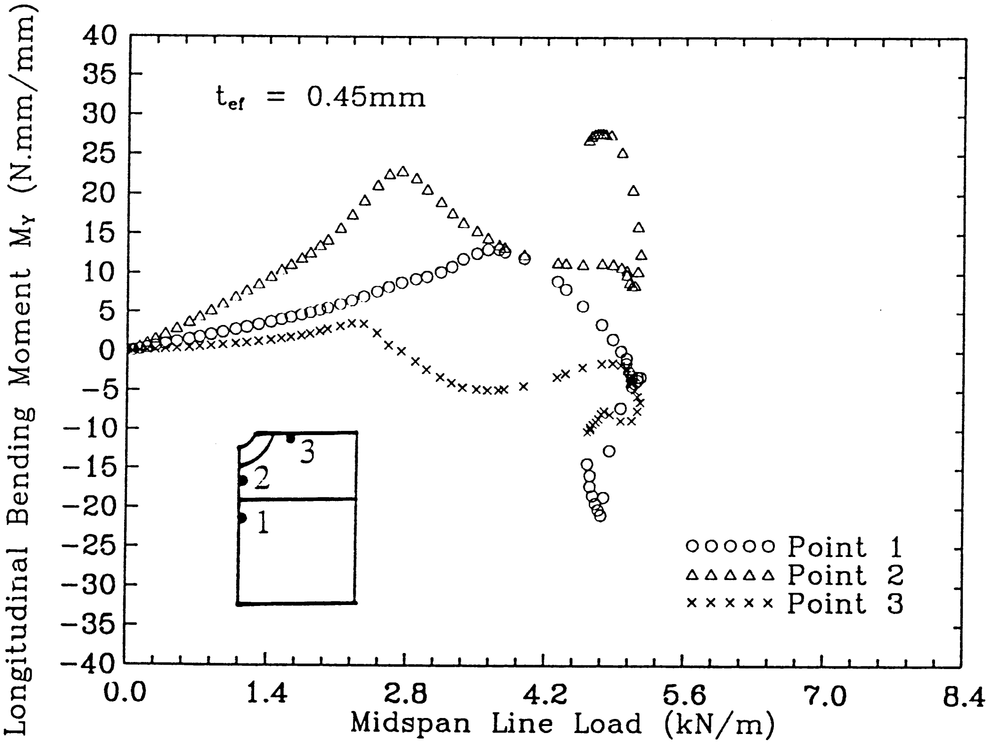

(d) Longitudinal Bending Moment

FIG.4.11 VARIATION OF STRESS RESULTANTS WITH LOAD: SHORT SPAN RIBBED PROFILE ROOFING SHEET

The large bi-directional tensile membrane stress resultants in region 2 may have caused the sheeting material to exceed effective fracture strain and then the sheeting to split. It is clear that within this load range, the sheeting is very susceptible to cracking due to the large bi-directional tensile stresses and longitudinal bending moment in the region 2.

(c) For the trapezoidal profile roofing sheet, the longitudinal tensile stress resultant at point 2 was increased to a maximum value at a line load about 4.2 kN/m and then decreased rapidly until the local plastic collapse occurred (see Fig. 3.11b). For the ribbed profile roofing sheet, the same stress resultant at point 2 monotonicly increased with the increasing load till the local plastic collapse at a line load about 5.04 kN/m. This difference is probably due to different sheeting cross-sections: the wide pan in the ribbed profile roofing sheet instead of the unscrewed crest in the trapezoidal profile roofing sheets.

The similar results were found in the short span roofing sheet of a 0.43 mm effective thickness.

4.4 Stresses in Long Span Roofing Sheet

The membrane and bending stress distributions in the long span roofing sheet regarding the global deformation were similar to those in the short span roofing sheet. The shear stresses in the side plate, however, were much smaller than those in the short span roofing sheet.

The local stress distributions around the central fastener hole were also similar to those in the short span sheeting. Three critical stress areas identified in the short span roofing sheet were found in the long span roofing sheet at nearly the same locations. The corresponding membrane stress resultants and bending moments at the three representative points are plotted in Figs. 4.12a-d for the sheeting of 0.43 mm effective thickness. Since the selected points are Gauss points rather than critical points in the critical regions, magnitudes of stress resultants and bending moments could not be accurately compared between the short and long span roofing sheets. However, local failure mechanisms of the long span sheeting can be identified from these figures. The different points with regard to the failure mechanisms between the short and long span roofing sheets are as follows:

(a) The longitudinal compressive membrane resultant at point 1 reached the

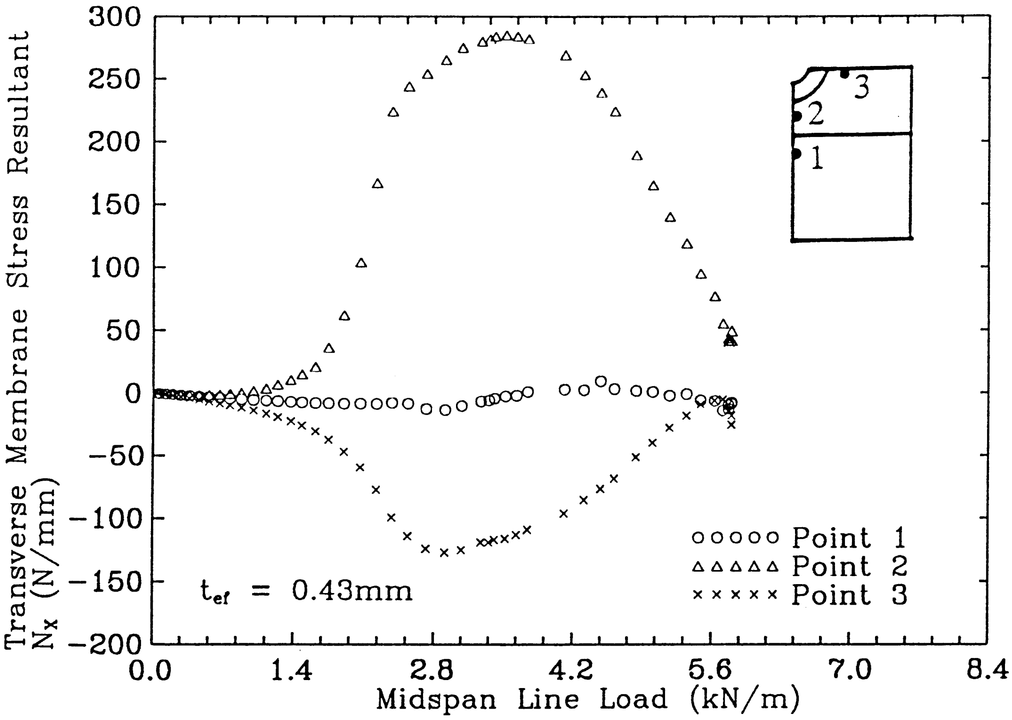

(a) Transverse Membrane Stress Resultant

FIG.4.12 VARIATION OF STRESS RESULTANTS WITH LOAD: LONG SPAN RIBBED PROFILE ROOFING SHEET

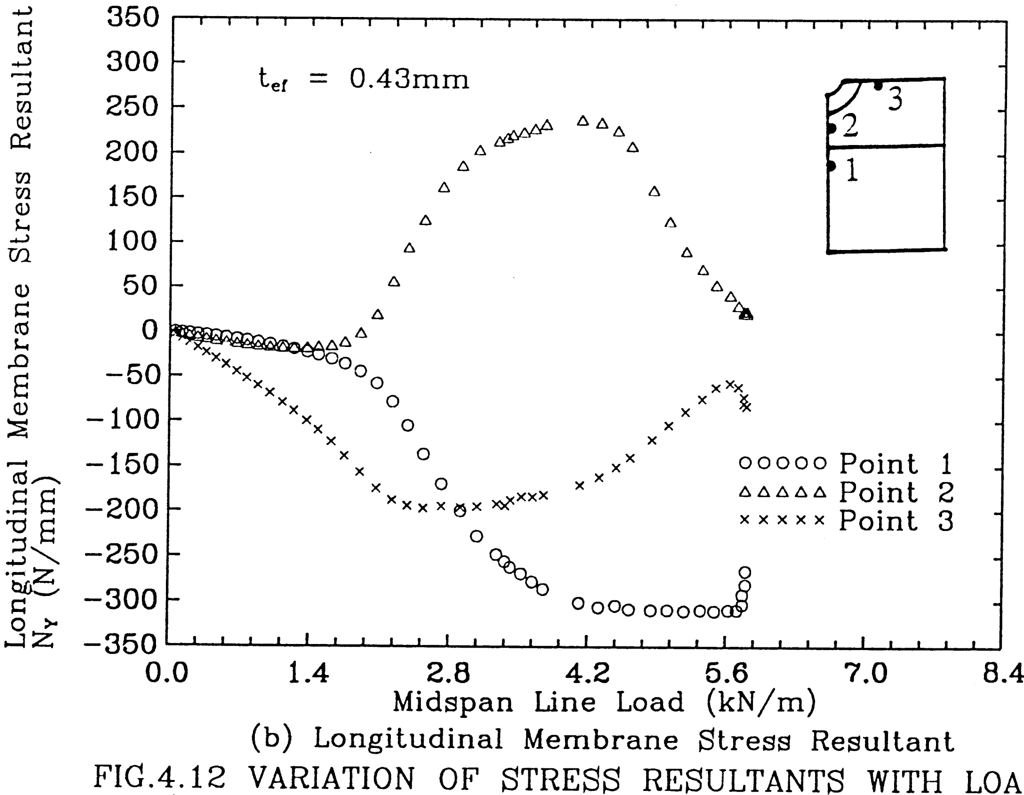

(b) Longitudinal Membrane Stress Resultant

FIG.4.12 VARIATION OF STRESS RESULTANTS WITH LOAD: LONG SPAN RIBBED PROFILE ROOFING SHEET

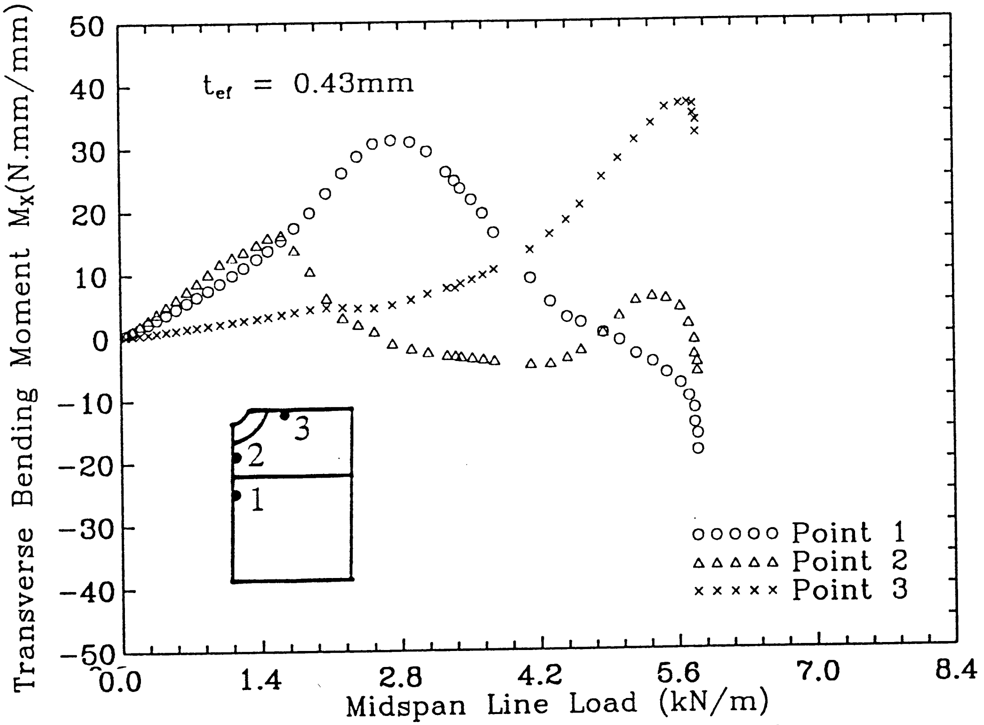

(c) Transverse Bending Moment

FIG.4.12 VARIATION OF STRESS RESULTANTS WITH LOAD: LONG SPAN RIBBED PROFILE ROOFING SHEET

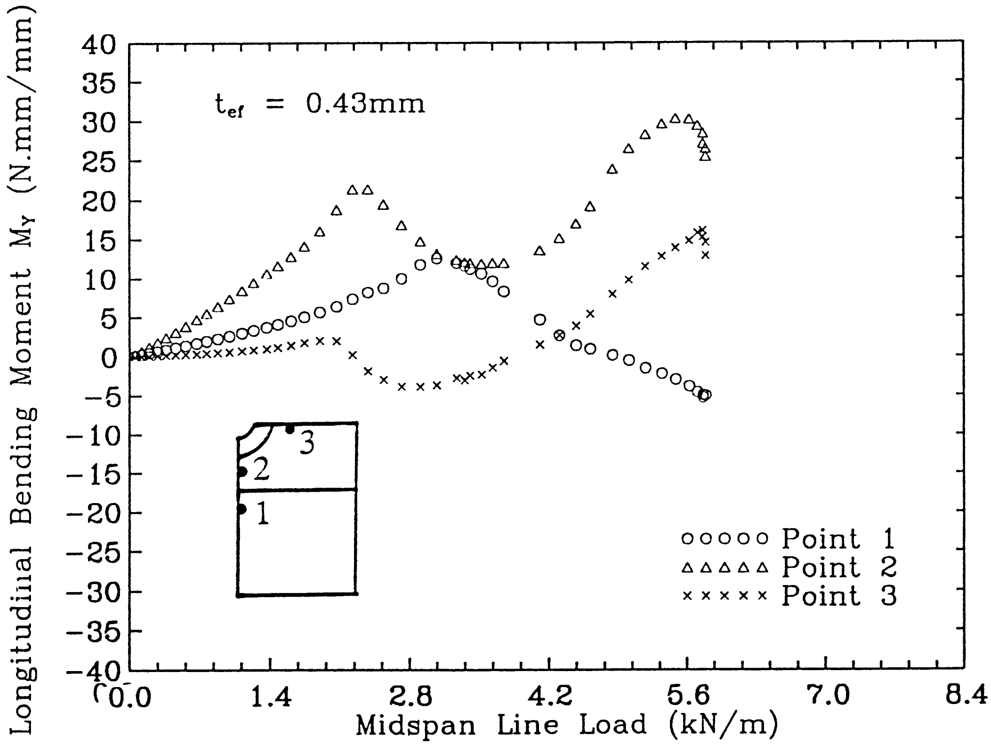

(d) Longitudinal Bending Moment

FIG.4.12 VARIATION OF STRESS RESULTNATS WITH LOAD: LONG SPAN RIBBED PROFILE ROOFING SHEET maximum value at a line load about 4.2 kN/m and remained this value till a line load of 5.74 kN/m, and then the local plastic collapse occurred (Fig. 4.12b).

(b) Both the longitudinal and transverse tensile membrane stress resultants at point 2 reached maximum values at a line load about 3.64 kN/m, and then decreased rapidly till the local plastic collapse (Fig. 4.12a-b). Therefore, when the line load increased above 3.64 kN/m, the possibility of sheeting cracking at point 2 due to excessive tensile strain became small. However, it should be noted that the longitudinal bending moment at point 2 became large again when the sheeting approached failure, which can still generate fatigue cracks under cyclic loads. The earlier occurrence of the maximum tensile stresses at point 2 indicates that within a lower load range, the long span roofing sheets may be more susceptible to fatigue damage than the short span roofing sheets.

(c) For point 3, the longitudinal compressive membrane resultant was dominant when the line load was small. As the sheeting approached the local failure, the transverse bending moment at point 3 increased rapidly and had a relatively large value. This large transverse bending moment could also induce the sheeting to crack at point 3 in the longitudinal direction when cyclic loads are applied.

5. ANALYSIS OF ROOFING SHEETS OF ARC-TANGENT PROFILE

5.1 Sheeting Deflections and Local Buckling

Presented in Fig. 5.1 are the upward deflections of the short span arc-tangent profile roofing sheet at point D (see Fig. 2.4), which is located at the longitudinal centre line of the unscrewed crest at the midspan. The linear and nonlinear finite element results using an effective sheeting thickness of 0.43 mm were compared with experimental results. The four stages in the load-deflection behaviour, as mentioned in the trapezoidal profile roofing sheets, can be seen in Fig. 5.1.

When line load is below about 1.4 kN/m, the results from linear elastic analysis match those from both the experiment and the elastic-plastic large deflection analysis well. The overall structural behaviour of the roofing sheet seems to be predominantly linear and elastic. The sheeting was in the elastic deformation stage.

As the line load increased, the load-deflection curves obtained from both the experiment and the elastic-plastic large deflection analysis started to deviate from that predicted by linear elastic analysis. Initially, nonlinear characteristic was weak and mainly attributed to sheeting cross-sectional distortions, as shown in Fig. 5.2. When the line load was increased to about 3.08 kN/m, local diamond-shaped deformations were observed under the head of the screw fastener at the central support during the test, and then the sheeting started to soften quickly due to the spreading of yielding and the further distortions of sheeting cross-sections. Fig. 5.3 shows the global deformations and the yield zones in the arc-tangent profile sheeting under a line load of 4.17 kN/m, which was just before initial failure of the sheeting. The large reaction force of the central screw fastener led to more extending yield zone over there than at the end supports. It is clear that the sheeting was now in the elastic-plastic transition stage.

With the further increase of load, the experiments showed that the local diamond-shaped deformation around the central screw fastener became larger and larger, the area of which was bounded by four line "knuckles". At a midspan line load about 4.2 kN/m, local buckling with a clear sound occurred at these knuckle regions. A sudden load drop was noted simultaneously. After that, it was observed that the sheeting cross-section distortions at the central support progressively developed without any load increase. Such structural behaviour was also predicted by the elastic-plastic large deflection analysis. The load-deflection curve predicted by finite element analysis, as shown in Fig. 5.1, exhibited strong snap-though buckling behaviour after the line load increased to a value of slightly higher than 4.2 kN/m. During the local snap through buckling, the load dropped down rapidly at first and then increased again to reach a new equilibrium. The sheeting cross-section at the central support, however, continuously distorted with further upward deflections, as shown in Fig. 5.2. It can be seen from Fig. 5.2 that when the line load was restored to 4.2 kN/m, the screwed crest at the central support was nearly flattened, and the curvature at the top of the screwed crest was inverted. In the meantime, the local upward deflections around the central screw fastener at the longitudinal centre line of the screwed crest jumped and formed a deep local dimple, as shown in Fig. 5.4. It is clear from the finite element results that the arc-tangent profile roofing sheet is more susceptible to local buckling due to its profile, compared with the trapezoidal and ribbed profile roofing sheets. It is also interesting to find the snap-through buckling predicted by the finite element analysis is similar to the snap-through buckling of the spherical shells under ring loads, which have been widely studied and reported in the literature (e.g., Evan-Iwanowski *et al*, 1963; Cagan and Taber, 1986).

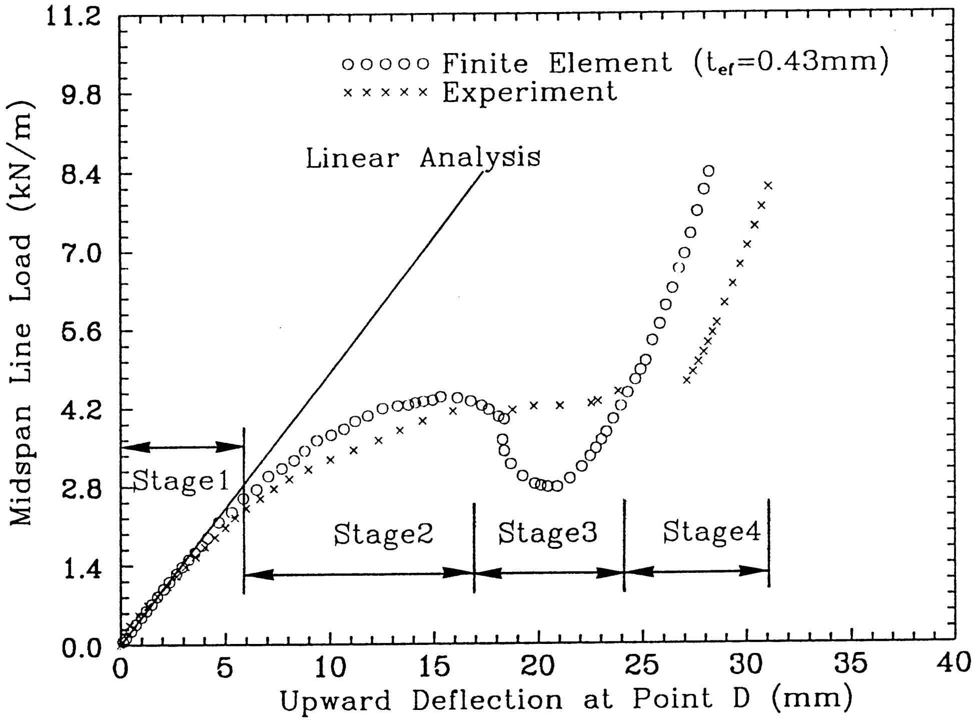

FIG.5.1 LOAD-DEFLECTION CURVES FOR POINT D: ARC-TANGENT PROFILE ROOFING SHEET

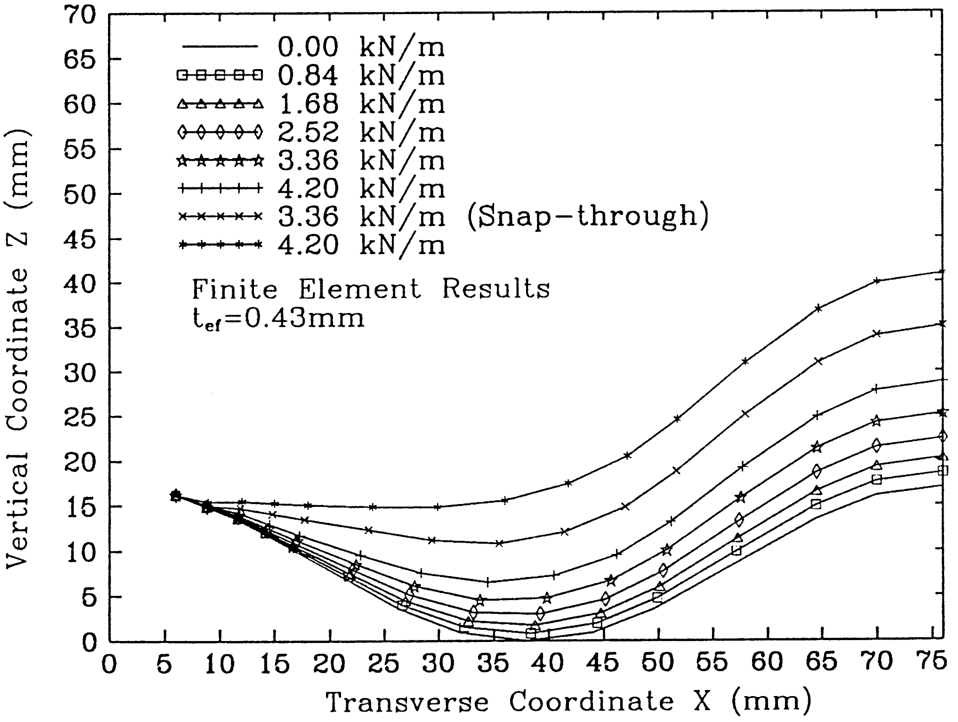

FIG.5.2 DISTORTION IN SHEETING PROFILE AT CENTRAL SUPPORT UNDER INCREASING LOADS: ARC-TANGENT PROFILE ROOFING SHEET

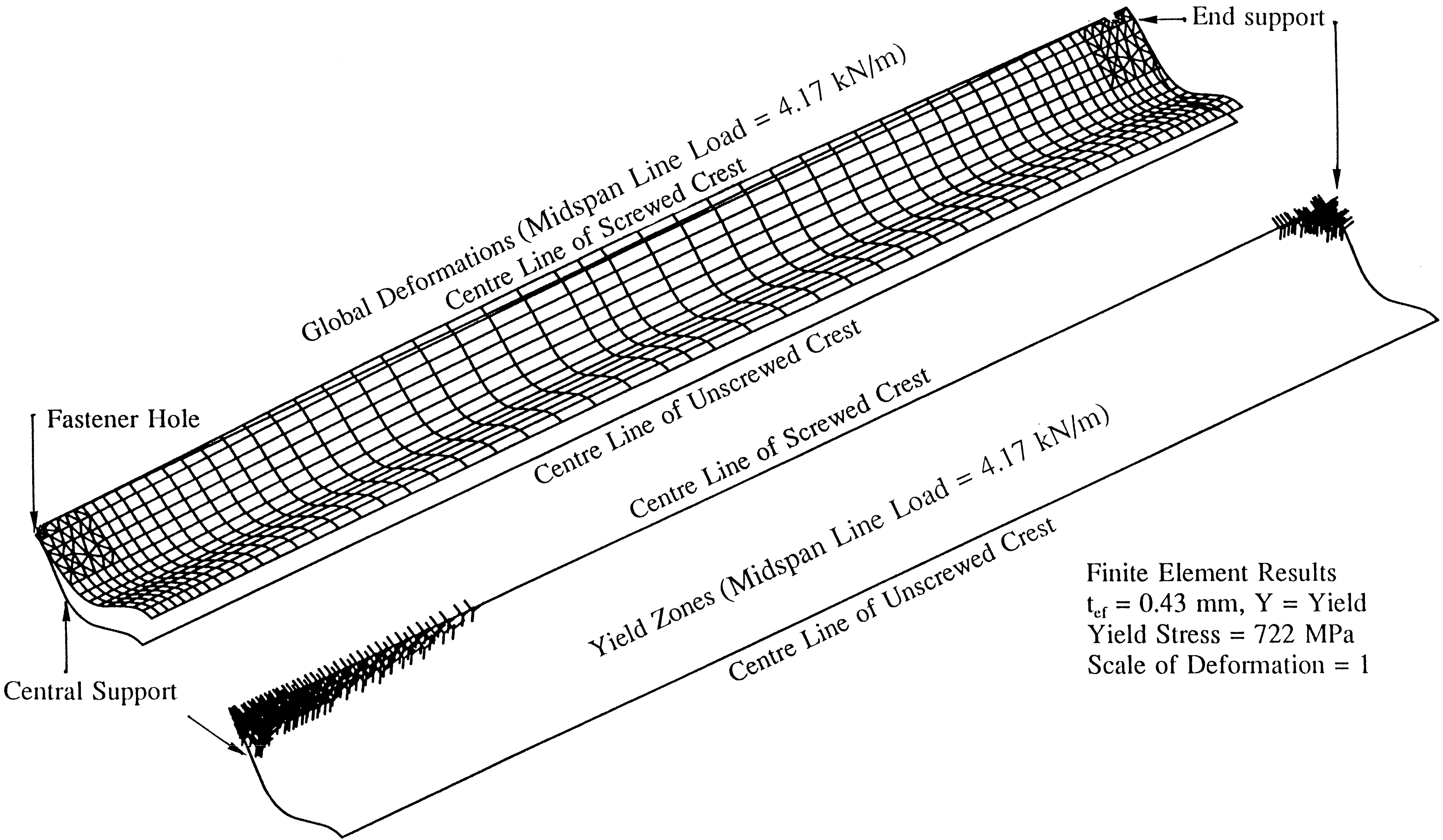

Finite Element Results
t_{ef} = 0.43 mm, Y = Yield
Yield Stress = 722 MPa
Scale of Deformation = 1

FIG. 5.3 GLOBAL DEFORMATIONS AND YIELD ZONES OF SHORT SPAN ARC-TANGENT PROFILE ROOFING SHEET UNDER FAILURE LOAD

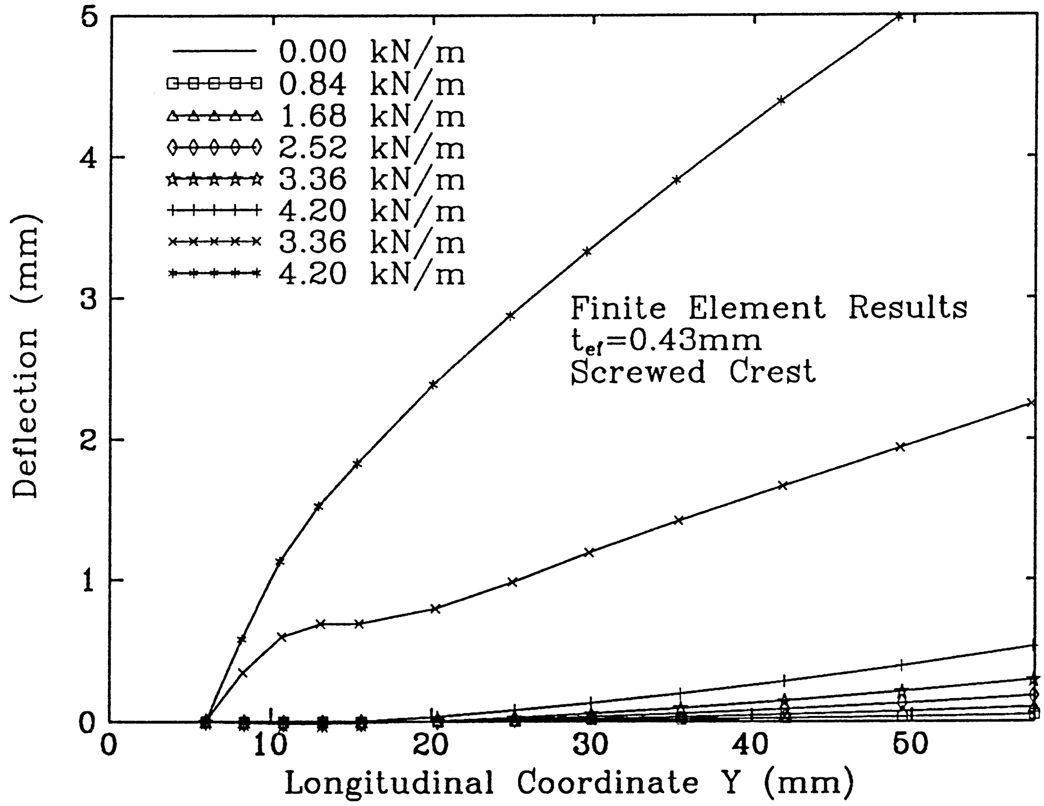

FIG.5.4 DEFLECTED SHAPES OF SCREWED CREST NEAR CENTRAL SUPPORT UNDER INCREASING LOADS: ARC-TANGENT PROFILE ROOFING SHEET

However, the finite element analysis somewhat predicted a much deeper snap-through than that in the experimental curve, as shown in Fig. 5.1. The reasons may be related to both the experimental arrangement and the finite element modelling of the sheeting. In the experimental arrangement aspect, the dial gauges used to read the upward deflections during the test could not provide a real picture of the sheeting buckling. A few readings during the sheeting snap-through or large cross-sectional distortion, as plotted in Fig. 5.1, were taken in the dynamic equilibrium, which may not be accurate. In the aspect of the finite element modelling, planar triangular elements used to replace curved triangular elements in the vicinity of the fastener holes (see Fig. 2.4) may be one of many factors affecting prediction of the snap-through since shell buckling is very sensitive to surface curvature, so does the neglect of the local initial geometric imperfections and residual stresses around the screw fasteners, which could be easily generated by the initial pre-tightening of the central screw fastener in the test.

After the snap-through buckling, the screwed crest around the central fastener tended towards tensile membrane behaviour in the longitudinal direction of the sheeting. The sheeting therefore displayed geometrically stiffening behaviour characterised by a nearly linear load-deflection response. This stiffening behaviour was observed in both the experiment and the finite element analysis, and continued until an overall cross-sectional buckling at the midspan occurred.

The fastener force-deflection relations and the fastener force-load relations predicted from finite element analysis were also in close agreement with the experimental results in the elastic deformation stage, the elastic-plastic transition stage and the geometrically stiffening stage. In the local snap-through buckling stage, there was also a discrepancy between the experiment and the finite element analysis as found in the load-deflection relations.

5.2 Stress Distributions

Global stress distributions were examined for the short span roof sheeting of a 0.43 mm effective thickness under a line load of 4.17 kN/m. Fig. 5.5 shows the stress distributions in the middle layer of the sheeting in both longitudinal and transverse directions. Fig. 5.6 displays the stress distributions in the top surface of the sheeting in both longitudinal and transverse directions. The local stress distributions around the fastener holes are not clearly shown in Figs. 5.5 and 5.6. Some general observations on global stress distributions for areas away from the fastener holes are made as follows:

(a) Transverse stresses in the middle layer of the sheeting were nearly zero, but transverse stresses in the top surface of the sheeting were very large. This stress distribution indicates that large bending moments existed in the transverse direction and caused the severe sheeting cross-sectional distortions. The transverse bending moments along the longitudinal centre line of the unscrewed crest were smaller than and had a sign opposite to those along the longitudinal centre line of the screwed crest. Approaching the sheeting valley, the transverse bending moments became smaller and smaller.

(b) Around the midspan, longitudinal stresses in the middle layer were compressive at the sheeting valley and tensile at both the screwed and unscrewed crests. Around the central support, the longitudinal stresses in the middle layer were compressive at the screwed crest and tensile at the valley. This stress distribution was attributed to the global bending of the roofing sheet. The longitudinal stress

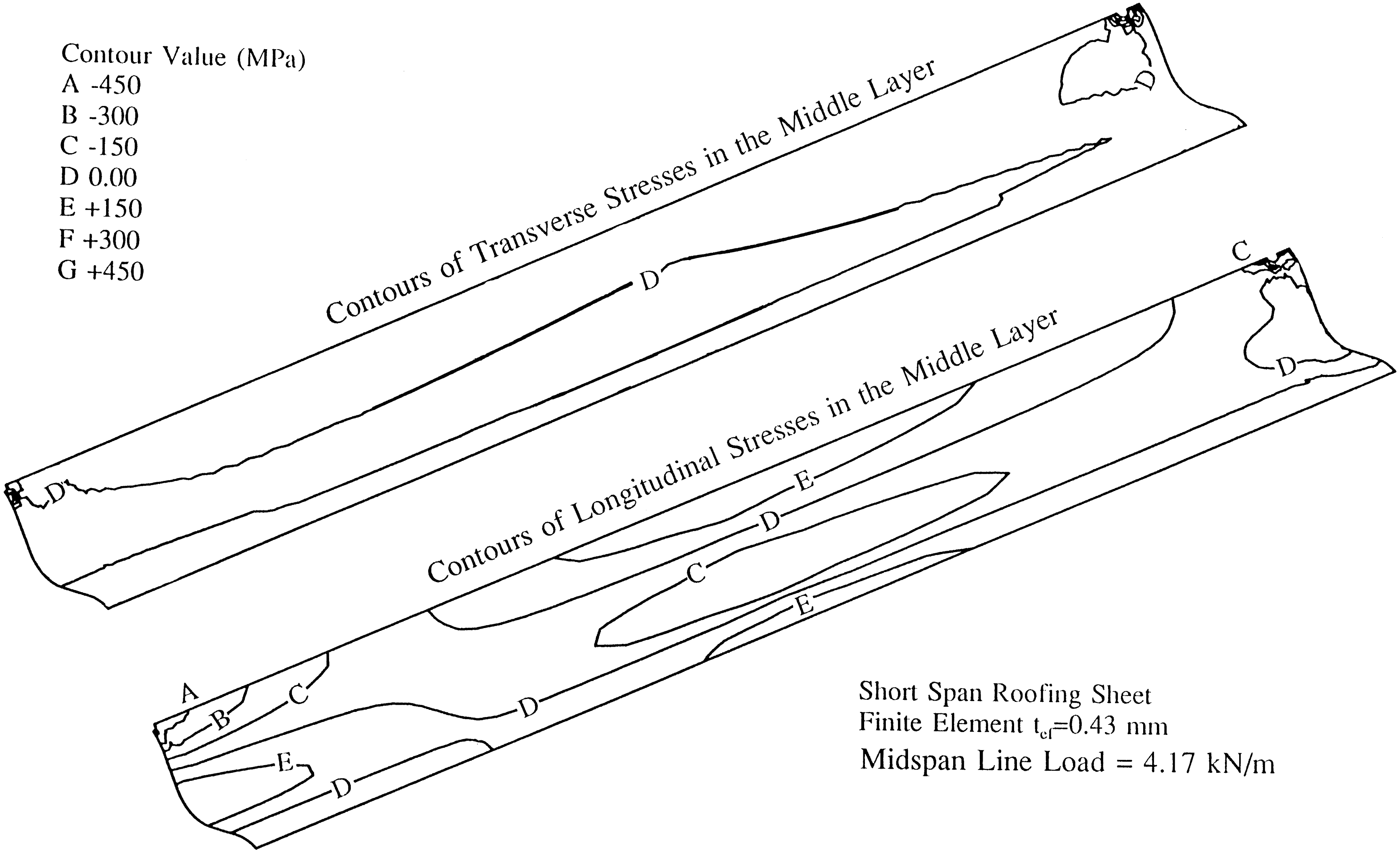

Short Span Roofing Sheet
Finite Element t_{ef}=0.43 mm
Midspan Line Load = 4.17 kN/m

FIG.5.5 GLOBAL CONTOURS OF STRESSES IN THE MIDDLE LAYER OF ARC-TANGENT PROFILE ROOFING SHEET

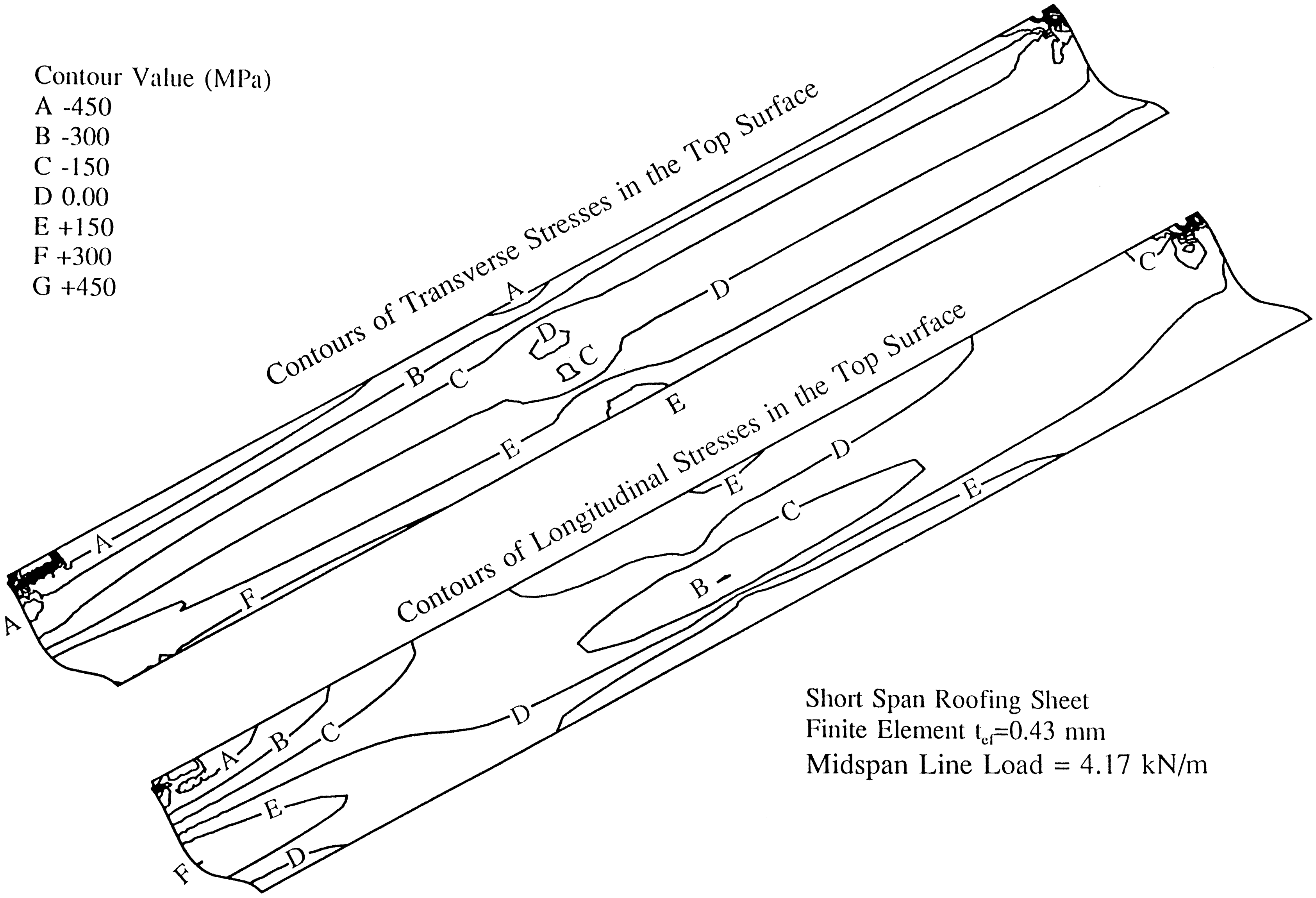

FIG.5.6 GLOBAL CONTOURS OF STRESSES IN THE TOP SURFACE OF ARC-TANGENT PROFILE ROOFING SHEET

distribution and magnitude in the top surface of the sheeting were similar to those in the middle layer and, therefore, the global longitudinal bending moments were small.

The membrane stress distributions in the vicinity of the fastener hole at the central support under a midspan line load of 4.17 kN/m are shown in Figs. 5.7 and 5.8. Both the longitudinal and transverse membrane stresses around the fastener hole were compressive, but the transverse membrane stresses were relatively smaller. It is interesting to note that the longitudinal membrane stresses were not only large but also within the local diamond-shaped deformation area. This indicates that the longitudinal compressive membrane stresses caused the sheeting local buckling around the four lines of the knuckles. A photograph from the experiment showing this buckling type is also presented in Fig. 5.7 to compare with the stress pattern around the screw fastener.

It is apparent that the local membrane stress distributions around the fastener holes of the arc-tangent profile roofing sheet were quite different from those of the trapezoidal and ribbed profile roofing sheets. For the trapezoidal and ribbed profile roofing sheets under the local failure loads, there were three critical areas identified with different signs of membrane stresses. For the arc-tangent profile roofing sheet before the local snap-through buckling, all membrane stresses around the fastener holes were compressive. This difference is mainly attributed to the shape of the screwed crests. Effects of different sheeting profiles on local stress distribution and local fatigue damage are further discussed in Section 5.4.

5.3 Load-Stress Relations at Critical Areas

Within the local diamond-shaped deformation area, four Gauss points were chosen to investigate the variations of the four main stress resultants with midspan line load: two points on the longitudinal centre line of the screwed crest and other two points on the transverse line at the central support (see Fig. 5.7). The x, y and z coordinates of the four points in millimetres are (1.00, 19.20, 16.85) for point 1, (0.38, 9.14, 16.94) for point 2, (10.67, 0.83, 13.90) for point 3 and (13.05, 0.94, 12.48) for point 4 in the global Cartesian coordinates shown in Fig. 2.4. The longitudinal and transverse membrane stress resultants at the four points are shown in Figs. 5.9a and 5.9b while the longitudinal and transverse bending moments at the four points are shown in Figs. 5.9c and 5.9d. a few important observations are made here.

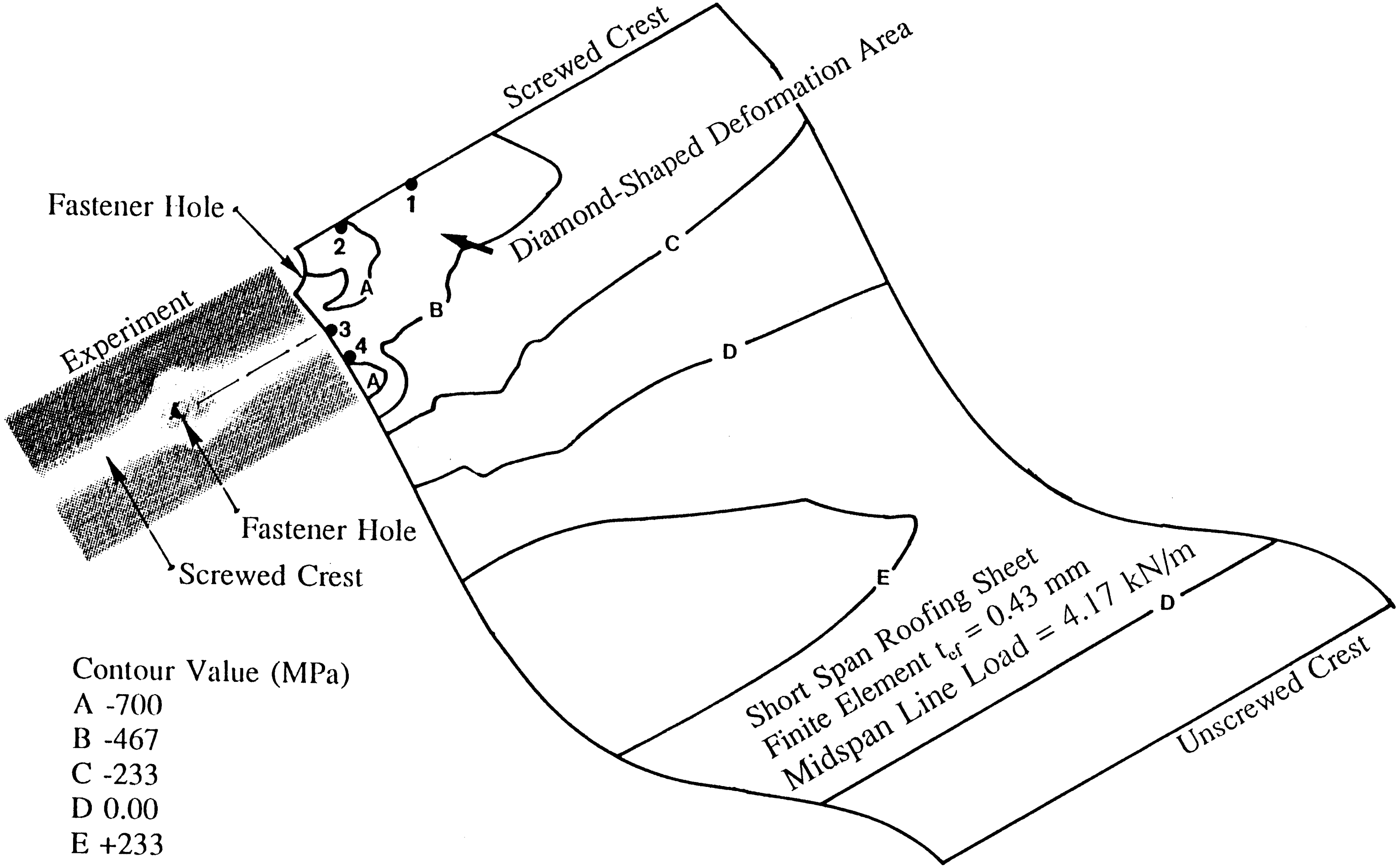

FIG. 5.7 CONTOURS OF LONGITUDINAL MEMBRANE STRESSES AT THE BEGINNING OF LOCAL SNAP-THROUGH STAGE: ARC-TANGENT PROFILE ROOFING SHEET

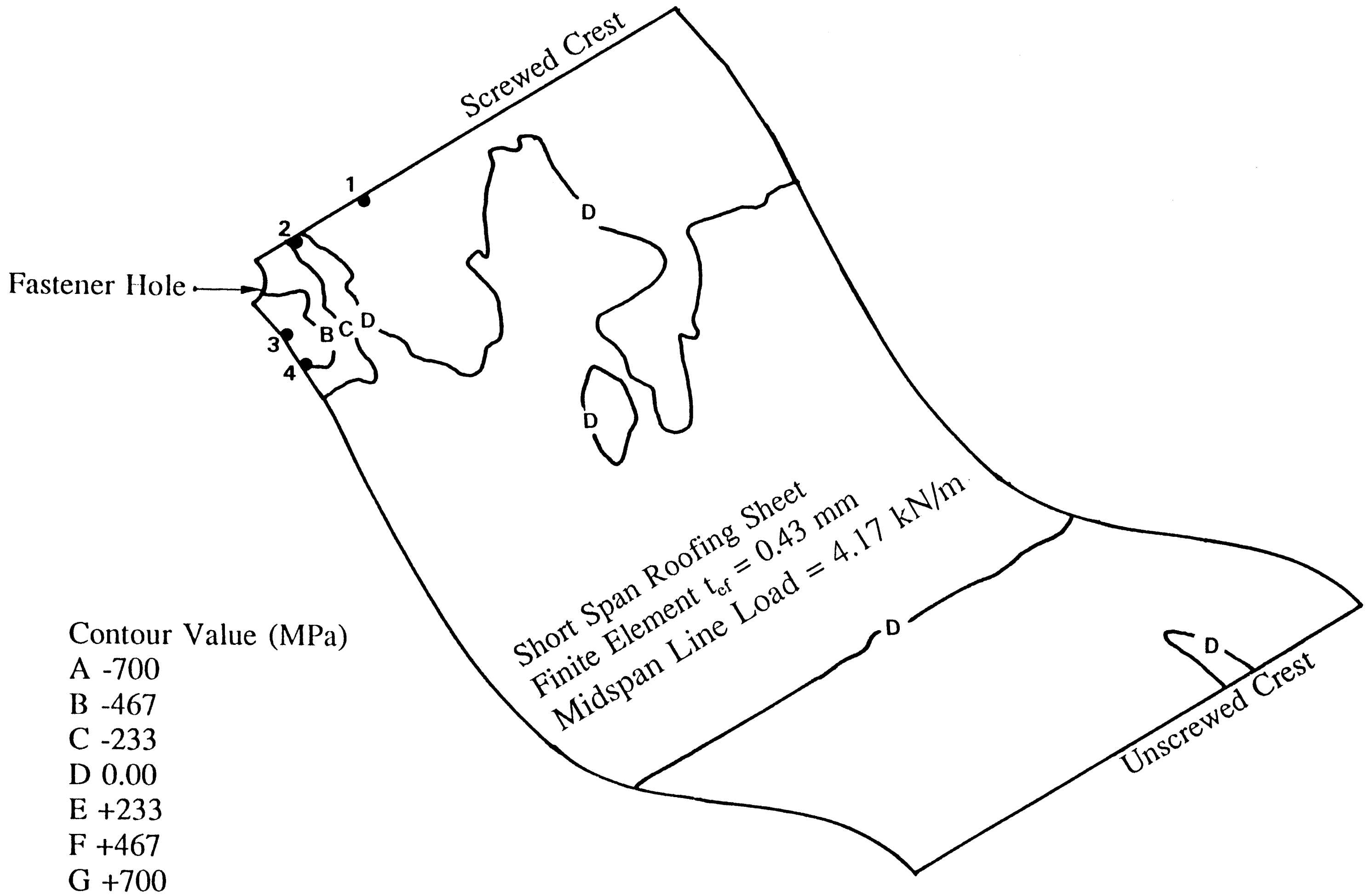

FIG. 5.8 CONTOURS OF TRANSVERSE MEMBRANE STRESSES AT BEGINNING OF LOCAL SNAP-THROUGH STAGE: ARC-TANGENT PROFILE ROOFING SHEET

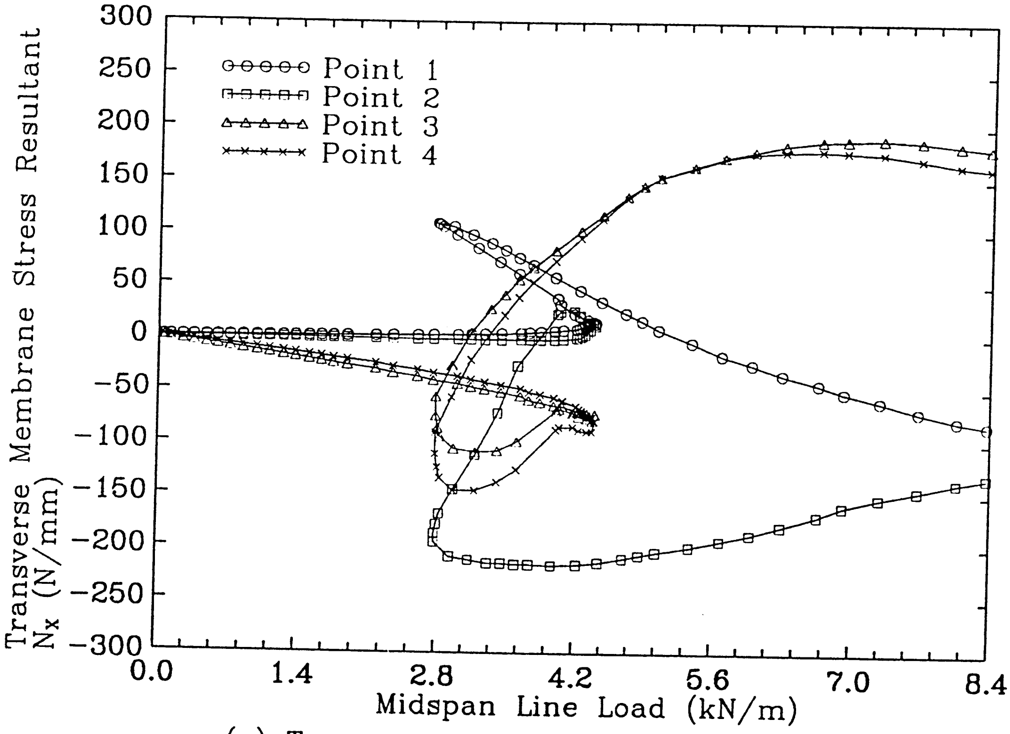

(a) Transverse Membrane Stress Resultant

FIG.5.9 VARIATION OF STRESS RESULTANTS WITH LOAD: ARC-TANGENT PROFILE ROOFING SHEET

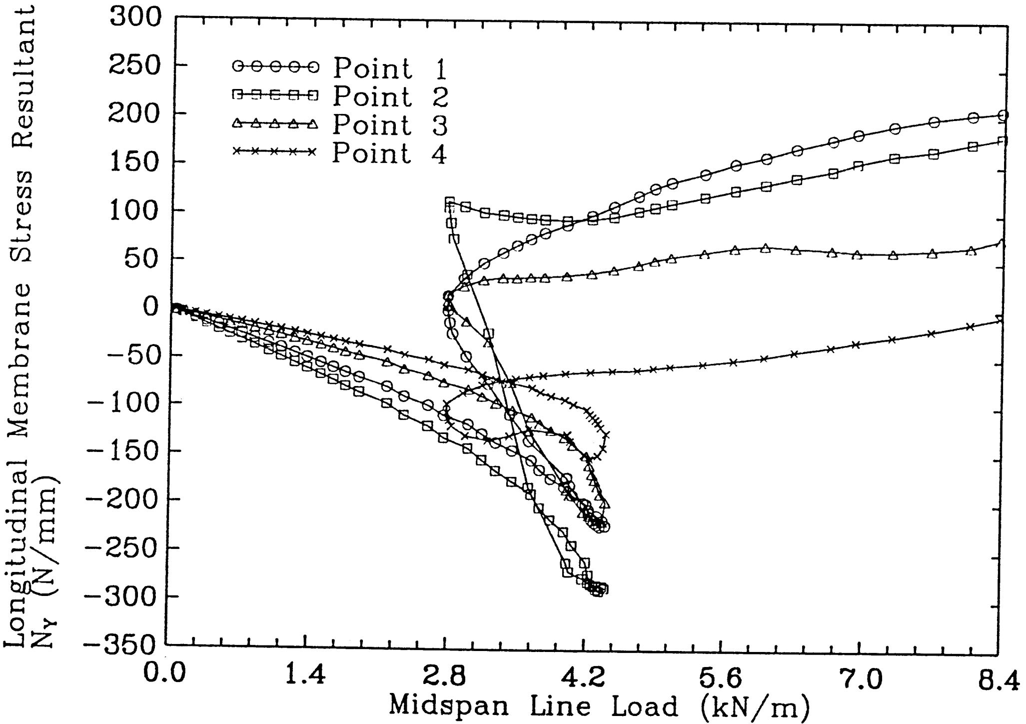

(b) Longitudinal Membrane Stress Resultant

FIG.5.9 VARIATION OF STRESS RESULTANTS WITH LOAD: ARC-TANGENT PROFILE ROOFING SHEET

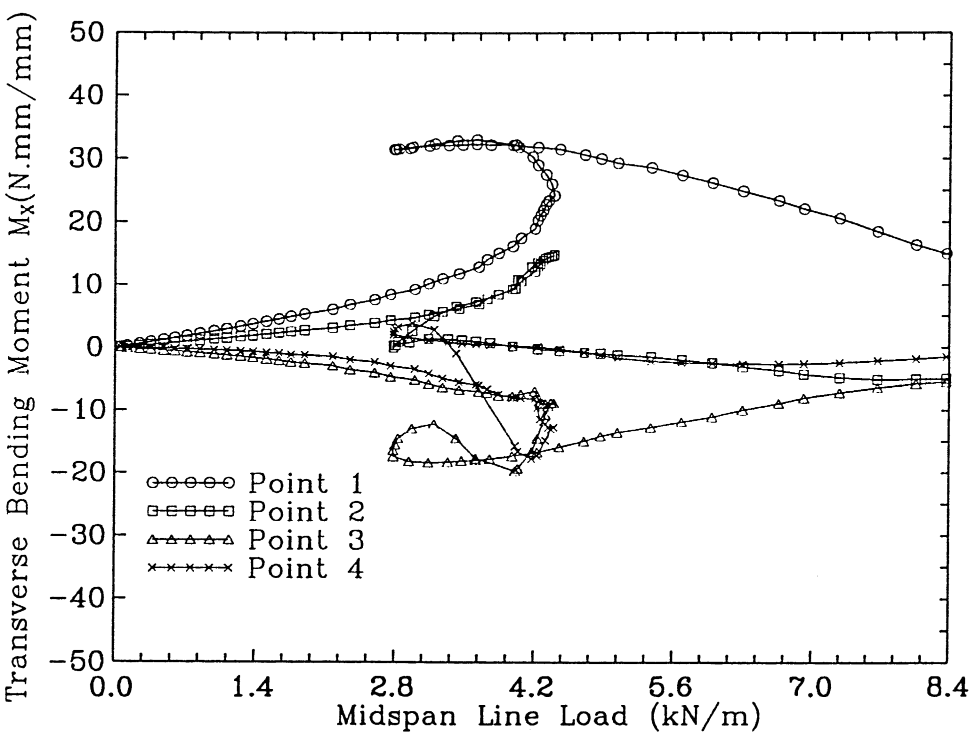

(c) Transverse Bending Moment

FIG.5.9 VARIATION OF STRESS RESULTANTS WITH LOAD: ARC−TANGENT PROFILE ROOFING SHEET

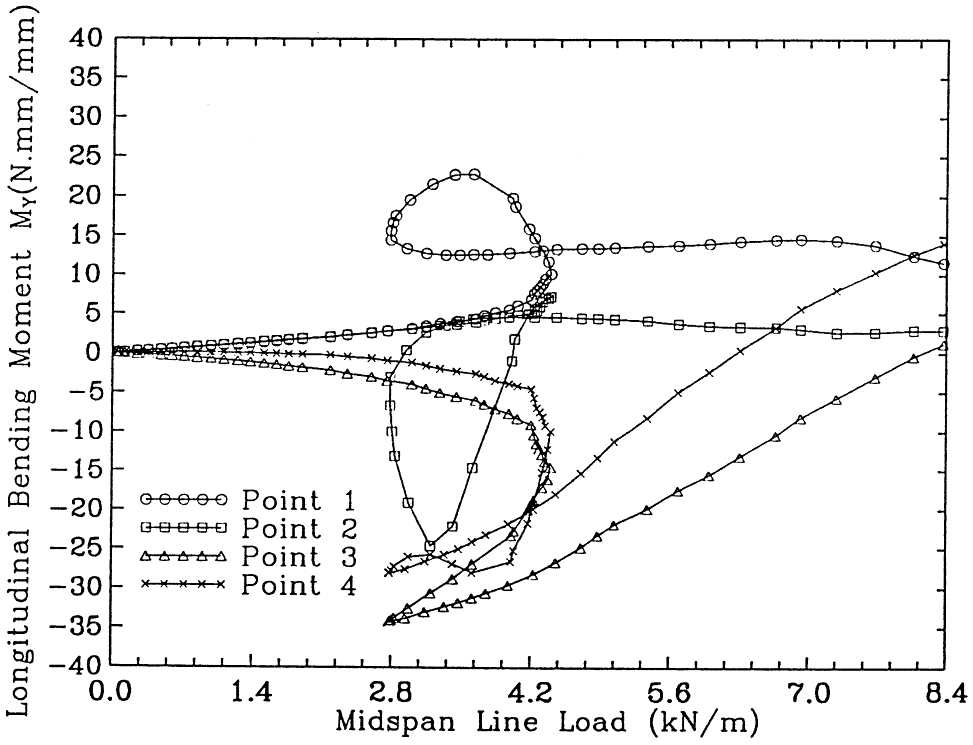

(d) Longitudinal Bending Moment

FIG.5.9 VARIATION OF STRESS RESULTNATS WITH LOAD: ARC−TANGENT PROFILE ROOFING SHEET

(a) Before the local snap-through buckling, all four points were loaded in longitudinal membrane compression (Fig. 5.9b). It is the large longitudinal compressive membrane stresses that caused the local snap-through buckling of the arc-tangent profile roofing sheet at a line load of about 4.34 kN/m. After the local snap-through buckling, the longitudinal membrane stress resultants at points 1 to 3 became tensile, and the longitudinal tensile membrane stress resultants at points 1 and 2 increased with increasing load.

(b) The transverse membrane stress resultants at all four points were small before the sheeting buckled (see Fig. 5.9a). After the sheeting buckled, points 3 and 4 were loaded in the large longitudinal membrane tension whilst point 2 was loaded in the large longitudinal membrane compression.

(c) When line load was small, both the longitudinal and transverse bending moments increased approximately linearly with the line load (Figs. 5.9c-d). When the line load approached the buckling load of 4.34 kN/m, the bending moments increased rapidly with only small load increase. After the local snap-through buckling, the bending moments decreased monotonicly.

5.4 Discussion

The abovementioned load-stress relations of the arc-tangent profile roofing sheet show that there was a sudden change in characteristics of both bending moments and membrane stress resultants as the local buckling of the sheeting occurred. This change would be expected to lead to different types and extents of sheeting fatigue damage. Before the sheeting buckled, bending moments are probably main resultant components to cause the sheeting to crack if cyclic loads are applied on the sheeting. As the amplitude of cyclic load approaches the local buckling failure load, one would expect much less load cycles required to cause the sheeting to crack because at this load level the magnitude of the alternative bending moments at points 1, 3 and 4 were quite large (Figs. 5.9c-d). After the sheeting buckled, the high tensile membrane stress resultants (Figs. 5.9a-b), together with the high bending moments, would easily cause the sheeting to crack as the sheeting material used here has a very low tensile strain fracture.

Such analysis based on load-stress relations is consistent with some fatigue test results. For instance, the constant repeated-loading tests conducted by Beck and Stevens (1979) and Mahendran (1990) on the arc-tangent profile roofing sheets showed that before and after the local buckling, the fatigue cracks exhibited different types, and when the amplitude of cyclic load exceeded the local buckling load, the fatigue performance deteriorated rapidly.

Since the load-stress relations at the critical areas of the trapezoidal and ribbed profile roofing sheets significantly differ from those of the arc-tangent profile roofing sheets, a great difference in fatigue performances between these roofing sheets would be expected. Particularly when the amplitude of cyclic load just exceeded the buckling load of the arc-tangent profile roofing sheet (about 4.2 kN/m), the fatigue resistance of the arc-tangent profile sheeting would be dramatically reduced, but for the trapezoidal profile roofing sheet, the small load increase would not change the fatigue resistance very much since the local plastic collapse load of the trapezoidal profile roofing sheet was higher than the local buckling load of the arc-tangent profile roofing sheet. However, this does not exclude the possibility that the fatigue performance of the arc-tangent profile sheet would be better than those of the trapezoidal and ribbed profile sheets in some load cases. For instance, when the midspan line load was around 3 kN/m, the large local tensile membrane stress resultants and longitudinal bending moments in the trapezoidal or ribbed profile roofing sheets may cause the sheeting to crack at less cycles than for the arc-tangent profile roofing sheets. However, any further practical comparison should be based on a reliable wind load model related to sheeting fatigue.

6. CONCLUSIONS

The following conclusions have been drawn from this investigation.

(1) A finite element modelling procedure has been proposed for three types of light gauge steel profiled roofing sheets subject to simulated wind uplift. The upward deflections, fastener reaction forces and limit loads of the roofing sheets predicted by the finite element analysis are in close agreement with the corresponding experimental results.

(2) In finite element modelling of the roofing sheets, the mesh around the fastener holes should be fine enough to obtain highly varying stress distributions. The nonlinear control parameters and techniques involved in computation iteration and incrementation procedures should be carefully selected to maintain the accuracy of

the solution when the sheeting is approaching local failure.

(3) Linear elastic finite element analysis is valid only at a low wind uplift. Elastic-plastic large deflection finite element analysis is generally required. Using base metal thickness as an effective sheeting thickness in finite element analysis usually produces a marginally conservative solution for failure load. The slight change of the effective sheeting thickness does not create a significant influence on sheeting performance.

(4) In terms of finite element analysis, the global deformations, local deformations, yield zones and cross-sectional distortions of the three types of profiled roofing sheets at different load levels have been clearly demonstrated. The four stages of the deflection behaviour of both the arc-tangent and trapezoidal profile roofing sheets, i.e., elastic deformation stage, elastic-plastic transition stage, local plastic collapse (or snap-through buckling) stage and geometrically stiffening stage, have also been predicted.

(5) Stress analyses show that the local plastic failure of both the trapezoidal and ribbed profile roofing sheets around fastener holes is initiated by local plastic collapse at the junction between the upper part of the side plate and the top plate near the fastener hole at the central support, where large longitudinal compressive membrane stresses exist. The local cracking of the short span ribbed profile roofing sheet, immediately after the local plastic collapse, is attributed to the high longitudinal tensile membrane stresses near the central fastener hole. The high longitudinal compressive membrane stresses around the central fastener hole cause the diamond-shaped deformation and the buckling of the arc-tangent profile roofing sheet.

(6) Load-stress relations of both the trapezoidal and ribbed profile roofing sheets indicate that when the sheeting undergoes cyclic loads of small amplitude, fatigue cracking would be expected to occur at a certain area around the fastener hole due to bending stresses. If the amplitude of the cyclic load increases, the high tensile membrane stresses and bending stresses around the fastener hole would be the main reason to cause the sheeting to crack. As to the arc-tangent profile roofing sheet, the load-stress relations show that before the local snap-through buckling, compressive membrane stresses were dominant for areas around the fastener holes. After the sheeting buckled, the high tensile membrane stresses around the fastener hole, along with the high bending stresses, would significantly reduce the sheeting

fatigue performance.

(7) The load-stress relations of the trapezoidal or ribbed profile roofing sheets are quite different from those of the arc-tangent profile roofing sheet. Therefore, one would expect large differences in fatigue performances between these roofing sheets under cyclic loads at different levels. Any reasonable comparison of fatigue performances between the roofing sheets, however, should be based on a reliable wind load model which could reflect real cyclic characteristics of wind load.

(8) The successful application of the finite element method to light gauge steel profiled sheets not only provides a method of conducting extensive parametric studies of the structural behaviour of the marketing roofing sheets under arbitrarily distributed wind pressure, but also opens the way for the design of new sheeting profiles and serves as a transfer function from cyclone induced wind load characterisation to sheeting fatigue life prediction.

7. ACKNOWLEDGMENTS

This research report forms part of an ongoing research program on the behaviour and strength of light gauge steel profiled roofing sheets under wind loads. The author wish to thank Mr G.F. Reardon, Technical Director of the Cyclone Testing Station, for his support and careful review of this report, and Dr J.G. Teng at the Department of Civil & Systems Engineering for many helpful discussions. Thanks also are due to Ms W.J. Zhang and Mr K. Abercombie for plotting some diagrams, and Lysaght Building Industries and W.A. Deutsher Pty Ltd for denoting the roofing sheets and screw fasteners.

8. REFERENCES

ASCE Fatigue and Fracture Reliability Committee (1982). "Fatigue reliability: variable amplitude loading." *Journal of Structural Division, ASCE,* Vol. 108, No. ST1, Jan., pp. 47-69.

Beck, V.R. and Stevens, L.K. (1976). " Constant repeated loading of corrugated sheeting." Proc. of Metal Structures Conf., The Institute of Engineers, Australia, November, pp. 40-45.

Beck, V.R. and Stevens, L.K. (1979). " Wind loading failures of corrugated roof cladding." *Civil Engineering Transactions, I.E.Aust*, Vol. CE21, No.1, pp. 45-56.

Bushnell, D. (1985). " *Computerised Buckling Analysis of Shells*." Martinus Nijhoff Publishers.

Cagan, J. and Taber, L.A. (1986). " Large deflection stability of spherical shells with ring loads." *Journal of Applied Mechanics*, Dec., Vol. 53, pp. 897-901.

Eaton, K.J. and Mayne J.R. (1975). " The measurement of wind pressures on two-storey houses at Aylesbury." *Journal of Industrial Aerodynamics*, Vol. 1, pp. 67-109.

Ellifritt, D.S. and Burnette, R. (1990). " Pull-over strength of screws in simulated building tests." *Proc. of 10th International Speciality Conference on Cold-formed Steel Structures*, St. Louis, Missouri, U.S.A.

Evan-Iwanowski, R.M., Loo, T.C. and Tierney, D.W. (1963). " Local buckling of shells." *Developments in Mechanics*, Vol. 2, Ostrach, S. and Scanlan, R.H., eds, Pergamon, New York, pp. 221-251.

FEA (1990). " *LUSAS User's Manual, LUSAS Theory Manual*." Version 10.0, Finite Element Analysis Ltd, Surry, U.K.

Gerhardt, H.J. and Kramer, C. (1986). " Wind induced loading cycle and fatigue testing of light weight roofing fixations." *Journal of Wind Engineering and Industrial Aerodynamics*, Vol. 23, pp. 237-247.

Hancock, G. (1991). " Behaviour of purlin with screw fastened sheeting under wind uplift and downwards loading." Postgraduate Course - *Behaviour and Design of Purlins, Sheeting and Screw-fasteners*, The University of Sydney, Australia, October.

Holmes, J.D. and Best, R.J. (1978). " Wind pressures on an isolated high-set house." James Cook University of North Queensland, *Wind Engineering Report 1/78*, Queensland, Australia, Jan.

Holmes, J.D., Melbourne, W.H. and Walker, G.R. (1990). " *A Commentary on the*

Australian Standard for Wind Loads." Courtney Colour Graphics Pty Ltd, Vic., Australia.

Irons, B.M. (1976). " The semi-loof shell element." *Finite Elements for Thin Shells and Curved Members*, Edited by Ashwell and Gallagher, Chap. 11, Wiley, London.

Javaherian, H., Dowling, P.J. and Lyons, P.R. (1980). " Nonlinear finite element analysis of shell structures using the semi-loof element." *Computers & Structures*, Vol. 12, pp. 147-159.

Lysaght Building Industries (1990). " *Design Manual: Steel Roofing and Walling.*" Sydney, Australia.

Mahendran, M. (1990). " Static behaviour of corrugated roofing under simulated wind loading." *Civil Engineering Transactions, I.E.Aust,* Vol. CE32, No. 4, pp. 212-218.

Mahendran, M. (1990). " Fatigue behaviour of corrugated roofing under cyclic wind loading." *Civil Engineering Transactions, I.E.Aust*, Vol. CE32, No. 4, pp. 219-226.

Martins, R.A.F. and Owen, D.R.J. (1981). " Elastic-plastic and geometrically nonlinear thin shell analysis by the Semi-Loof element." *Computers & Structures*, Vol. 13, pp. 505-513.

Mehta, K.C., Levitan, M.L., Iverson, R.E. and McDonald, J.R. (1992). " Roof corner pressures measured in the field on a low building." *Journal of Wind Engineering and Industrial Aerodynamics*, 41-44, pp. 181-192.

Morgan, J.W. and Beck, V.R. (1977). " Failure of sheet-metal roofing under repeated wind loading." *Civil Engineering Transactions, I.E.Aust*, Vol. CE19, No.1, pp. 1-5.

Nilson, A.H. (1973). " Analysis of light gauge steel shear diaphragms." *Second Specialty Conference on Cold-Formed Steel Structures,* University of Missouri-Rolla, Rolla, Mo., Oct., pp. 325-363.

Redfearn, D. (1984). " A test rig for proof-testing building components against wind loads." *BRE Information Paper IP19/84*, Garston, Building Research Establishment.

SAE Fatigue Design and Evaluation Technical Committee (1988). " *Fatigue Design Handbook.*" Published by Society of Automotive Engineers.

Salaheldin, M., Schmidt, L.C. and Upfold, R.W. (1987). " Deflection behaviour of statically loaded corrugated sheet." *Proc. of First National Structural Engineering Conference*, Melbourne, Aug., pp. 541-545.

Standards Association of Australia.(1984). " *AS1397-Steel Sheet and Strip--Hot-Dipped Zinc Coated or Aluminium Zinc-Coated.*" Sydney, SAA.

Standards Association of Australia (1991). " *AS1391-Methods for Tensile Testing of Metals.*" Sydney, SAA, 1991.

Stathopoulos, T. (1984). " Wind loads on low-rise buildings: a review of the state of the art." *Engineering Structure*, Vol. 6, April, pp. 119-135.

Walker, G.R. (1975). " *Report on Cyclone Tracy - Effect on Buildings - Dec. 1974.*" Vol.1, Australian Department of Housing and Construction, Melbourne.

Walker, G.R. (1980). " A review of the impact of cyclone Tracy on Australian building regulations and practice." *Civil Engineering Transactions, I.E.Aust*, Vol. CE22, No. 2, pp. 100-107.

Xu, Y.L. and Reardon, G.F. (1992). " Behaviour of different profiled roofing sheets subject to wind uplift." *Technical Report,* No. 36, Cyclone Testing Station, James Cook University, Australia (also will be published in *Engineering Structures*).